



THE HONG KONG
POLYTECHNIC UNIVERSITY

香港理工大學

Pao Yue-kong Library

包玉剛圖書館

Copyright Undertaking

This thesis is protected by copyright, with all rights reserved.

By reading and using the thesis, the reader understands and agrees to the following terms:

1. The reader will abide by the rules and legal ordinances governing copyright regarding the use of the thesis.
2. The reader will use the thesis for the purpose of research or private study only and not for distribution or further reproduction or any other purpose.
3. The reader agrees to indemnify and hold the University harmless from and against any loss, damage, cost, liability or expenses arising from copyright infringement or unauthorized usage.

IMPORTANT

If you have reasons to believe that any materials in this thesis are deemed not suitable to be distributed in this form, or a copyright owner having difficulty with the material being included in our database, please contact lbsys@polyu.edu.hk providing details. The Library will look into your claim and consider taking remedial action upon receipt of the written requests.

**COOPERATIVE PLANNING AND
MULTI-OBJECTIVE OPERATION OF
ELECTRIC VEHICLE CHARGING STATIONS**

ZHANG XIAN

PhD

The Hong Kong Polytechnic University

2019

The Hong Kong Polytechnic University

Department of Electrical Engineering

**Cooperative Planning and
Multi-Objective Operation of
Electric Vehicle Charging Stations**

ZHANG XIAN

A thesis submitted in partial fulfillment of the requirements
for the degree of Doctor of Philosophy

December 2018

CERTIFICATE OF ORIGINALITY

I hereby declare that this thesis is my own work and that, to the best of my knowledge and belief, it reproduces no material previously published or written, nor material that has been accepted for the award of any other degree or diploma, except where due acknowledgement has been made in the text.

_____ (Signed)

ZHANG Xian (Name of student)

Abstract

In future smart grid, electric vehicles (EVs) would play a vital role to reduce air pollution and carbon emissions caused by conventional transportations while EV batteries could contribute to the power system dispatch as distributed energy storage devices. However, large-scale uncoordinated EV charging would bring challenges and difficulties to the control and operation of a power system due to the rapid growth of charging load demand, additional energy losses, deterioration of power quality, decrease of power grid economic efficiency, etc.

Considering the infrastructure development of EV charging stations (CSEs) as one of the key factors to the widespread use of EVs, this thesis conducts studies from the aspects of the planning and operation of EV CSEs to meet the rapidly growing charging demand of EVs and eliminate any potential threats as a result. Because EV load prediction is the precondition of the planning and operation of CSEs and distribution system (DS), the forecast methodology of EV demand is also one of the concerns of this thesis.

The forecasting of EV load can be divided into long-term forecast and short-term forecast according to the time duration. For the long-term prediction, grey system forecasting theory model and nonlinear autoregressive (NAR) neural network model are firstly utilized in this thesis to forecast the annual growth in the number of EVs including electric buses (EBs) and non-EBs (including private electric cars, electric taxis, etc.). The effectiveness, rationality, precision and adaptability of the two models are evaluated and compared. Simulation results show that the NAR neural network model has a better performance in long-term forecasting of EVs than the grey system forecasting model. Moreover, the deep belief network (DBN) method is firstly applied for accurate EV demand forecasting, the effectiveness of which is proved by comparing with other typical

algorithms. For short-term forecasting, EV charging load is difficult to forecast accurately due to the non-stationary feature of traffic flow (TF) and erratic nature of charging procedures. In this thesis, TF is predicted by a novel deep learning based convolutional neural network (CNN) approach, and the model and data uncertainties are evaluated to formulate the prediction intervals (PIs). EVs' arrival rate is calculated based on the historical data and the proposed mixture model, and the EV charging process is studied by a novel probabilistic queuing model considering charging service limitations and drivers' behaviors. The proposed methods are assessed by using real TF data and the results demonstrate that the errors of the proposed method are reduced by about 30% compared to other widely-used approaches, and the probabilistic forecasting approach has better reliability and sharpness indices than other methods, which leads to high potential for practical use.

According to the forecasting results, sufficient number of CSEs should then be planned to meet the future charging demand of EVs while new feeders in the DS should be timely constructed to provide the required supply to the CSEs. It is a common assumption in the present work that the CS planning and power system planning are managed by a single entity to carry out centrally, which is quite contrary to the reality. In fact, in the deregulated environment, DS and EV CS owners / operators are independent market participants and responsible for their own planning with different or even conflicting interests and objectives. Therefore, coordination of these interests and objectives is a critical and complicated problem for extensive integration of EVs in the liberalized market environment. In addition, the electricity market mechanism should be fully studied in the planning strategy making process. In this thesis, Nash bargaining theory is employed to formulate the cooperative planning for CSEs and DS for the first time. A negotiated planning model of CSEs and DS is established to achieve the most fair and Pareto-efficient payoff allocation for the two independent participants. Additionally, a novel locational marginal price (LMP) model to alleviate DS congestions with

consideration of schedulable EV charging and flexible demands is proposed to model the real market environment while the deep belief network (DBN) method is firstly applied for the accurate forecasting of TF. Simulation results of a 38-node DS with high penetration of EVs and flexible demands have demonstrated that the realistic negotiated planning process and the consideration of DS market mechanism would improve the DS gain payoffs by 8.21% than those in the centralized plan, and the payoff gap between DS and CS is also reduced by 10.73%, which would boost the planning enthusiasm and lead to a more fair planning solution.

Once CSes are constructed, the operation of CSes should be investigated to ensure the high efficiency and reliability of CSes and DS. In this thesis, the application potential of EVs in CSes are accounted in the electric power dispatch, especially with several conflicting and competing objectives such as providing vehicle-to-grid (V2G) service and coordinating with wind power. Further, to solve this firstly proposed highly constrained multi-objective optimization problem (MOOP) with the consideration of uncertainties of EVs and wind power, a decomposition based multiple group search optimization (MGSO/D) is proposed to efficiently reduce the computational complexity and innovatively incorporate the producer-scrounger model to effectively improve the diversity and spanning of the Pareto-optimal front (PF) while uncertainties are accounted by the estimation error punishment. The performance of MGSO/D and the effectiveness of the uncertainty model are investigated using the IEEE 30-bus and 118-bus system with wind farms and CSes. Four indices, namely convergence metric, span metric, spacing metric and l_{max}/l_{min} metric, are utilized to measure the solution quality of MGSO/D and other three well-established Pareto heuristic methods. The PF solutions obtained by the proposed MGSO/D in both small-size and large-scale cases show its superiority over other three algorithms on all 4 indices and demonstrate that it can propagate the search to obtain the uniformly distributed and diverse PF more effectively.

Furthermore, a battery schedule framework is studied in this thesis to dispatch batteries between battery charging stations (BCS) and battery-swapping station (BSS) efficiently. Compared with the battery-swapping technology, fast charging technology has disadvantages that it takes a relatively long time and shortens the battery life much faster. The EV battery-swapping technology is a promising method to avoid the inconvenience of fast charging because of its flexibility. In this thesis, to improve the effectiveness of battery dispatch between BCS and BSS, an original two-direction battery dispatch mechanism to reduce the transportation cost are established and solved by the particle swarm optimization algorithm (PSO) method. The simulation results demonstrate that the optimized battery travel distance is reduced about 50% compared with the random travel. Moreover, considering the serving ability limitations, the K-means clustering algorithm is innovatively utilized to pre-partition the BCS and BSS to make the battery dispatch more efficient for the large-scale system, and the simulation results confirm the travel distance could be further shortened up to 15% by the pre-partition method.

Acknowledgements

First and foremost, I would like to express my sincere gratitude to my chief supervisor, Dr. Kevin K. W. Chan, for his continuous support, care and encouragement throughout my PhD study and research. He patiently guided me solve all kinds of academic problems. His knowledge, experience and intelligence always impress me and enlighten me. It is my honor to study under his guidance.

I would also like to give special thanks to the members in the research team for the comfortable and invigorative academic atmosphere they have created during my research period. I wish to give special thanks to my good friends, Ms. X. Gao, Mr. X. Lu, Mr. M Liu and Mr. W Xu. They have given me so many valuable suggestions and practical helps on my life and research. My sincere appreciations also go to many other coworkers, with whom I have a wonderful and unforgettable research journey.

Moreover, I would like to thank my dear parents Zufeng Zhang and Xiaoqing Huang for their selfless and unconditional love, support, and encouragement ever since I was born. I also owe many thanks to my husband Guibin Wang for his help, encouragement and support throughout my PhD study and life. He is my most powerful backing. I would like to thank my baby Wenjing Wang. His birth gives me motivation to do better.

Last but not least, I would like to acknowledge the support from my Ph.D. studentship awarded by The Hong Kong Polytechnic University.

Table of Contents

Abstract	I
Acknowledgements	V
Table of Contents	VI
Lists of Figures, Tables and Abbreviations	X
Chapter I	
Introduction	1
1.1 Background and Literature Review	1
1.2 Incentives of Thesis.....	6
1.3 Primary Contributions	11
1.4 Thesis Layout	14
1.5 List of Publications	15
Chapter II	
Probabilistic Forecasting of Electric Vehicle Charging Load	17
2.1 Introduction	17
2.2 Long-term Forecasting Models	18
2.2.1 Grey System Forecasting Theory Based Model	18
2.2.2 Nonlinear Autoregressive Neural Network Based Model	20
2.2.3 Performance Criteria of Grey System Forecasting Theory Based Model and NAR Neural Network Theory Based Model	21
2.2.4 Deep Belief Network Based Forecasting	22
2.3 Deep Convolutional Neural Networks with PIs.....	24
2.3.1 Convolutional Neural Network Layer.....	25
2.3.2 Deep CNN Architecture	27

2.3.3 PIs Formulation.....	29
2.3.4 Evaluation of Forecasting Performance.....	31
2.4 Probabilistic EV Load Forecasting.....	32
2.4.1 EV Arrival Rate Estimation.....	33
2.4.2 EV Charging Queuing Model that considers Driver Behaviors.....	37
2.4.3 Stochastic Process Analysis for EV Load Determination.....	39
2.5 Case Studies.....	40
2.5.1 Forecasting Results of Grey System Theory.....	40
2.5.2 Forecasting Results of Nonlinear Autoregressive Neural Network...	44
2.5.3 DBN method Forecasting Results Analysis.....	47
2.5.4 DCNN TF Forecasting Results Analysis.....	48
2.5.5 Charging Load Forecasting Results Analysis.....	55
2.6 Summary.....	59

Chapter III

Negotiated Planning of Distribution System and EV Charging Stations in Deregulated Electricity Markets..... 61

3.1 Introduction.....	61
3.2 Framework of the Proposed Model.....	61
3.3 The Mathematical Model.....	62
3.3.1 Nash Bargaining Model: General Formulation.....	62
3.3.2 Nash Bargaining of the Cooperative Planning.....	63
3.3.3 EV Participated Market Mechanism.....	67
3.3.4 The Centralized Planning Model for Comparison.....	70
3.3.5 Scenario-based Approach for Uncertainty Consideration.....	71
3.4 Solution Methodology.....	73
3.5 Case Studies.....	75
3.5.1 Test System and Experiment Data Description.....	76
3.5.2 Scenarios Description.....	79

3.5.3 Results of the Centralized Planning Benchmark.....	80
3.5.4 The Nash Bargaining Solution.....	80
3.5.5 Discussion: A Comparison between the two Schemes	80
3.5.6 Nash Solutions with Fixed Electricity Prices.....	82
3.5.7 Nash Solutions with Different Disagreement Points	83
3.6 Summary	84

Chapter IV

Multiple Group Search Optimization based on Decomposition for Multi-Objective Dispatch with Electric Vehicle and Wind Power Uncertainties...85

4.1 Introduction.....	85
4.2 Formulation of the Multi-objective Power Dispatch Problem.....	86
4.2.1 Optimization Objectives Considering Uncertainties.....	86
4.2.2 MOOP Constraints.....	90
4.3 Multiple Group Search Optimization based on Decomposition	92
4.3.1 General Framework.....	92
4.3.2 Decomposition of the Proposed MOOP.....	92
4.3.3 Innovatively Incorporated Producer-Scrounger Model	93
4.3.4 Solving Process	95
4.3.5 Performance Metrics of the Proposed MGSO/D Method	97
4.4 Numerical Results and Analysis	98
4.4.1 Investigation on the Modified IEEE 30-Bus System.....	98
4.4.2 Investigation on the Modified IEEE 118-Bus System.....	104
4.4.3 Group Member Number Effects on MGSO/D Performance	106
4.5 Summary	108

Chapter V

Optimal Dispatch of Electric Vehicle Batteries between Battery Swapping Stations and Charging Stations 109

5.1 Introduction	109
5.2 Assumptions and modeling	109
5.2.1 Battery Swapping Charging Network	110
5.2.2 The Basic 2-Direction Battery Dispatch Model.....	111
5.2.3 The Extended Battery Dispatch Model by K-means Pre-partition Method	112
5.3 Solving strategies	113
5.3.1 PSO Based Optimal EV Battery Dispatch	114
5.4 Case studies	115
5.4.1 The Basic 2-Direction Battery Dispatch Model Case	115
5.4.2 The Extended Battery Dispatch Model Case with K-means Clustering Method	117
5.5 Summary	119
Chapter VI	
Conclusions and Future Works	120
6.1 Conclusions	120
6.2 Future Works.....	123
Appendix.....	125
References	127

Lists of Figures, Tables and Abbreviations

List of Figures

Fig. 1.1	Illustration of overall organizational structure of the thesis	14
Fig. 2.1	The DBN framework for EV growth forecasting	22
Fig. 2.2	The flowchart of the proposed DBN framework for forecasting	23
Fig. 2.3	The flowchart of the DCNN implement	25
Fig. 2.4	Basic structure of a CNN layer	26
Fig. 2.5	Architecture of the DCNN	28
Fig. 2.6	An overview of PIs formulation	29
Fig. 2.7	Flowchart of the FCS charging load determination	33
Fig. 2.8	The distribution of EV daily travel distances	35
Fig. 2.9	Trips in progress by time of day in UK	37
Fig. 2.10	Capacity constrained queuing model that considers driver behaviors	38
Fig. 2.11	State transition diagram of the Markov chain that considers EV behaviors	39
Fig. 2.12	The forecasted results of EBs by the grey system theory	42
Fig. 2.13	The forecasted results of non-EBs by the grey system theory	42

Fig. 2.14	The forecasting setting interface of EBs	44
Fig. 2.15	The forecasting setting interface of non-EBs	45
Fig. 2.16	The forecasted results of EBs by NAR	46
Fig. 2.17	The forecasted results of non EBs by NAR	46
Fig. 2.18	The graphic display of the test system	48
Fig. 2.19	Forecasting results by different methods on node 37	48
Fig. 2.20	Validation test for BPNN with different number of hidden neurons	49
Fig. 2.21	Validation test for SAE with different number of hidden layers	50
Fig. 2.22	Deterministic TF forecast absolute residual in summer at J5-J6 M42	52
Fig. 2.23	Deterministic TF forecast absolute residual in winter at J5-J6 M42	52
Fig. 2.24	Probabilistic one-hour ahead TF forecast results during the spring, summer, fall, and winter of 2014	54
Fig. 2.25	The PDF of EV daily travel distances estimated using the mixture model	56
Fig. 2.26	Probabilistic one-hour ahead charging load forecast results during the spring, summer, fall, and winter of 2014	57
Fig. 2.27	The Pearson (linear) correlation between TF and charging load in different seasons	58
Fig. 2.28	Forecasted charging load for different values of C and K	58

Fig. 2.29	Forecasted charging load for different values of σ and δ	58
Fig. 3.1	Framework of the proposed model	62
Fig. 3.2	The programming flow chart	73
Fig. 3.3	Normalized load patterns of different load categories in the UK	76
Fig. 3.4	The 38-bus DS and the centralized planning result	77
Fig. 3.5	The Nash Bargaining Solution without and with fixed electricity prices	81
Fig. 4.1	Flowchart of MGSO/D to solve the proposed problem	96
Fig. 4.2	The best PFs obtained for case 1	100
Fig. 4.3	The best PFs obtained for case 2	101
Fig. 4.4	The best PFs obtained for case 3	102
Fig. 4.5	PFs for different uncertain parameter ϕ of V2G power in Case 4	103
Fig. 4.6	PFs for different uncertain parameter h of wind power in Case 4	104
Fig. 4.7	The best PFs obtained for Case 5	106
Fig. 4.8	Comparison of the PFs of the best runs for $Y=3, 10$ and 20	108
Fig. 5.1	Battery swapping charging network structure	110
Fig. 5.2	Basic battery dispatch model	110
Fig. 5.3	The pre-partition step of the extended battery dispatch model	113

Fig. 5.4	Flowchart of the BCS service K-means clustering	113
Fig. 5.5	Flowchart of the PSO based optimal EV battery dispatch	114
Fig. 5.6	The random travel path of the basic battery dispatch model	115
Fig. 5.7	The optimal travel path of the basic battery dispatch model	116
Fig. 5.8	The iteration curve of the proposed PSO method	116
Fig. 5.9	The BSS/BCS partition results in a larger area	117
Fig. 5.10	The random path, optimal path, and iteration curve of the extended model before partition	118
Fig. 5.11	The optimal path of the extended model after partition	119

List of Tables

Table 2.1	The EB and Non-EB number in Shenzhen from 2006-2015	41
Table 2.2	The EB forecasting result residual error	43
Table 2.3	The non EB forecasting result residual error	43
Table 2.4	The association degree and variance ratio of grey system method	43
Table 2.5	Accuracy level reference table	43
Table 2.6	The EB forecasting result residual error of NAR	45
Table 2.7	The non EB forecasting result residual error of NAR	46
Table 2.8	TF Forecasting Error Comparison at Node 33 and 37	48
Table 2.9	Validation Test for SVM with Different Kernel Function Types	50
Table 2.10	Deterministic one-hour ahead TF forecasting error	51
Table 2.11	Probabilistic one-hour ahead forecasting error	53
Table 2.12	Correlation coefficients of TF and charging load	56
Table 3.1	Reinforcement/Construction costs for substations	78
Table 3.2	The SS offers and load/CS bids	79
Table 3.3	Costs of CSes	79
Table 3.4	Lengths of candidate feeders	79

Table 3.5	Outcomes of two methods of planning	81
Table 3.6	Nash solutions with fixed electricity prices	83
Table 3.7	Electricity prices in the LMP model	83
Table 3.8	Nash solutions with different disagreement points	84
Table 4.1	Parameter setting	99
Table 4.2	Cost coefficients of wind and V2G power	99
Table 4.3	Resulting statistics of performance metrics in case 1	99
Table 4.4	Comparison of best solutions in case 1 and the scheduled EV charging energy losses	100
Table 4.5	Resulting statistics of performance metrics in case 2	101
Table 4.6	The components of the reference PF in case 3	102
Table 4.7	Resulting statistics of performance metrics in case 3	103
Table 4.8	Resulting statistics of performance metrics in case 5	105
Table 4.9	Resulting statistics of performance metrics in case 6	107
Table 5.1	The BSS/BCS geographic location in the extended model	117

List of Abbreviations

ACE	Average coverage error
AIC	Akaike information criterion
ANN	Artificial neural networks
BCS	Battery charging station
BIC	Bayes information criterion
BP	Back propagation
BPNN	Back-propagation neural network
BPSO	Binary particle swarm optimization algorithm
BSS	Battery swapping station
CNN	Convolutional neural network
CS	Charging Station
DBN	Deep belief network
DCNN	Deep convolutional neural network
DisCos	Distribution companies
DoD	Depth of discharge
DS	Distribution system
DSO	Distribution system operator
EA	Evolutionary algorithm
EB	Electric bus
EM	Expectation-maximization
ER	External repository
EV	Electric Vehicle
FCS	Fast charging station
GSO	Group search optimization
IS	Interval Sharpness
LMP	Locational marginal price

MAE	Mean absolute error
MAPE	Mean absolute percentage error
MGSO/D	Multiple group search optimization based on decomposition
MILP	Mixed integer linear programming
MOEA/D	Multi-objective evolutionary algorithm (EA) based on decomposition
MOOP	Multi-objective optimization problem
NAR	Nonlinear autoregressive
NBS	Nash bargaining solution
NLP	Nonlinear programming
NSGA-II	Non-dominated sorting genetic algorithm-II
OPF	Optimal power flow
pcu	passenger car unit
PDF	Probability density function
EV	Plug-in Electric Vehicle
PF	Pareto-optimal front
PI	Prediction interval
PHEV	Plug-in hybrid Electric Vehicle
PICP	Prediction interval coverage probability
PINC	Prediction interval nominal confidence
POZ	Prohibited operating zone
RBM	Restricted Boltzmann machines
RE	Renewable energy
RMSE	Root mean square error
SOC	State of charge
SVM	Support vector machine
SVR	Support vector regression
TF	Traffic Flow
UC	unit commitment

V2G	Vehicle to Grid
VPP	Virtual power plant
WT	Wavelet decomposition

Chapter I

Introduction

1.1 Background and Literature Review

Worsening global environmental problems have accelerated the development of electric vehicles (EVs). The widespread use of EVs will reduce vehicular fossil fuel consumption and contribute to environmental sustainability [1]. It has been estimated by the Electric Power Research Institution that EVs could reduce energy-related greenhouse gas (GHG) emissions approximately 163–612 million metric tons per year by 2050 [11]. Currently, several countries [2-4] have actively promoted the development of the EV industry, and various EV models are being rolled out to the market by auto manufacturers [5]. From 2009 to 2016, the global sales of EVs reached approximately two million [8]. It is predicted by the International Energy Agency (IEA) that global EV sales could reach five million per year by 2020, and the EV industry could obtain 50% of the automobile market share by 2050 [9]. The growing EV population has required massive investments in charging facilities in recent years. For example, in China, 4.8 million distributed charging piles and more than 12,000 fast charging stations (FCSes) are planned for construction by 2020 [10-11].

The rapid development of EVs brings new opportunities and challenges for the power system. EVs could benefit the power system dispatch if EV batteries could be utilized as distributed energy storage devices. For instance, casual charging could be shifted to a valley load period to relieve the peak generation [19]. Due to advances in V2G technologies [91-92], EV batteries now have more flexibility that can allow them to provide contributions to the operation of the system. As presented in [92], EVs with V2G can be utilized as portable power plants to

improve the reliability as well as reserves of power systems, and decrease system dependencies on expensive units. In [93] a joint optimization model for generators and EVs with V2G modes is developed to demonstrate the potential for EVs to participate in power dispatch. Furthermore, the integration of renewable energy with EV charging stations (CSEs) has become a recent hot research topic. In [12], it is demonstrated that coordinated EV charging can promote the integration of photovoltaic power plants. Voltage rise problems caused by photovoltaic power plants could also be alleviated by coordinated EV charging [13]. A virtual power plant composed of a wind power plant and a fleet of EVs is proposed in [14], and the profit of this virtual plant could be maximized by dispatching the output power of the virtual plant and the energy storage of EVs.

Alternately, uncoordinated charging of a large amount of EVs would have significant adverse impacts on the secure and economically feasible operation of power systems [15], and reduce the widespread use of EVs. Harmonic currents generated by EV charging loads could harm the stable operation of substations [16], and harmonic voltages that result from EV charging would be problematic for the stable operation of distribution systems [17]. Due to the uncertain nature of EV charging behavior, power losses and voltage deviations brought on by a high penetration of EVs are also the concerns of system operators, and these issues need to be properly addressed to mitigate their negative impacts [89]. In addition, inconveniences associated with EV charging are another problem that significantly limits the popularization of EVs. Long charging times and the lack of charging facilities significantly reduce consumers' willingness to purchase EVs [19] [45].

The development of CSEs is one of the critical factors needed to accelerate the industrialization and large-scale development of EVs. So far, a majority of the attention of the researchers has been placed on how to eliminate the threats caused by EVs and to promote the adoption of EVs by improving the planning and operation of EV CSEs. Moreover, because accurate forecasts of EV charging loads are essential for the planning and operation of charging facilities [18-19], the

forecasting of EV charging loads has attracted much attention as well. The current state of the research regarding EV demand forecasting, planning and operation of CSEs is summarized as follows.

- (1) For long-term forecasting of EV load, parametric technologies such as the autoregressive integrated moving average (ARIMA) [173] are commonly used to forecast the number of EVs while nonparametric methods such as artificial neural networks (ANN) [38] and support vector regression (SVR) [174] are also widely used. For short-term EV load forecasting, historical data is often used in existing literature [25-26]. In [25], an EV sales forecasting model is established and it was based on consumer preferences in EVs that were extracted from historical data. Then, a daily EV load curve is forecasted based on EV charging behaviors. In [26], EV loads are forecasted in terms of the number of EVs connected to the power grid using historical data from the National Renewable Energy Laboratory and the Idaho National Laboratory. Meanwhile driving behavior needs to be considered in the EV load forecasting process [25-29] to account for the EV mobility characteristics. A queuing theory based on an EV charging demand stochastic model is proposed in [26], and a more accurate forecast result is obtained using real-time data and proper analysis of uncertainties. The number of EVs using charging facilities during different hours, charging start time, travel distance, and the charging duration are considered for the study of load demand forecasting for battery-swap stations in [27]. The half-hourly V2G capacity is estimated using dynamic real-time EV scheduling based on an accurate EV load model that considers constraints on meeting demand while ensuring EV charging ability in [28]. Due to the stochastic nature of EV charging behavior, the Monte Carlo simulation is frequently utilized for forecasting EV demand [29].
- (2) Due to the ever-increasing penetration of EVs, adequate charging facilities and a charging distribution system needs to be coordinately planned and developed to support the successful deployment of charging scheduling and cooperative

control. However, research regarding coordinated planning of charging facilities and charging DS is still in the early stages with the focus currently primarily on the planning of CSes [45-52]. In [45], a multi-objective model is developed for rapid CS planning that considered traffic constraints in the planning schedule. A two-step screening method with a service radius for EV CSes and environmental factors is proposed in [46] to identify CS sites. In [47], a probabilistic method is proposed to optimize the locations and capacities of EV parking lots that considered uncertain parameters in EV owner driving patterns. In [45] and [48], a data envelopment analysis of CS planning is utilized to evaluate different objectives and obtain the size and location of CSes. CS planning methods in urban areas and around freeways are studied in [49] and [50], respectively. Customer behavior, such as charging preferences and demand response, is another important factor that influences CS planning results, and these were discussed in [51] and [52]. The existing power grid without additional investments will limit the integration of a large number of EVs in the future [53-55]. Environmental considerations are considered in an analysis of the potential for the system to support a large amount of EV charging, and it is found that the reliability of a power grid would be jeopardized if EV penetration is high [53-54]. Emissions and system costs are assessed by distribution system operators (DSOs) to accommodate a high penetration of EVs in [55]. However, studies regarding power system planning to accommodate the fast growing use of EVs are relatively sparse [56-59]. It is concluded in [56] that the transmission capacity would need to be properly expanded to accommodate high EV electricity consumption. A scenario-based planning approach for DS that considers the uncertainties of EV penetration is presented in [57], and it indicates that coordinated charging would defer DS planning and improve investment efficiency. Co-planning of charging facilities and the power system has also been proved effective in accommodating EV integration [58-59]. A load density method to determine

the optimal capacity of CSEs is proposed in [58], and the DSs and CSEs are co-planned to minimize the overall cost of investment, operation, and maintenance. A collaborative planning model for DS and CSEs to minimize the cost of investment and energy losses while maximizing charging service abilities is developed in [59].

- (3) In addition to the issue of CS planning, the optimized operation of CSEs is also critical to guarantee the efficiency, stability, and reliability of CSEs and the DS. So far researchers have devoted large amount of effort to EV charging demand management. EV demand response to the load shift in a smart grid is presented in [60]. A layered and distributed charging load dispatch mechanism for large populations of EVs, is proposed in [61] to directly reduce generation cost. In [98], an optimal economic dispatch model for EVs and wind power based on an enhanced particle swarm optimization algorithm (PSO) that considers uncertainties is proposed. A summary of the existing dynamic approaches for static EV charging and their suitability is addressed in [62]. In [63], a distributed EV charging control method based on energy demand forecasting is developed to smooth the daily grid load profile while satisfying the charging demand of EVs. A novel cooperative charging strategy for a smart charging station is proposed in [64]. In [65], two queueing-based optimization frameworks are proposed for CSEs to maximize system revenue. The demand-side management of plug-in hybrid EV charging at low-voltage transformers in a smart grid is studied in [66]. Optimization models were proposed in [67-68] to maximize the unilateral payoffs of the distribution system and EV owners. In addition, future smart grids will have high penetration of REs due to their advantages in reducing the pollution of conventional generators [94]. Coordinated dispatch of EVs and REs shall therefore be investigated. In [70], cooperative dispatch with renewable generation (RE) has been investigated extensively to promote the integration of EVs in modern smart grid. While cost

reduction is frequently discussed for power grid with both EVs and REs [95], it is often considered together with reduction of emissions [96].

(4) Different from FCSEs, BSSes provide a battery swapping service for EV owners instead of battery charging. Compared to fast charging technology, the battery-swapping technology has the advantage that it reduces the service time and the battery transportation cost. The battery swapping method is promising because it may overcome the difficulties of long charging time and the lack of charging facilities, thereby achieving the high EV charging efficiency [71]. Moreover, BSSes have shown better performance for smoothing the load profile than FCSEs due to their flexible battery charging characteristics [72]. Research on the optimal operation of BSSes has begun in recent years. A charging power dispatch model is established in [73] to reduce fluctuations and peak-valley differences in load demand in the distribution system. A two-stage optimal charging model with the objectives of charging cost minimization and charging power smoothing is studied in [74] that considered bus running operation and battery discharging characteristics. Unit commitment and economic dispatch problems of the smart grid with BSSes are investigated in [75] and [76].

1.2 Incentives of Thesis

To eliminate any negative impacts caused by EVs and increase the penetration of EVs, infrastructure development of EV CSEs is a critical factor. Many studies have investigated the planning and operation of CSEs. Moreover, the forecasting of EV charging loads is a precondition for the planning and operation of CSEs. Therefore, this thesis focuses on accurate forecasting of EV charging demands (long-term and short-term), and the cooperative planning and multi-objective operation of CSEs to overcome the following difficulties currently faced to promote the wide adoption of EVs.

1) The grey system forecasting theory has been used for population forecasting [20] and power system load forecasting [21]. Also, the nonlinear autoregressive (NAR) neural network has been used in the establishment of the aquaculture water nitrite prediction model and for the classification and prediction of audience rating [22-24]. Both of them are effective long-term forecasting methods, but they have never been applied to forecast growth in the number of EVs. Therefore, it is the first incentive of this thesis to first apply and benchmark those two models to forecast the annual growth in the number of EVs using history data.

2) It is a common practice to obtain the EV numbers in the CS indirectly from the *traffic flow* (TF) information [18][59][113][131]. Therefore, the accurate forecast of TF at the candidate CS locations is the first and important step for the planning and operation of CS and DS. Generally, this forecast could be influenced by different factors such as charging infrastructure, socioeconomic level and the government policy, many of which are not easy to be quantified. Multilayer neural network (NN) solves problems in a way similar to the human brain and is quite efficient in dealing with incomplete ambiguous data without strong regularity [156]. It is thus well suited for complicated forecasting problems. However, it is difficult to optimize the weights (neurons) in most kinds of multilayer NNs and limits their forecasting performance. If the initial weights are too large, only poor local minima could be found. If the initial weights are too small, the gradients in the early layers are tiny when training with back propagation (BP), making it infeasible to obtain the optimal weights in the multilayer NNs [156]. In comparison, the core characteristics of the proposed deep belief network (DBN) method lies in that the composition of visible and hidden layers results in a fast-unsupervised process by pre-training a multilayer NN, thus the neurons in the hidden layer could be efficiently optimized to recognize different TF characteristics. Then, the supervised fine-tuning is utilized to adjust the learned features for better prediction. Therefore, the second incentive is applied DBN to predict TF in the CS construction planning horizon.

3) Queuing theory [30] is an effective approach for studying aggregated EV charging behaviors, and it accounts for various uncertainties in the EV charging process. The V2G capacity for regulation was estimated using the queuing theory in [31]. Charging demand can also be forecasted based on the queuing model [28], [32-33]. However, the proper application of queuing theory needs to consider EV mobility and aggregative characteristics, and this has rarely been done. Traffic flow (TF) theory [34] is a promising method to solve this problem, and its use has rapidly progressed in recent years. The spatial and temporal dynamics of EV charging loads in a highway charging station (CS) was studied in [35] using queuing theory and the TF model. The arrival rate was estimated using the TF model in [36], and the CS capacity was obtained using the forecasted arrival rate and proposed queuing model. There are a large number of TF forecasting studies due to the rapid development of smart traffic technologies. Parametric technologies, such as the autoregressive integrated moving average [26] and other time-series methods [37], have been often used for TF predictions. Nonparametric methods, such as artificial neural networks (ANN) [38] and the support vector machine (SVM) [39], have also been widely used due to their excellent ability to present TF stochastic characteristics [40]. However, the complicated nonlinear features of TF data cannot be fully extracted using these methods. Therefore, this problem inspires the application of deep learning methods for TF forecasting due to their good performance for discovering various structures in traffic data [41-44]. Deep learning methods, such as stacked autoencoders (SAE) [41-42] and the deep belief network [43-44], can represent the inner features of TF without any prior knowledge, and they have superior performance for TF predictions. However, there are two major disadvantages of the existing deep learning-based forecasting methods. First, the performance of the proposed approaches is still not satisfactory. Second, the charging procedures that are needed to utilize the proposed approaches to solve EV load forecasting problems are not well considered. Consequently, the third incentive for this thesis is to address a novel deep learning based

convolutional neural network approach to reveal the low-dimensional and nonlinear structure of TFs and achieve a higher forecasting performance. The incorporated behavior considered queuing models will simulate charging procedures properly.

4) In the deregulated environment, DS and EV CS owners are independent market participants and responsible for DS and CS planning with different or even conflicting interests and objectives. However, most current studies [45-59] assume that charging facility planning and power system planning are managed by a single entity and carried out in a centralized manner, which is not really the case in practice. In fact, coordination of these interests and objectives is a critical and complicated problem for extensive integration of EVs in a liberalized market environment. Additionally, the electricity market mechanism needs to be taken into consideration in the planning process. Unfortunately, so far, this is still absent from many systematic investigations. Nash bargaining, which assumes that game players bargain directly with each other to come to binding agreements [77], is innovatively utilized in this work to analyze the agreement binding process to determine the planning schedules of CSEs and DSEs. Nash bargaining theory has been applied for solving transmission investment cost sharing [77-80] and transmission cost allocation [81-83] problems. Different from non-cooperative games [85], Nash bargaining focuses on the payoff allocation and is very suitable for CS and DS co-planning in a deregulated market environment. As the fourth incentive of this thesis, Nash bargaining is first applied to formulate cooperative planning for CSEs and DSEs, then a novel locational marginal price (LMP) model to alleviate DS congestion that considers schedulable EV charging and flexible demands in order to represent real market conditions.

5) Owing to the variety of system participants and complexity of system operation, power dispatch involved in both REs and EVs in CSEs should be beneficial to model as MOOPs, and the uncertainties of REs and EVs in CSEs should be properly handled. However, research that has considered those aspects

is rare. Optimal dispatch models that accounted for the uncertainties in both REs and EVs were formulated in [19] and [98], but not solved in a multi-objective manner. A microgrid operation scheduling framework with EVs and REs was proposed and solved using a mixed integer linear programming (MILP) based multi-objective optimization (MOO) method in [99], but the uncertainties of REs and EVs were not mentioned. However, there are many barriers to applying the Pareto optimization algorithms into MOOP with REs and EVs. The use of a weighted sum is a common approach [100], but many trials are claimed by adjusting the weights, and this is not efficient for obtaining non-convex Pareto-optimal front (PFs). The Pareto-based MOO algorithms, such as the non-dominated sorting genetic algorithm-II (NSGA-II) [101] and the strength evolutionary algorithm (SPEA) [102], have been utilized in two-objective MOOPs to achieve the compromise between fuel costs and air pollutant emissions. A two-objective MOOP that considered the uncertainties of REs and PHEVs was solved using NSGA-II in [103]. Nevertheless, the broadening of these algorithms to adapt to more optimization objectives for EVs in CSes and REs is still insufficient. Therefore, there is a need to set up an innovative multi-objective dispatch model that considers the uncertainties of EVs and wind power, and there is a need to efficiently solve the highly constrained MOOPs with large dimension objectives using advanced algorithms. Group search optimization (GSO) is a recently proposed algorithm based on the producer-scrounger model inspired by animal searching behavior [104]. It was improved to become a multi-objective GSO algorithm (MGSO) in [105] for large-scale MOOPs that shows superiority in convergence and span metrics compared with NSGA-II and SPEA-II. Another up-to-date widely used algorithm is the multi-objective evolutionary algorithm (EA) based on decomposition (MOEA/D) that combines the advantages of weighted sum methods and EAs. It has been shown that MOEA/D performed better than NSGA-II in many benchmark problems [106]. Therefore, the fifth incentive of the thesis is to propose a complicated MOOP that considers the uncertainties of EVs

in CSEs and REs and solves this using a novel MGSO/D inspired by the merits of the producer-scrounger model and decomposition.

6) Although some progress has been obtained in the research of BSS, in-depth studies of BSS operation are rather underdeveloped [72-75]. Most existing research treats BSS as a special kind of load and ignores its difference from common loads. Since the battery charging process occurs separately from the vehicle in the battery swapping mode, the battery swapping charging network is usually consisted of BSS and battery charging stations (BCS) independently. In this mode, the logistics between BSS and BCS becomes an urgent problem to solve to ensure the economic and safe operation of a battery swapping charging network. However, studies regarding battery transportation between BCS and BSS are insufficient. The last incentive for this thesis is to propose an original two-direction battery dispatch mechanism between BSSes and BCSes to reduce the transportation cost based on the K-means clustering algorithm.

1.3 Primary Contributions

1) Two promising forecasting approaches based on grey system forecasting and the NAR neural network respectively are first used to establish the forecasting models for the annual growth of EV number in the future. Their effectiveness is fully evaluated and simulation results show a better performance of the NAR neural network model in long-term forecasting of EVs than the grey system forecasting model.

2) DBN method is first applied for accurate forecast of TF in the CS construction planning horizon. And its superior effectiveness is confirmed by comparing with other typical long-term forecasting algorithms.

3) A comprehensive ensemble method is developed to address the complicated EV load forecasting problems. First, TF is forecasted using an original deep-learning based convolutional neural network (CNN) method in which an ensemble

approach that considers both model and data uncertainty is employed to effectively formulate TF prediction intervals (PIs). Therefore, the complicated nonlinear features of TF are learned more effectively, and superior forecasting performance is obtained. Second, a mixture model-based method is used to approximate the arrival rate of EVs according to the historical data. Third, an advanced MMCK queuing model is formulated for the first time to predict the EV charging load in the CSEs, which accounts for CS service limitations and the inherent randomness of EV driver behaviors. The proposed probabilistic forecasting methods are assessed using real TF data, and case study results show that uncertainties in the EV charging load can be learned comprehensively using the proposed methods. Compared with other widely-used approaches, the proposed approach resulted in better reliability and sharpness indices, giving it a high potential for practical utilization.

4) A cooperative game-theory (Nash bargaining) based planning model is proposed to reflect a more realistic process of DS and CS planning to reach a negotiated solution for profit sharing, cost recovery, and nondiscriminatory benefits. This approach is based on an efficient deep belief network (DBN) method for forecasting the future growth of EV demand. The use of Nash bargaining theory is more accurate than simply assuming this system is managed by a single utility. Then, a novel DS-based locational marginal price (LMP) model capable of alleviating congestion and promoting responses in EV charging is modeled to simulate a deregulated market environment. Simulation results show that the proposed model can obtain a fair planning solution and boost planning enthusiasm, and is proved for its immediate and far-reaching significance to promote the development of CSEs and EVs.

5) The complicated MOOP considering uncertainties of EVs and REs is proposed for the first time and solved using a novel MGSO/D inspired by the merits of the producer-scrounger model and decomposition. The MGSO/D explicitly decomposes the MOOP into several scalar subproblems that leads the

proposed algorithm to lower computational complexity at each generation. Then, the subproblem is optimized based on the innovatively incorporated producer-scrounger model that only uses information from its several adjacent subproblems. Therefore, the resulting PFs would have better diversity and spanning metrics than other well-established evolutionary algorithms. Furthermore, the cost functions of wind generators and V2G power supplies of EVs are derived according to the probability distributions to study the probabilistic behaviors of REs and EVs. Case studies have illustrated that these uncertainties have significant impacts on simulation results, and MGSO/D has a superior solution searching ability to solve high-dimensional MOOPs with complex constraints and objectives. This demonstrates its large potential to accommodate similar problem characteristics.

6) A bi-direction battery dispatch between the BCS and BSS models is proposed to reduce battery transportation costs, and the K-means clustering algorithm is innovatively utilized to pre-partition the BCS and BSS to make the battery dispatch more efficient in a large-scale system that considers serving ability limitations. The feasibility and efficiency of the proposed model is demonstrated in an urban battery logistics case. The results show that compared with random transportation, optimal dispatch of EV batteries is feasible and efficiently reduces battery transportation costs, which will contribute to the development of battery swapping technologies and the wide application of EVs in the future.

1.4 Thesis Layout

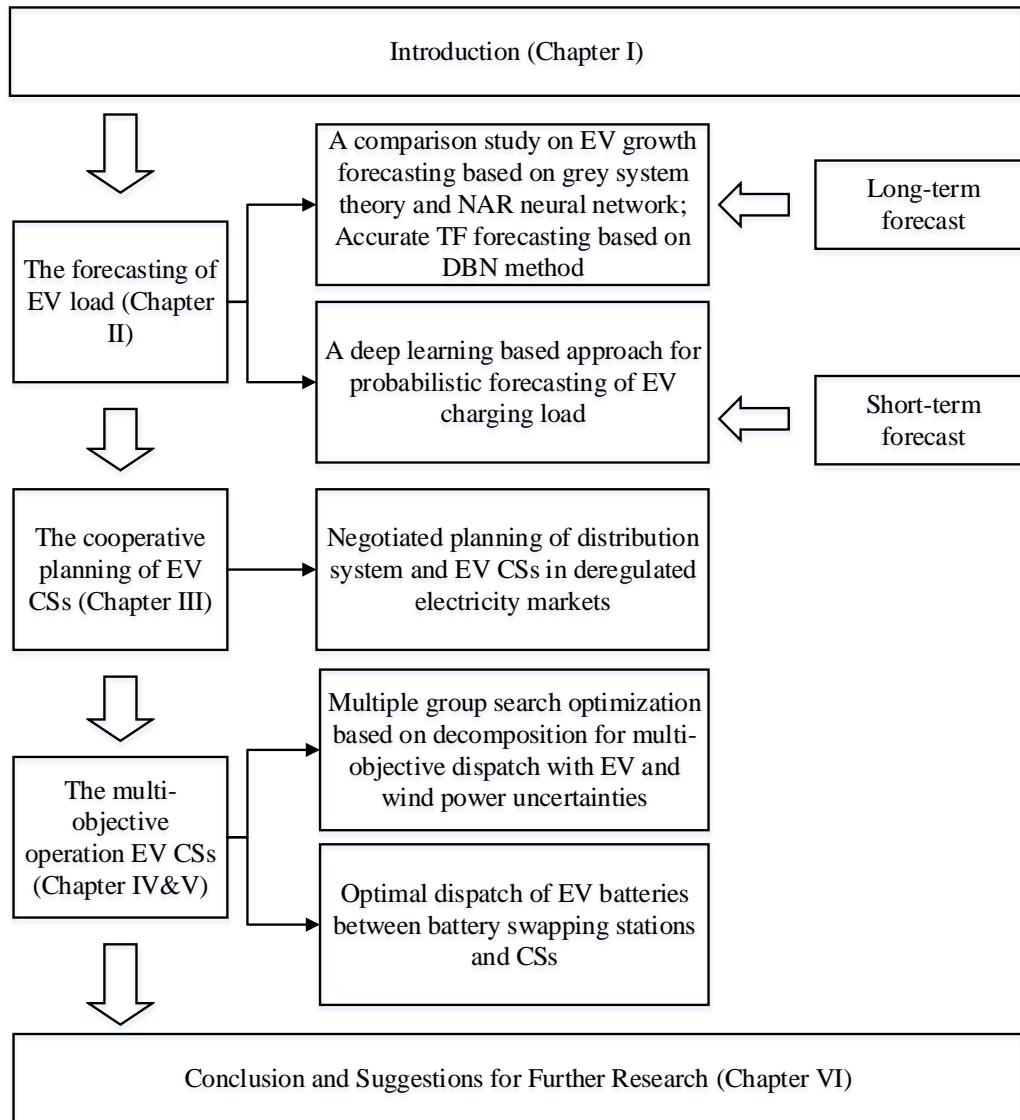


Fig. 1.1 Illustration of overall organizational structure of the thesis

The rest of this thesis consists of five chapters. Chapter II first presents a comparison study on EV growth forecasting based on the grey system theory and the NAR neural network. Second, DBN method is applied to the accurate TF forecasting. Then, a deep learning-based approach for probabilistic forecasting of EV charging load is proposed. Chapter III outlines a negotiated planning approach for a distribution system and EV charging stations in a deregulated electricity market. Chapter IV presents an improved multiple group search optimization method based on decomposition for multi-objective dispatch that considers

electric vehicle and wind power uncertainties. Chapter V investigates the optimal dispatch of electrical vehicle batteries between battery swapping stations and charging stations. Finally, the conclusions of the thesis are discussed in Chapter VI with suggestions for future work. The overall organization of this thesis is shown in Fig. 1.1.

1.5 List of Publications

Journal paper

1. X. Zhang, K. W. Chan et al, "Negotiated Planning of Distribution System and EV Charging Stations in Deregulated Electricity Markets," resubmitted to IEEE Transactions on Industrial Informatics, TII-18-1679, 28 Jun 2018.
2. X. Zhang, K. W. Chan et al, "Multiple Group Search Optimization based on Decomposition for Multi-Objective Dispatch with Electric Vehicle and Wind Power Uncertainties," submitted to IEEE Transactions on Sustainable Energy, TSTE-00028-2019, 8 Jan 2019.
3. X. Zhang, K. W. Chan et al, "Deep Learning-Based Probabilistic Forecasting of Electric Vehicle Charging Load with a Novel Queuing Model," resubmitted to IEEE Transactions on Industrial Informatics, TII-18-2693, 14 Oct 2018.
4. X. Zhang, K. W. Chan et al, "Flexible and Robust Multi-objective Planning for Electric Vehicle Charging Facilities under Uncertainty in a Coupled Traffic-Power System," submitted to Applied Energy, APEN-D-18-09939. 10 Oct 2018.
5. X. Zhang, K. W. Chan et al, "Game-Theoretic Planning for Integrated Energy System with Independent Participants Considering Ancillary Services of Power-to-Gas Stations," submitted to Energy, EGY-D-18-08149. 13 Dec 2018.

6. G. Wang, X. Zhang et al, "Robust Planning of Electric Vehicle Charging Facilities with an Advanced Evaluation Method," IEEE Transactions on Industrial Informatics, vol. 14, no.3, pp. 866-876.

Conference paper

7. X. Zhang, G. Wang, "Optimal dispatch of electric vehicle batteries between battery swapping stations and charging stations," Power and Energy Society General Meeting (PESGM), 2016.
8. X. Zhang, K. W. Chan et al, "A comparison study on electric vehicle growth forecasting based on grey system theory and NAR neural network," IEEE Int. Conf. on Smart Grid Communication, pp. 711-715, Sydney, Nov 2016.

Chapter II

Probabilistic Forecasting of Electric Vehicle Charging Load

2.1 Introduction

Accurate forecasting of EV charging demand is important for the unit commitment (UC), economic dispatch, optimal power flow (OPF) and electric power market transaction in power systems. Furthermore, EV demand forecasting is the precondition for the planning and operation of CSEs. It is therefore necessary to establish an efficient method for the forecasting of EV load by establishing reasonable models.

According to the time duration, the forecasting of EV charging load can be divided into long-term forecast and short-term forecast. Grey system forecasting theory and NAR neural network are methodologies for long-term forecasting [20-24] which can be applied for EV charging demand forecasting. In this chapter, they are explored to establish two separate models to forecast the annual growth in the number of EVs from the history data. Their rationality, effectiveness, precision and adaptability are evaluated and compared. Moreover, DBN method is innovatively applied for accurate TF forecasting in the CS construction planning horizon. And its effectiveness is compared with other typical long-term forecasting algorithms.

For short-term forecasting, due to the non-stationary feature of traffic flow (TF) and erratic nature of charging procedures, it is hard to forecast the EV charging load accurately. In this chapter, a deep learning based approach for probabilistic

forecasting of EV charging load is proposed. In this forecast model both the driver behaviors and FCS service would be considered, and the EV charging load in the FCSes are predicted with the following steps. The first step is to predict TF by a novel deep-learning based CNN method. Then the TF PIs are formulated by evaluating the model and data uncertainties. EV arrival rates are calculated based on historical data and the proposed mixture model. The EV charging process is studied using a novel probabilistic queuing model that takes into consideration charging service limitations and driver behaviors. At last, a novel probabilistic queuing model is proposed to predict the EV charging load in the CSes .

2.2 Long-term Forecasting Models

2.2.1 Grey System Forecasting Theory Based Model

EV number growth data are complicated, orderly and have overall functionality. Grey system forecasting theory tries to find inherent laws in the seemingly disorganized data. Grey forecasting theory firstly distinguishes differences in trends of factors, and then finds hidden laws in history data in certain time horizon after processing the data. After that, grey system theory generates data sequence with regularity and forecasts the trend of data by setting up several differential equations.

GM (1, 1) is the most widely used grey model, which is a first-order differential model to forecast one variable. The mathematical model of GM (1, 1) is as follows [107]:

1) The general form of GM (1, 1)

A time series is used to reflect the character of the prediction object to structure the GM (1, 1) model, which forecasts the features at a specific time in the future or the time when a feature increases to a certain value. In general, the raw time series $\mathbf{X}_i^{(0)}$ can be written as follows:

$$\mathbf{X}_i^{(0)} = \{x_1^{(0)} \ x_2^{(0)} \ \dots \ x_n^{(0)}\} \quad i = 1, 2, 3, \dots, n \quad (2.1)$$

At first, $\mathbf{X}_i^{(1)}$ is generated by first-order accumulation and eliminating the randomness and volatility of the data:

$$\mathbf{X}_i^{(1)} = \{x_1^{(1)} x_2^{(1)} \dots x_n^{(1)}\} \quad i = 1, 2, 3, \dots, n \quad (2.2)$$

Among them,

$$x_s^{(1)} = \sum_{S=1}^i x_s^{(0)} \quad (2.3)$$

The first-order differential is

$$\frac{dx^{(1)}}{dt} + ax^{(1)} = \mu \quad (2.4)$$

2) Identification algorithm

Let grey number parameter series be \hat{a} , $\hat{a} = [a, \mu]^T$, \hat{a} can be solved by the least square method:

$$\hat{a} = (\mathbf{B}^T \mathbf{B})^{-1} \mathbf{B}^T \mathbf{Y}_n \quad (2.5)$$

In the equation, B is the matrix after processing and \mathbf{Y}_n is a data column.

$$\mathbf{B} = \begin{pmatrix} -1/2 & (x_1^{(1)} + x_2^{(1)}) & 1 \\ \dots & \dots & \dots \\ -1/2 & (x_{n-1}^{(1)} + x_n^{(1)}) & 1 \end{pmatrix} \quad (2.6)$$

$$\mathbf{Y}_n = (x_2^{(0)} x_3^{(0)} \dots x_n^{(0)})^T \quad (2.7)$$

The GM (1,1) model are as above.

The results of the GM (1, 1) model, the predicted value are:

$$\hat{\mathbf{X}}_{k+1}^{(1)} = (x_1^{(0)} - \frac{u}{a})e^{-ak} + \frac{u}{a} \quad (2.8)$$

or

$$\hat{\mathbf{X}}_k^{(1)} = (x_1^{(0)} - \frac{u}{a})e^{-a(k-1)} + \frac{u}{a} \quad (2.9)$$

3) The transformation of the predicted value

The result of the GM (1, 1) model is the first-order cumulative result. To obtain the result on the time $k \in \{n+1, n+2, \dots\}$, $\mathbf{X}_{k+1}^{(1)}$ in the GM (1,1) model should be transformed to $\mathbf{X}_{k+1}^{(0)}$ as follows:

$$\hat{\mathbf{X}}_{k+1}^{(0)} = (\hat{\mathbf{X}}_{k+1}^{(1)} - \hat{\mathbf{X}}_k^{(1)}) \quad (2.10)$$

2.2.2 Nonlinear Autoregressive Neural Network Based Model

NAR neural network theory model could be defined as:

$$y_n = f(y_{n-1}, \dots, y_{n-k}, x_n, \dots, x_{n-1}) \quad (2.11)$$

In the formula, x is the input data; y is the output data; n is a time series; f is a nonlinear function.

In the model, although these data are the factors influencing the predictable number of electric vehicles, there are default input data, such as socio-economic level, charging infrastructure, policies and regulations, which cannot be quantified. Therefore, the history output is taken as the input data, and the model is constructed as follows:

$$y_n = f(y_{n-1}, \dots, y_{n-k}) + k\varepsilon_n \quad (2.12)$$

where k is the autoregressive order, which is a constant and ε_n is a random variable following a Gaussian distribution.

The output of each y in the NAR model will be the input data in the next calculation as the adjustment parameters for the next output, completing the adjustment of the neural network [22].

In the neural network training for the model, a neural network is firstly created, then the autoregressive order k should be set. Input sequence is $\{y_i, y_{i+1}, \dots, y_{i+k-1}\}$, $i = 1, 2, \dots, n$. And the target output is $\{y_{i+k}\}$, $i = 1, 2, \dots, n$. For each input sample, the network output and the target output comparison algorithm will automatically adjust the network parameters to minimize the mean square error. In MATLAB implementation, fitness function is used to construct the network.

Next, network parameters of NAR neural network should be determined. NAR neural network is mainly composed of input layer, output layer and hidden layer. Because the model sample of our prediction model has only one output variable, the number of neurons in the output layer is set to 1. The order of auto-regression and the number of the hidden layer neurons are determined by a variety of factors.

At present, there is no mature theoretical basis. The most reasonable approach is selecting a reasonable set of parameters to test in a number of comparative ways, and deciding the final parameters according to the test results.

2.2.3 Performance Criteria of Grey System Forecasting Theory Based Model and NAR Neural Network Theory Based Model

The performance of the proposed approach could be comprehensively assessed via different indices.

1) *Residual error*: This index is the difference value between the actual value and the forecasted value

$$\mathbf{e}_k = \mathbf{X}_k - \hat{\mathbf{X}}_k \quad (2.13)$$

where the \mathbf{e}_k is the residual error, while \mathbf{X}_k and $\hat{\mathbf{X}}_k$ is the actual value and the forecasted value, respectively.

2) *Relative error*: The relative error could be stated as

$$\mathbf{e}_k = (\mathbf{X}_k - \hat{\mathbf{X}}_k) / \mathbf{X}_k * 100\% \quad (2.14)$$

3) *The mean value of the residual error*:

$$\bar{\mathbf{e}} = \frac{1}{n} \sum_{i=1}^n \mathbf{e}(i) \quad (2.15)$$

4) *The mean value of the original data*:

$$\bar{x} = \frac{1}{n} \sum_{i=1}^n x_i^{(0)} \quad (2.16)$$

5) *The standard deviation of the original data*:

$$S_1 = \sqrt{\frac{1}{n} \sum_{i=1}^n (x_i^{(0)} - \bar{x})^2} \quad (2.17)$$

6) *The standard deviation of the residual error*:

$$S_1 = \sqrt{\frac{1}{n} \sum_{i=1}^n (\mathbf{e}(i) - \bar{\mathbf{e}})^2} \quad (2.18)$$

7) *Rariance ratio*:

$$C = \frac{S_1}{S_2} \quad (2.19)$$

2.2.4 Deep Belief Network Based Forecasting

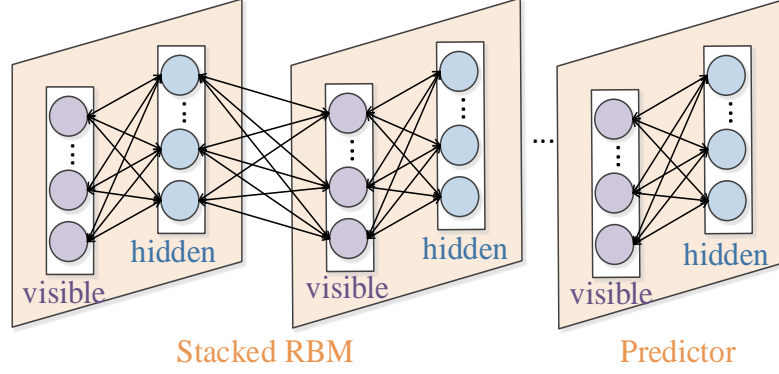


Fig. 2.1 The DBN framework for EV growth forecasting

DBN consists of restricted Boltzmann machines (RBMs) layer by layer for pre-learning and a logistic regression layer for prediction, as shown in Fig. 2.1. The historic EV data is the input and firstly trained by the stacked RBMs in an unsupervised way. The purpose of each RBM is to extract a probability distribution $P(v, h)$ from visible layer v_i to hidden layer h_j to learn the unobservable patterns in the training data, which could be obtained by solving the following optimization according to the Bayesian theory [124].

$$\max \sum_{v \in S} \log P(v, h) = \sum_{v \in S} \log(e^{-E(v, h)} / Z) \quad (2.20)$$

where S is the training data; Z is the partition function for normalization; and $E(v, h)$ is the energy function assigned to the state of the network:

$$E(v, h) = -\sum_{i=1}^{n_v} a_i v_i - \sum_{j=1}^{n_h} b_j h_j - \sum_{i=1}^{n_v} \sum_{j=1}^{n_h} h_j W_{j,i} v_i \quad (2.21)$$

in which a_i and b_j are the visible unit offset and the bias weight of the hidden unit, respectively, and $W_{j,i}$ is the matrix of connection weights of visible and hidden units. The size of $W_{j,i}$ is $n_v \times n_h$. All the parameters could be acquired during the solving process of (3.1) by stochastic gradient ascent algorithm [125]. The learning of RBMs works well even it is not exactly following the gradient of the log probability of the training TF data [157]. Besides, adding more layers always improves the lower bound on the log probability and ensures the weights are initialized correctly [123]. Therefore, the DBN is very effective to pre-train the

weights and makes it an efficient way to reveal low-dimensional, nonlinear structure of the TFs to achieve higher forecasting performance than other technologies.

In the final stage of the whole network, the fine-tuning is utilized as the predictor to coordinate the parameters of the DBN, which could be solved by well-known back propagation (BP) in a supervised manner [124]. As a summary, the flowchart of the proposed DBN method is shown in Fig. 2.2.

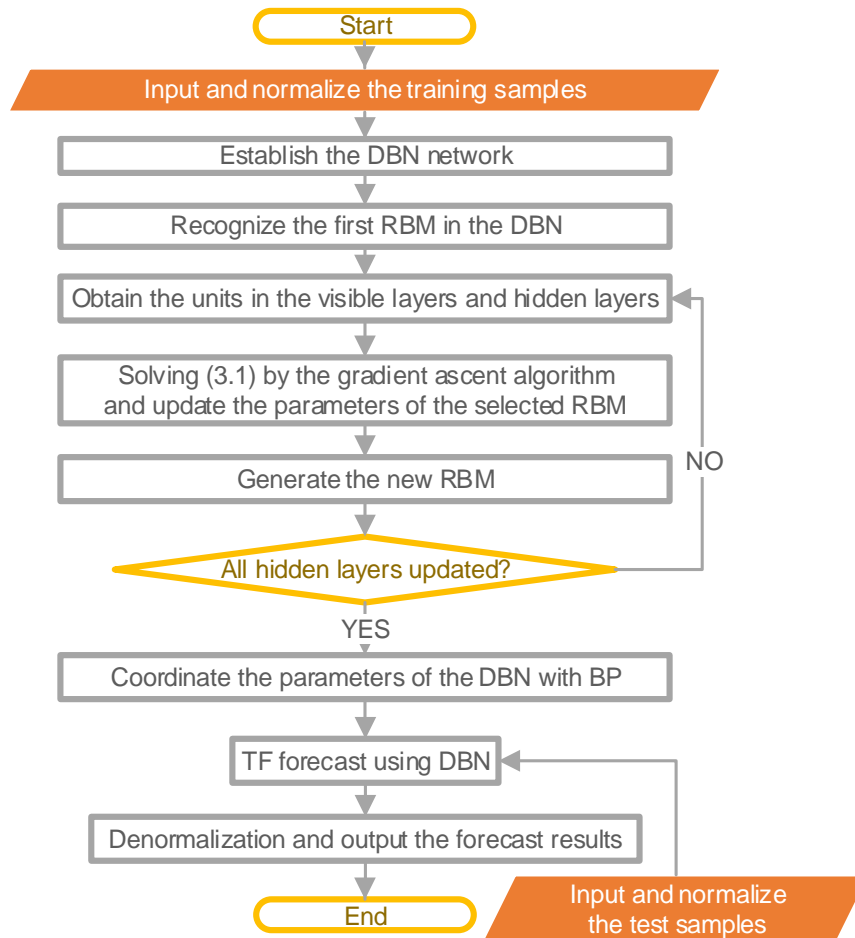


Fig. 2.2 The flowchart of the proposed DBN framework for forecasting

The purpose of implementing the DBN model is to predict the typical hourly TF in the planning horizon by studying the hourly TF data of the past few years and finding the patterns of TF variations. Meanwhile, the general growth trends of the previous years could be used to improve the DBN training results [158]. Therefore, the forecasting procedures are summarized as follows:

Step 1) Growth trends prediction: In this step, the average monthly TF of the coming year is forecasted by the past 3-year's data by the proposed DBN method.

Step 2) Hourly prediction: For each hour of the future typical day, the historical data of the past 3 years is trained by the DBN to obtain the daily TF patterns.

Step 3) Ensemble: the hourly-predicted curve is modified by the growth trends obtained by the Step 1 according to the ensemble approach [159] to get the more accurate results.

2.3 Deep Convolutional Neural Networks with PIs

Due to the chaotic nature of TF, EV charging loads possess high volatility and variability. Therefore, a deep convolution neural network (DCNN) based comprehensive approach is proposed here to reduce the influence of uncertainties on charging demand accuracy. The prediction is a hybrid of wavelet decomposition (WT), DCNN, PI construction, and queuing-based charging demand forecasting. The raw TF data are first normalized and decomposed into couples of frequencies. DCNNs are then designed for each frequency and trained to predict the behavior of each frequency. Consequently, wavelet reconstruction and anti-normalization are used to synthesize prediction frequencies to obtain a deterministic point forecast of TF. PIs are formulated according to model and data uncertainties. Finally, charging load forecasting is conducted based on the proposed data estimation and queuing model. The flowchart of the DCNN implementation is shown in Fig. 2.3, and the details are elaborated below.

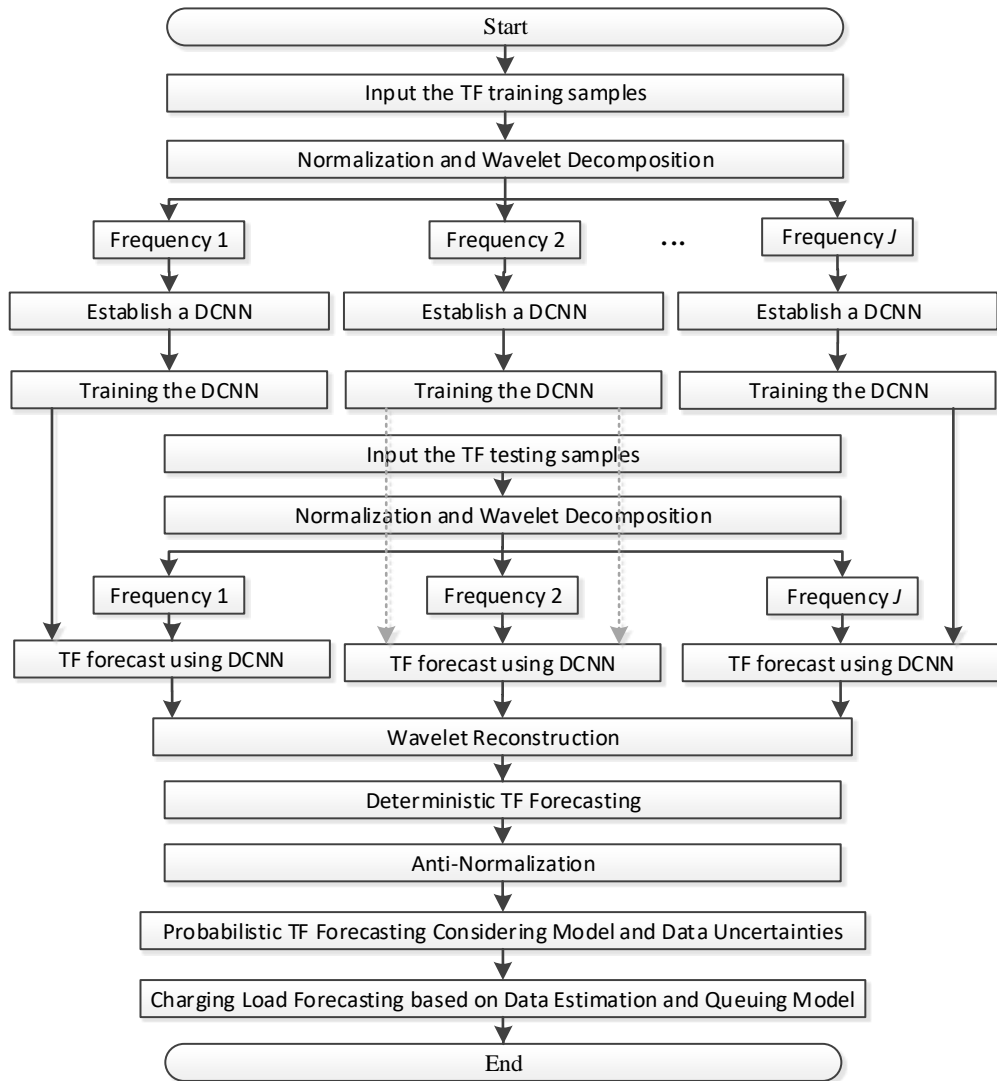


Fig. 2.3 The flowchart of the DCNN implementation

2.3.1 Convolutional Neural Network Layer

CNN is a type of feed-forward artificial neural networks (ANN) that has gained popularity in face recognition and language processing applications. As shown in Fig. 2.4, a pair of convolution and pooling layers in succession is referred to as 1 *CNN layer* [108]. It can be seen in Fig. 2.4 that either the convolution or the pooling layer consists of several maps, and each map has several neurons that share the same neuron kernel (also called weight). The data processed by the CNN are converted to 2-dimensional maps and gives a compact representation of a large set of hidden features. This ability makes CNN learn in an effective way to extract nonlinear structures in TF.

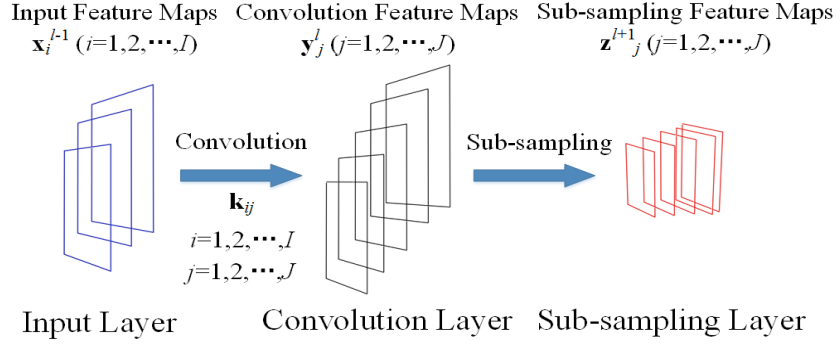


Fig. 2.4 Basic structure of a CNN layer

(1) Convolution Layer: The convolution layer handles small local receptive fields of input data in a sliding-map manner. At the current convolution layer l , the previous $(l-1)$ layer's feature maps are convolved with learnable kernels and passed through the activation function to form the output feature map before being transmitted to the pooling layer. This process is described in general as follows:

$$\mathbf{y}_j^l = f\left(\sum_{i \in M_j} \mathbf{x}_i^{l-1} \otimes \mathbf{k}_{ij}^l + b_j^l\right) \quad (2.22)$$

where \mathbf{y}_j^l is the output of the j th map in layer l ; \mathbf{x}_i^{l-1} is the input of the i th map in layer $l-1$; M_j represents a selection of input maps; \otimes denotes the convolutional operation; and \mathbf{k}_{ij} and b_j represent the weight and bias of the corresponding convolutional layer, respectively. Learning in an NN progresses by incrementally adjusting the biases and weights. The vector of weights and bias are defined as a *filter* and represents some feature of the input such as a kind of shape. The filter works in a sliding-window fashion on small local receptive fields of data. In this work, the sigmoid function $S(x)=1/(1+e^{-x})$ is utilized as the activation function $f(\cdot)$, and the weight \mathbf{k}_{ij} is trained with the well-known back-propagation algorithm [175].

A convolution layer is quite different from the fully connected hidden layer of other learning methods. Each convolutional unit represents some features of a local region of the input since it receives input only from a local area. The units of the convolution layer can be self-structured into a few feature maps, where all units in the same feature map share the same weights but receive inputs from different

lower layer locations [107]. The unique feature of CNNs of many weights sharing the same filter improves performance significantly by reducing both the memory footprint and the number of parameters to be estimated [109]. This is because a single bias and a single vector of weights is used across all the receptive fields that share that filter, rather than each receptive field using its own bias and vector of weights [176]. This indicates that the CNN learns the filter in an easy and efficient way without too much pre-processing, and this independence from prior knowledge in feature design is a major advantage of CNNs. Therefore, the architecture of the CNN involves more connections than weights and presents some degree of translation invariance [177], making it much easier to train. The CNN also has fewer parameters to be estimated compared with other NNs.

(2) Pooling Layer: A pooling layer generates several down-sampled versions of the input maps according to the following rules:

$$\mathbf{z}_j^{l+1} = f(\beta_j^{l+1} \text{down}(\mathbf{y}_j^l) + c_j^{l+1}) \quad (2.23)$$

Each output map has its own multiplicative bias β and an additive bias c . And $\text{down}(\cdot)$ represents a sub-sampling function. Also, the average function is adopted in this work

$$\mathbf{z}_{i,j,k} = \sum_{p,q} \alpha_{p,q} \mathbf{y}_{i+p,j+q,k} \quad (2.24)$$

where $\mathbf{y}_{i,j,k}$ and $\mathbf{z}_{i,j,k}$ represent each element of \mathbf{y} and \mathbf{z} , respectively, and $\alpha_{p,q}$ is the average filter with size $p \times q$.

Pooling layers intersperse convolution layers to reduce the computational burden and build up spatial and configural invariance. The pooling operation has 2 main advantages. First, it reduces the dimensionality of the convolutional layer output. Furthermore, the pooling summarizes the neighboring feature activations, leading to the robustness of the forecast by the translation of input data [110].

2.3.2 Deep CNN Architecture

A DCNN is composed of multiple CNN layers [108]. Due to the complications of the TF series, a novel modified DCNN forecasting strategy is proposed in this study, and Fig 2.5 shows a simple DCNN architecture with wavelet decomposition (WT), 2 convolution layers, and 1 final fully connected layer. First, original TF data series are usually nonlinear and non-stationary, and this will deteriorate the accuracy of traffic forecasting accuracy. The idea used to overcome this obstacle is to decompose the data series into several frequencies with better behavior of the data variance and outliers. In the beginning of the DCNN, a fast-discrete WT algorithm [111] is adopted for data decomposition to obtain a better forecast performance. The WT $W(m, n)$ of signal $g(x)$ with respect to a mother wavelet $\phi(x)$ is defined as

$$W(m, n) = 2^{-(m/2)} \sum_{t=0}^{T-1} g(t) \phi\left[\frac{(t - n2^m)}{2^m}\right] \quad (2.25)$$

where m and n denote 2 integer variables that determine the parameters of scaling and translation of ϕ , t is the discrete time index, and T is the length of the signal $g(t)$.

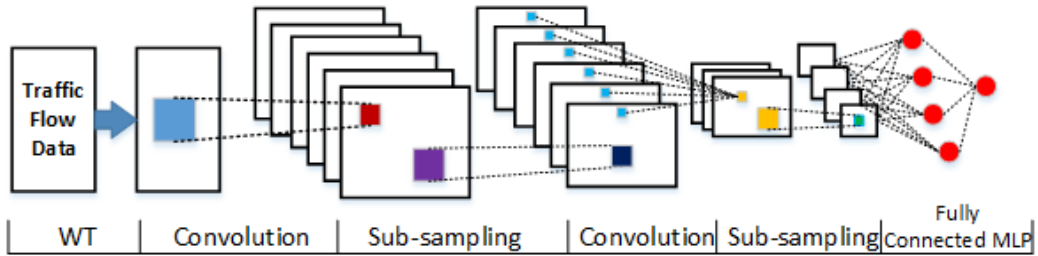


Fig. 2.5 Architecture of the DCNN

Next, the normalized and wavelet decomposed training samples are fed into the DCNN containing consecutive multiples CNNs, the structure of which has been discussed in Section 2.3.1. At the end of the DCNN, several fully-connected hidden layers are added on top of the final DCNN layer to combine the features across all maps before feeding to the output layer. The fully connected layer is stated as

$$\mathbf{y}^l = \mathbf{K}^l \mathbf{x}^{l-1} + \mathbf{b}^l \quad (2.26)$$

where \mathbf{K}^l is the weight from layer $l-1$ to layer l ; and \mathbf{b}^l is the additive bias.

2.3.3 PIs Formulation

(1) An Overview of PI formulation

The overall PIs formulation framework is illustrated in Fig. 2.6. The estimated regression, $\hat{y}(\mathbf{x}_i)$, model uncertainty variance, σ_m^2 , and data uncertainty variance, σ_d^2 , are obtained using forecasters based on CNN training to formulate PIs and are elaborated as follows.

(2) Estimated regression

The i th true forecast target, t_i , can be described as $t_i = y(\mathbf{x}_i) + \varepsilon(\mathbf{x}_i)$, where \mathbf{x}_i is the vector of the input data; $y(\mathbf{x}_i)$ is the true regression mean; and $\varepsilon(\mathbf{x}_i)$ is the noise. According to the definition of mean value, the *estimated regression*, $\hat{y}(\mathbf{x}_i)$, of the trained DCNN is the mean value of targets conditioned on \mathbf{x}_i , $E[t_i | \mathbf{x}_i]$ [178], which can be considered as an estimation of the true regression, $y(\mathbf{x}_i)$:

$$\hat{y}(\mathbf{x}_i) = E[t_i | \mathbf{x}_i] = (1 / N_E) \sum_{q=1}^{N_E} \hat{y}_q(\mathbf{x}_i) \quad (2.27)$$

where q is the number of DCNN models. Then values of $E[t_i | \mathbf{x}_i]$ can then be derived based on the trained N_E DCNNs with the target t_i . An ensemble of DCNN models with a larger number, N_E , can achieve a less biased estimate, $\hat{y}(\mathbf{x}_i)$, of the true forecast target, t_i .

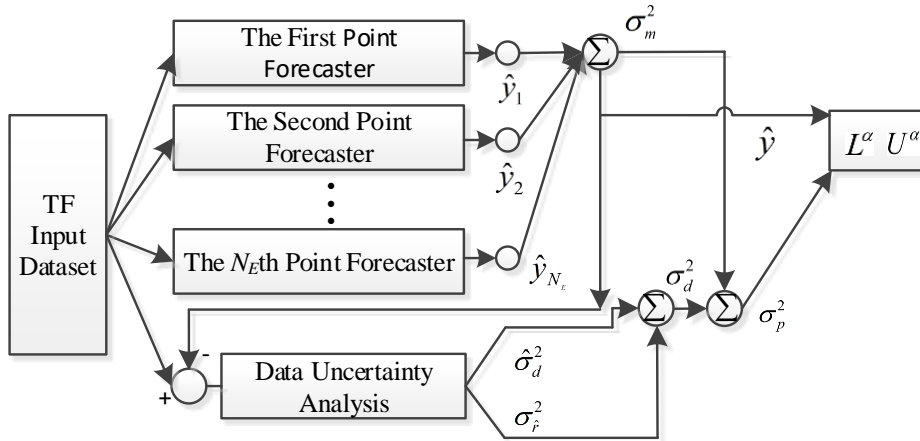


Fig. 2.6 An overview of PIs formulation

(3) Model uncertainty variance and data uncertainty variance

There are two major types of uncertainties in DCNN prediction: *model uncertainty* and *data uncertainty*. Model uncertainty usually originates from the erroneous specification of the DCNN structure and parameters, local minimum of the training process, and finite training samples. Meanwhile, data uncertainty usually comes from the stochastic nature of the data noise, such as the noise caused by chaotic weather conditions.

The total forecast error, $\sigma_p(\mathbf{x}_i)$, is the difference between the forecast target, t_i , and the estimated regression, $\hat{y}(\mathbf{x}_i)$: $\sigma_p(\mathbf{x}_i) = t_i - \hat{y}(\mathbf{x}_i) = [y(\mathbf{x}_i) - \hat{y}(\mathbf{x}_i)] + \varepsilon(\mathbf{x}_i)$, and $[y(\mathbf{x}_i) - \hat{y}(\mathbf{x}_i)]$ is the error involved in the estimation of the true regression, $y(\mathbf{x}_i)$, which accounts for model uncertainty. According to the variance definition discussed by [111], the variance of the model uncertainty can be evaluated from the variance in the outputs of the trained N_E DCNN models according to the following equation:

$$\sigma_m^2(\mathbf{x}_i) = (1 / (N_E - 1)) \sum_{q=1}^{N_E} (\hat{y}_q(\mathbf{x}_i) - \hat{y}(\mathbf{x}_i))^2 \quad (2.28)$$

By contrast, the error involved in the true forecast targets, t_i , accounts for the data uncertainty, which is difficult to estimate since there is only 1 observation of TF at each time point. Therefore, it is presumed in this work that the mean and variance of data uncertainty are also conditioned on \mathbf{x}_i . The variance of the measured target t_i conditioned on \mathbf{x}_i are defined as the variance of data, $\sigma_d^2(t_i | \mathbf{x}_i)$, which is expressed as follows, according to the variance definition [112]:

$$\sigma_d^2(t_i | \mathbf{x}_i) = E[(t_i - E[t_i | \mathbf{x}_i])^2 | \mathbf{x}_i] \quad (2.29)$$

According to (2.27), $E[t_i | \mathbf{x}_i]$ could be replaced with $\hat{y}(\mathbf{x}_i)$ and the output of $\sigma_d^2(\mathbf{x}_i)$ could be further stated as

$$\sigma_d^2(t_i | \mathbf{x}_i) = \hat{r}(\mathbf{x}_i) = E[(\hat{y}(\mathbf{x}_i) - t_i)^2 | \mathbf{x}_i] \quad (2.30)$$

Similar to the process for obtaining $E[t_i | \mathbf{x}_i]$, $E[(\hat{y}(\mathbf{x}_i) - t_i)^2 | \mathbf{x}_i]$ can be derived by training the DCNN with the target $(\hat{y}(\mathbf{x}_i) - t_i)^2$, the regression of which is denoted as $\hat{r}(\mathbf{x}_i)$. $\sigma_d^2(\mathbf{x}_i)$ in (2.30) can then be derived.

To reduce the bias of data uncertainty, N_S DCNNs with the regression, $\hat{r}(\mathbf{x}_i)$, are ensemble-trained, and the estimated noise variance is:

$$\hat{\sigma}_d^2(t_i | \mathbf{x}_i) = (1/N_S) \sum_{l=1}^{N_S} \hat{r}_l(\mathbf{x}_i) \quad (2.31)$$

The variance of $\hat{r}(\mathbf{x}_i)$ model uncertainty is:

$$\sigma_r^2(\mathbf{x}_i) = (1/(N_S - 1)) \sum_{l=1}^{N_S} (\hat{r}_l(\mathbf{x}_i) - \hat{r}(\mathbf{x}_i))^2 \quad (2.32)$$

Hence, the data noise variance is the combination of (2.31)- (2.32)

$$\sigma_d^2(\mathbf{x}_i) = \hat{\sigma}_d^2(t_i | \mathbf{x}_i) + \sigma_r^2(\mathbf{x}_i) \quad (2.33)$$

Based on the variance of model uncertainty, PIs could be obtained $\sigma_m^2(\mathbf{x}_i)$ in (2.28), and the variance of data uncertainty, $\sigma_d^2(\mathbf{x}_i)$ in (2.33), the variance of the total forecast errors is:

$$\sigma_p^2(\mathbf{x}_i) = \sigma_m^2(\mathbf{x}_i) + \sigma_d^2(\mathbf{x}_i) \quad (2.34)$$

(4) PIs formulation based on forecast errors

Therefore, the 100(1- α)% PI nominal confidence (PINC) of t_i , which is an interval denoted as $I^\alpha(\mathbf{x}_i)=[L^\alpha(\mathbf{x}_i), U^\alpha(\mathbf{x}_i)]$, can be formulated using the lower bound, $L^\alpha(\mathbf{x}_i)$, and upper bound, $U^\alpha(\mathbf{x}_i)$.

$$L^\alpha(\mathbf{x}_i) = \hat{y}(\mathbf{x}_i) - z_{1-\alpha/2} \sqrt{\sigma_p^2(\mathbf{x}_i)} \quad (2.35)$$

$$U^\alpha(\mathbf{x}_i) = \hat{y}(\mathbf{x}_i) + z_{1-\alpha/2} \sqrt{\sigma_p^2(\mathbf{x}_i)} \quad (2.36)$$

(2.35) and (2.36) are the mathematical expressions of confidence intervals, meaning that the target, t_i , is within the confidence interval $[L^\alpha(\mathbf{x}_i), U^\alpha(\mathbf{x}_i)]$ with a probability of 100(1- α)%. $z_{1-\alpha/2}$ is the critical value of the standard normal distribution and depends on the required PINC level 100(1- α)%.

2.3.4 Evaluation of Forecasting Performance

Mean absolute error (MAE), mean absolute percentage error (MAPE), and root mean square error (RMSE) are employed to evaluate the deterministic forecast performance as follows

$$\text{MAE} = (1/N) \sum_{i=1}^N |t_i - \hat{y}(\mathbf{x}_i)| \quad (2.37)$$

$$\text{MAPE} = (1/N) \sum_{i=1}^N \frac{|t_i - \hat{y}(\mathbf{x}_i)|}{(1/N) \sum_{i=1}^N t_i} \times 100\% \quad (2.38)$$

$$\text{RMSE} = \sqrt{(1/N) \sum_{i=1}^N |t_i - \hat{y}(\mathbf{x}_i)|^2} \quad (2.39)$$

where N is the number of training samples. PI coverage probability (PICP) and average coverage error (ACE) are employed as reliability indices to evaluate how well the probabilistic forecast results match the observed values:

$$\text{PICP} = (1/N) \sum_{i=1}^N r_i^\alpha \times 100\% \quad (2.40)$$

$$\text{ACE} = \text{PICP} - \text{PINC} \quad (2.41)$$

where r_i^α is the PI coverage probability indicator

$$r_i^\alpha = \begin{cases} 1 & t_i \in I^\alpha(\mathbf{x}_i) \\ 0 & t_i \notin I^\alpha(\mathbf{x}_i) \end{cases} \quad (2.42)$$

The interval sharpness (IS) is used to measure the sharpness of the PI by encouraging narrower PIs

$$\text{IS} = \frac{1}{N} \sum_{i=1}^N \begin{cases} -2\alpha\delta^\alpha(\mathbf{x}_i) - 4(L^\alpha(\mathbf{x}_i) - t_i) & t_i < L^\alpha(\mathbf{x}_i) \\ -2\alpha\delta^\alpha(\mathbf{x}_i) & t_i \in I^\alpha(\mathbf{x}_i) \\ -2\alpha\delta^\alpha(\mathbf{x}_i) - 4(t_i - U^\alpha(\mathbf{x}_i)) & t_i > U^\alpha(\mathbf{x}_i) \end{cases} \quad (2.43)$$

where $\delta^\alpha(\mathbf{x}_i)$ is the width of PI and calculated as $U^\alpha(\mathbf{x}_i) - L^\alpha(\mathbf{x}_i)$.

2.4 Probabilistic EV Load Forecasting

Experiments indicate that high temperature caused by large charging power is unfavorable for the lifetime of batteries [179], thus refueling via charging posts at home or in parking lots leads to less battery degradation. However, EV owners will also choose to charge using FCSes when their vehicle urgently needs charging or they are reluctant to wait for an extended period. Uncertainties are involved in this EV charging process. As shown in Fig. 2.7, a practical estimation method for the arrival rate is proposed using the daily travel distance distribution and travel

patterns. Then, an EV queuing model is established for EV load forecasting that considers various uncertainties and constraints.

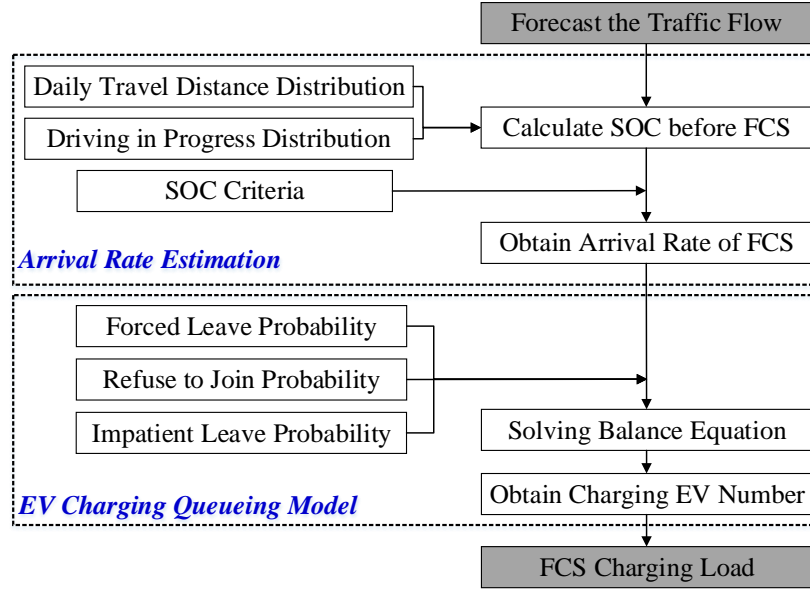


Fig. 2.7 Flowchart of the FCS charging load determination

2.4.1 EV Arrival Rate Estimation

Only a small part of EVs in the TF will go to the FCS on their travel path to receive the charging service, and the number of EVs arrive to the FCS in one time interval is denoted as the average EV arrival rate, λ . As an important input for the charging load forecasting, the FCS charging load cannot be precisely determined if the EV arrival rate is not properly estimated [28][36]. Generally, EV drivers' willingness to go to an FCS on their travel path determines the arrival rate and is highly related to an EV's state-of-charge (SOC) condition, SOC , while the charging duration time, μ , is determined by the SOC and the charging power. It is straightforward to understand that the travel distance, D_{ev} , is the key data source used to estimate EV SOC, which has been applied in [18], [29], [113] and [114]. The relationship between them is briefly represented as

$$SOC = 1 - p_{ev} D_{ev} / E_{ev} \quad (2.44)$$

where E_{ev} is an EV's battery capacity; and p_{ev} is an EV's driving consumption power. Due to the variations in EV types, EV parameters and TF data are first normalized to the standard *passenger car unit* (pcu) in this work. The biggest barrier in the current research is that FCSes are still in the primary stage of development, thus real data of travel distance before FCS D_{ev} is difficult to obtain directly. Therefore, the data of *daily travel distance*, D_{ev}^T , and *driving in progress distribution*, $g(t)$, which are much more easily obtained from historical data [115], are used as the indirect data source for estimating the travel distance of EVs when arriving at the FCS, D_{ev} . From D_{ev}^T and $g(t)$, the SOC and arrival rate can be determined.

(1) *Daily travel distance distribution estimation based on the mixture model:*

Most of the previously mentioned studies assumed that D_{ev}^T follows a simple probability density function (PDF), such as a normal distribution, which does not reflect the actual and cannot reflect the complexity of EV charging behaviors. The EV daily travel distance data in this study is obtained by interview surveys to EV users, which is a common practice when investigating daily vehicle miles traveled (VMT) [182]. As shown in Fig. 2.8, daily travel distance distribution curve is more complicated and several peaks can be seen. To get a more general results, the mixture model based approach is used to analyze the complicated D_{ev}^T distribution $p(\mathbf{X}|\Theta)$. The mixture model is able to model random variables using a combination of selected PDFs:

$$p(\mathbf{X}|\Theta) = \sum_{m=1}^M \pi_m p_m(x|\theta_m) \quad 0 \leq \pi_m \leq 1, \quad \sum_{m=1}^M \pi_m = 1 \quad (2.45)$$

where $\mathbf{X} = \{x_1, x_2, \dots, x_m\}$ is the random variable set; Θ is the PDF parameter; π_m is the weight coefficient of the m th PDF p_m ; and M is the PDF number.

The Expectation-maximization (EM) algorithm [116] is adopted by using a 2-step iteration to obtain the parameters of the mixture model, which maximizes the expectation of the likelihood,

$$L(\Theta | \mathbf{X}, \mathbf{Y}) = \prod_{i=1}^N \sum_{m=1}^M y_{m,i} \pi_m p_m(x_i | \theta_m) \quad (2.46)$$

where N is the number of data samples; \mathbf{Y} is an auxiliary variable set marking where the data sample belongs to which PDF in the mixture model.

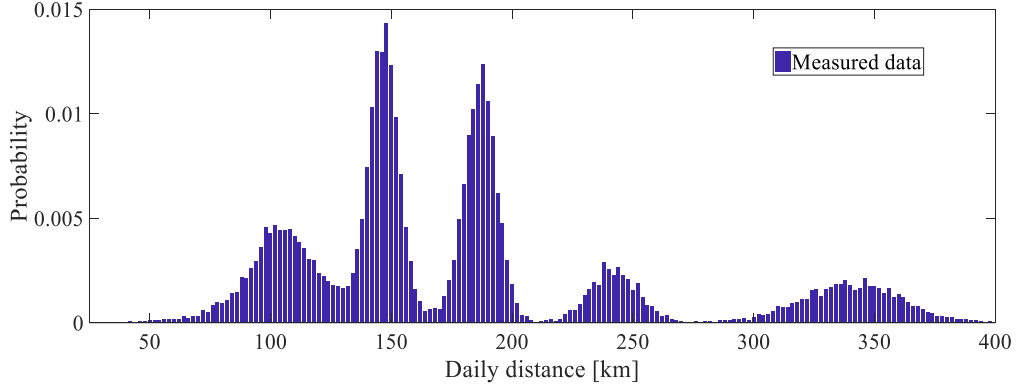


Fig. 2.8 The distribution of EV daily travel distances

Before applying the EM algorithm, the parameters Θ and the auxiliary variables \mathbf{Y} are initialized using the K-means clustering method [117]. The PDF number M is another critical index that can be obtained using the Akaike information criterion (AIC) and the Bayes information criterion (BIC). These are expressed, respectively, as follows:

$$BIC = M \ln(N) - 2 \ln \arg \max_{\Theta} L(\Theta | \mathbf{X}) \quad (2.47)$$

$$AIC = 2M - 2 \ln \arg \max_{\Theta} L(\Theta | \mathbf{X}) \quad (2.48)$$

The optimal M is selected by increasing M one by one until $BIC(M) - BIC(M+1)$ and $AIC(M) - AIC(M+1)$ are smaller than a pre-set terminating criterion.

The EM algorithm is carried out iteratively, and in the q th iteration, the calculation of the expectation of the likelihood function (2.46) under the current estimation of $\Theta^{(q)}$ is the first step:

$$Q(\Theta | \Theta^{(q)}) = E[\ln L(\Theta | \mathbf{X}, \mathbf{Y}) | (\mathbf{Y}, \Theta^{(q)})] \quad (2.49)$$

Determining the parameters to maximize the expectation in this iteration is the second step:

$$\Theta^{(q+1)} = \arg \max_{\Theta} Q(\Theta | \Theta^{(q)}) \quad (2.50)$$

The 2-step algorithm is executed iteratively until the pre-set stopping criterion is reached, and the distributions $p(\mathbf{X})$ are obtained with the parameters optimally estimated using the proposed mixture model. It should be noted the proposed method is universally applicable and not limited to specific distributions.

(2) *Driving in Progress Distribution*: Travel patterns vary with time over the course of a day, and can be represented as the *driving in progress distribution*, $g(t)$. This is also a critical distribution for obtaining the arrival rate at FCSes. As shown in Fig 2.9 [118], $g(t)$ is formulated to demonstrate the probability that the EV is currently driving. For instance, $g(5) = 8\%$ indicates that the EV has a probability of 8% of being on the road. Based on the definition of $g(t)$, D_{ev}^T is estimated using the mean travel distance of EVs at time t , $D_{ev,t}$, where

$$D_{ev}^T = D_{ev,t} \int_{t_0}^t g(h)dh \quad (2.51)$$

It is assumed that EV drivers prefer to charge when the SOC is below to the criterion SOC_{min} , and their mean SOC is SOC_m ($0 \leq SOC_m \leq SOC_{min}$). According to (2.44) and (2.51), the daily travel distance of EVs arriving to the FCS D_{ev} at time t $D_{ev,t}^T$ is estimated as

$$D_{ev,t}^T = (E_{ev}(1 - SOC_m)) / (p_{ev} \int_{t_0}^t g(h)dh) \quad (2.52)$$

The probability that an EV passing by an FCS at time t will choose to charge, P_t , is determined using the daily travel distance distribution $p(\mathbf{X})$ as

$$P_t = \int_{D_{ev,t}^T}^{D_{ev,t-1}^T} p(x)dx \quad (2.53)$$

Therefore, the arrival rate at time t λ_t is

$$\lambda_t = \zeta P_t f_t \quad (2.54)$$

where ζ is the penetration rate of EV during the total TF; and f_t is the forecasted TF at time t .

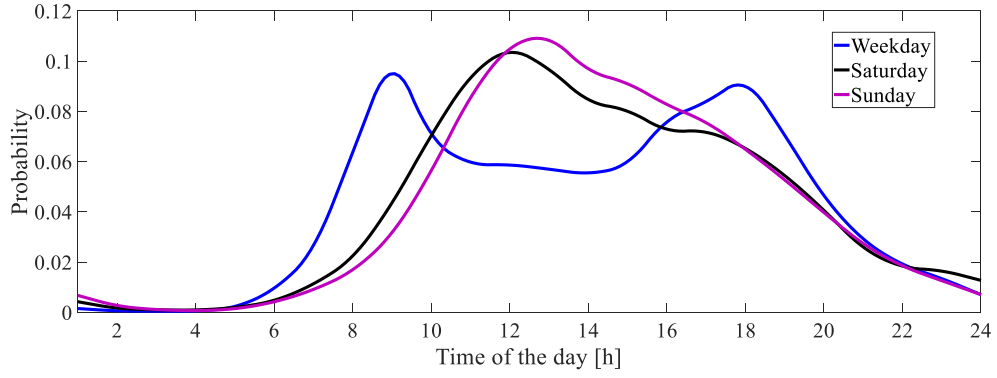


Fig. 2.9 Trips in progress by time of day in UK [118]

2.4.2 EV Charging Queuing Model that considers Driver Behaviors

The capacity of an FCS K is the maximum number of EVs the FCS can accommodate. Currently, most countries are still in the early stages of EV development, and the service ability of FCSes is facing a serious shortage. Meanwhile, many FCSes are built in downtown areas or near the expressways. Therefore, the capacity of an FCS is very limited. Thus, the limitations of FCS capacity deserve full consideration. As shown in Fig. 2.10, an EV charging process is set up as a Markov MMCK model. MMCK is the Kendall notation [184]: It assumes the FCS has C servers and can accommodate a maximum of K EVs; The arrival of EVs is governed by a Markovian-Poisson process [181], in which the arrival EV number, n , in a given time interval follows a Poisson distribution, $P(n)$, with an average EV arrival rate, λ , in each time interval.

$$P(n) = e^{-\lambda} (\lambda^n / (n!)) \quad n \in \Omega^{EV} \quad (2.55)$$

Also, the charging duration time t_c of EVs follows an exponential distribution:

$$f(t_c) = \mu e^{-\mu t_c} \quad (2.56)$$

where μ is the average EV leave rate for each time interval, which is the number of EVs that finish charging and leave the FCS. Here the subscript t is omitted in order to simplify the expression.

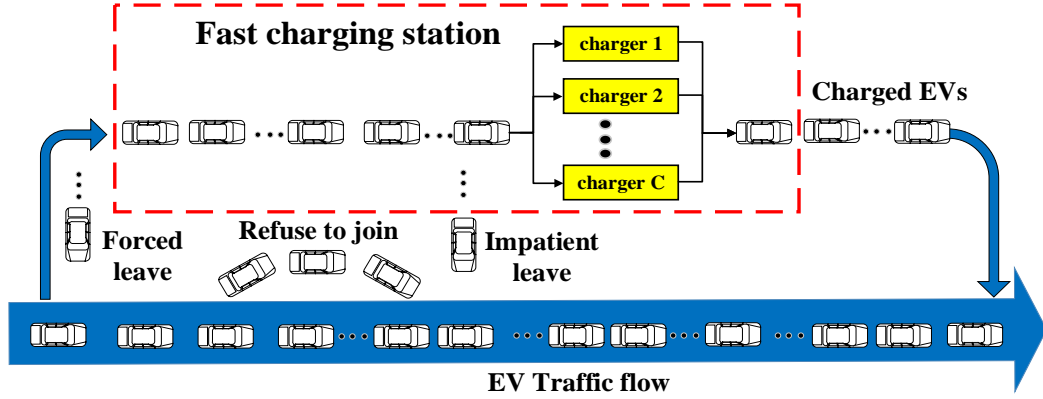


Fig. 2.10 Capacity constrained queuing model considering drivers' behaviors

As shown in Fig. 2.10, sometimes EVs leave the FCS without getting charged. Such EV driver behavior may result from the insufficiency of total number of available chargers, the limitation of FCS capacity, et al., and we categorize the underlying causes of EV leaving behaviors into 3 types: *forced leave*, *refuse to join*, and *impatient leave*. Category 1: *Forced leave*. If the FCS has accommodated K EVs already, other EVs are forced to leave the FCS because there is no space in the queue. Category 2: *Refuse to join*. When arriving to the FCS, the EV finds the waiting line is too long and thus refuses to join the queue, even if the total EV number in the FCS is less than K . Based on categories 1 and 2, the probability that an EV will choose to queue is relevant to the EV number in the FCS, w , and is assumed to be

$$\alpha_w = \begin{cases} 1 & w < C \\ e^{-(w-C)\sigma} & \sigma \geq 0, C \leq w < K \\ 0 & w = K \end{cases} \quad (2.57)$$

where the exponential function indicates that the probability decreases faster for EVs choosing to queue when w increases, and σ is the parameter that defines the probability decrease rate. Category 3: *Impatient leave*. Even if the waiting line is not too long, the queuing EVs may still choose to leave the FCS when they get too impatient. The number of EVs left in the queue during each time interval is relevant to w and assumed to be

$$b_w = \begin{cases} 0 & w \leq C \\ \delta \ln(w - C + 1) & \delta \geq 0, C < w \leq K \end{cases} \quad (2.58)$$

where the logarithm function suggests the number of EVs that leave grows as w increases, and δ is the parameter that defines the probability of leaving the FCS. According to (2.57) and (2.58), the average arrival rate and the average leaving rate, considering categories 1-3, can be stated as $\lambda_w = \alpha_w \lambda$ and $\mu_w = \mu - b_w$, respectively.

2.4.3 Stochastic Process Analysis for EV Load Determination

Based on the described queuing model, FCS EV charging loads can be obtained using the stochastic Markov chain analysis. According to the stochastic process theory, P_w , the steady-state probability of the Markov chain being in state w , should satisfy the balance equation [119]:

$$\sum_{w \in S} P_w = 1, \quad P_w \sum_{v \in S} q_{wv} = \sum_{v \in S} P_v q_{vw} \quad \forall w \in S, w \neq v \quad (2.59)$$

(2.59) means that the sum of all state probabilities should be 1. Also, the probability in and out of each state should be equal, and q_{wv} is the transition rate from state w to v . S is the state space.

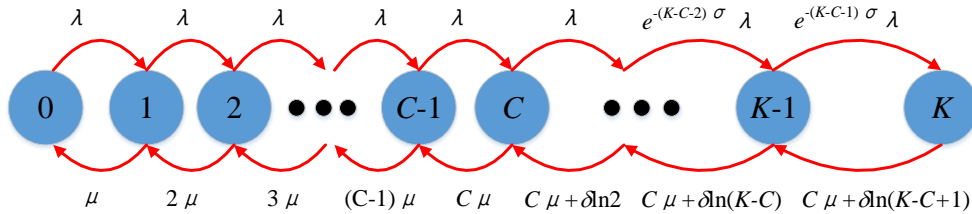


Fig. 2.11 State transition diagram of the Markov chain that considers EV behaviors

The Markov chain of FCS is shown in Fig. 2.11. The state transitions in the FCS only belong to the following 2 types: *arrives* and *leaves*. Therefore, based on (2.59), the FCS balance equation can be expressed as:

$$(\lambda_w + \mu_w)P_w = \lambda_{w-1}P_{w-1} + \mu_{w+1}P_{w+1} \quad (2.60)$$

By solving (2.57)-(2.60) (the detailed solving process is shown in the appendix), the probability that the FCS has w EVs is

$$P_w = \begin{cases} (\rho^w / w!) P_0 & 0 < w \leq C \\ \frac{e^{-\frac{(w-C)(w-C-1)\sigma}{2}} \rho^w}{C! \prod_{i=1}^{w-C} [C + \eta \ln(i+1)]} P_0 & C < w \leq K \end{cases} \quad (2.61)$$

The P_0 in (2.61) could also be obtained by solving (2.57)-(2.60)

$$P_0 = \left\{ \sum_{w=0}^C \frac{\rho^w}{w!} + \sum_{w=C+1}^K \frac{e^{-\frac{(w-C)(w-C-1)\sigma}{2}} \rho^w}{C! \prod_{i=1}^{w-C} [C + \eta \ln(i+1)]} \right\}^{-1} \quad (2.62)$$

where $\rho = \lambda/\mu$ and $\eta = \delta/\mu$ are defined for conciseness. Hence, the charging EV number in an FCS can be expressed as

$$\begin{aligned} N_{ch} &= \sum_{w=0}^C w P_w + C \sum_{w=C+1}^K P_w \\ &= \sum_{w=0}^C w \frac{\rho^w}{w!} P_0 + C \sum_{w=C+1}^K \frac{e^{-\frac{(w-C)(w-C-1)\sigma}{2}} \rho^w}{C! \prod_{i=1}^{w-C} [C + \eta \ln(i+1)]} P_0 \end{aligned} \quad (2.63)$$

and the charging load of the FCS, P^{FCS} , can be determined using N_{ch} and the power of the charging post for each EV, p^{EV} :

$$P^{FCS} = N^{ch} p^{EV} \quad (2.64)$$

2.5 Case Studies

2.5.1 Forecasting Results of Grey System Theory

The total EV number in Shenzhen, Guangdong province, China from 2006 to 2015 is utilized as the test database for long-term prediction, which is summarized in Table 2.1. The EVs are classified as electric buses (EBs) and non-EBs (including private electric cars, electric taxis, et al.) because they have obvious different application purposes and developing characteristics. From the Table 2.1 it is noticeable for the fast growth rate of EVs in recent years.

In the proposed forecasting model based on the grey system theory, every three years data of EV number is used to forecast the future EV number in the next year, and the forecasted number is compared by the actual EV number to verify the

effectiveness of the proposed model. The forecasted results of EBs and non-EBs are plotted in Fig. 2.12 and Fig. 2.13, respectively.

Table 2.1 The EB and Non-EB number in Shenzhen from 2006-2015

Year	EB number	Non-EB number
2006	500	1000
2007	900	1250
2008	1200	3500
2009	1700	6200
2010	2100	7320
2011	2500	9300
2012	3100	10800
2013	4200	13500
2014	5400	19000
2015	7000	27500

It could be roughly observed in Fig. 2.12 and Fig. 2.13 that the forecasting result is quite acceptable. To ensure that the established model has enough prediction accuracy in the practical application, three index, residual error, degree of association and variance ratio is calculated to check out the effectiveness of the proposed method. The residual error of EBs and non EBs is shown in Table 2.2 and Table 2.3, respectively. And the association degree and variance ratio of EB and non EB forecasting is demonstrated in Table 2.4. According to the accuracy inspection level, which is shown in Table 2.5, the forecasting relative error belongs to level 4, and the association rate belongs to level 1, while the variance ratio belongs to level 1, which indicates that the grey system method is suitable to forecast the EV numbers in Shenzhen, but the accuracy is not good enough for some situations.

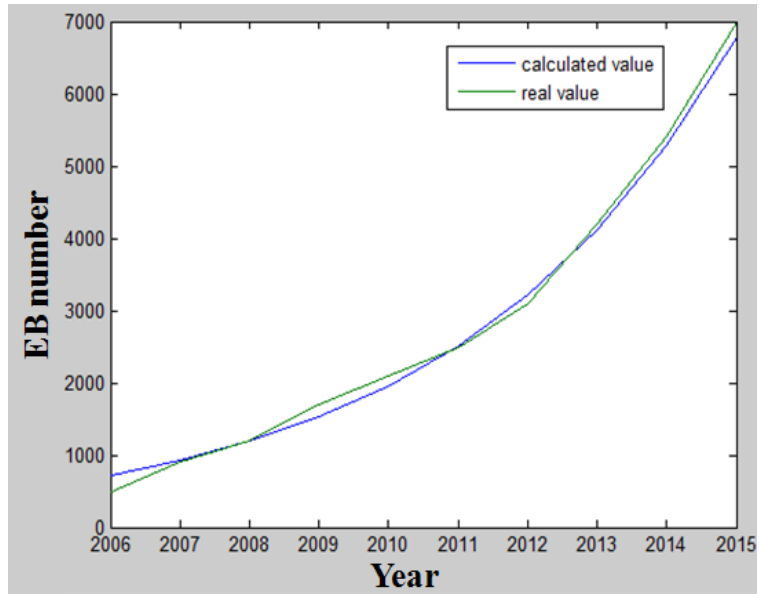


Fig.2.12 The forecasted results of EBs by the grey system theory

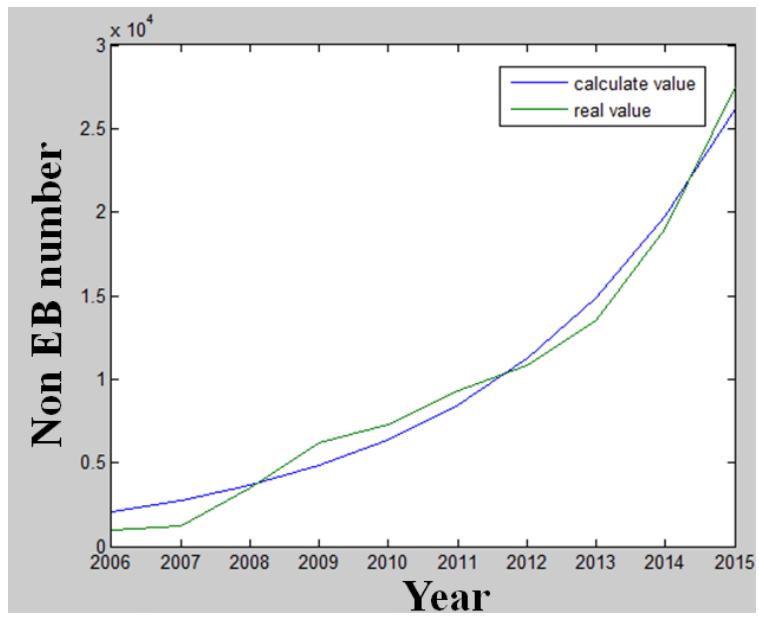


Fig. 2.13 The forecasted results of non-EBs by the grey system theory

Table 2.2 The EB forecasting result residual error

Year	Actual EB number	Forecasted EB number	residual error e	relative error %
2006	500	722	-222	44.4
2007	900	926	-26	2.9
2008	1200	1187	13	1.1
2009	1700	1523	177	7
2010	2100	1953	147	7
2011	2500	2505	-5	0.2
2012	3100	3202	-112	3.6
2013	4200	4119	81	1.9
2014	5400	5283	117	2.2
2015	7000	6775	225	3.2

Table 2.3 The non EB forecasting result residual error

Year	Actual non-EB number	Forecasted non-EB number	residual error e	relative error %
2006	1000	2068	-1068	106.8
2007	1250	2742	-1492	119.4
2008	3500	3635	-135	3.9
2009	6200	4820	1380	22.3
2010	7320	6390	930	12.7
2011	9300	8472	828	8.9
2012	10800	11232	-432	4.0
2013	13500	14891	-1391	10.3
2014	19000	19741	-741	3.9
2015	27500	26172	1328	4.8

Table 2.4 The association degree and variance ratio of grey system method

	EB forecasting	Non EB forecasting
association degree	0.599	0.556
variance ratio C	0.066	0.136

Table 2.5 Accuracy level reference table

Accuracy level	relative error %	association degree	variance ratio C
Level 1	0.01	0.90	0.35
Level 2	0.05	0.80	0.50
Level 3	0.10	0.70	0.65
Level 4	0.20	0.60	0.80

2.5.2 Forecasting Results of Nonlinear Autoregressive Neural Network

Then the nonlinear autoregressive neural network is applied to forecast growth of EV number using the same historical data in Table 2.1. The autoregressive process order is set to 3 and the hidden neuron number is set to 10 in this case. The forecasting setting interface of EBs and non-EBs are demonstrated in Fig. 2.14 and Fig. 2.15. The forecasted results of EBs and non-EBs are demonstrated in Fig. 2.16 and Fig. 2.17, respectively. The residual error of EBs and non EBs is shown in Table 2.6 and Table 2.7.

Comparing the forecasting results of two models, residual errors of the model based on the NAR network is shown to be less than those of the model utilizing the grey system theory. It could be concluded that the NAR method has a better performance in the forecasting of EV numbers than the grey system theory.

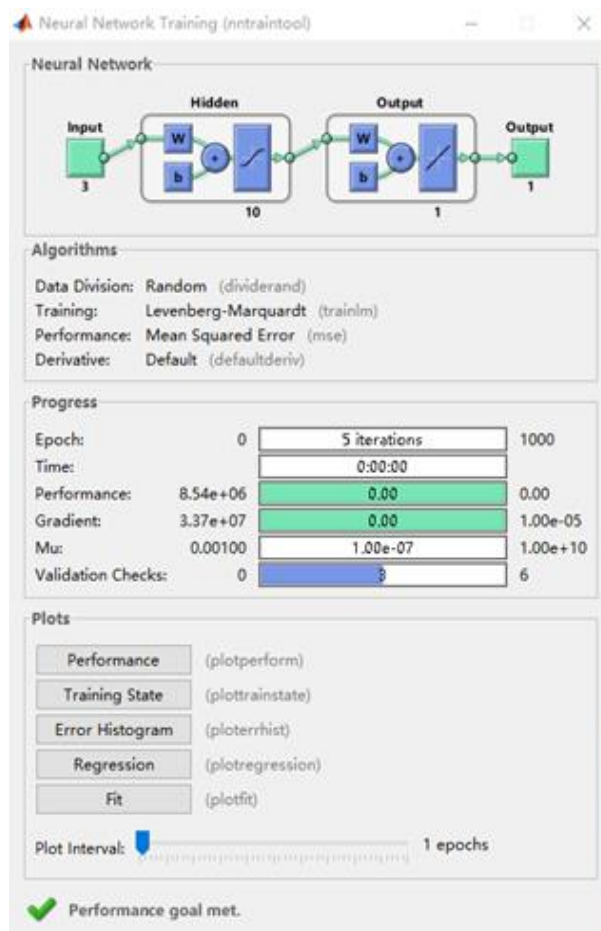


Fig. 2.14 The forecasting setting interface of EBs

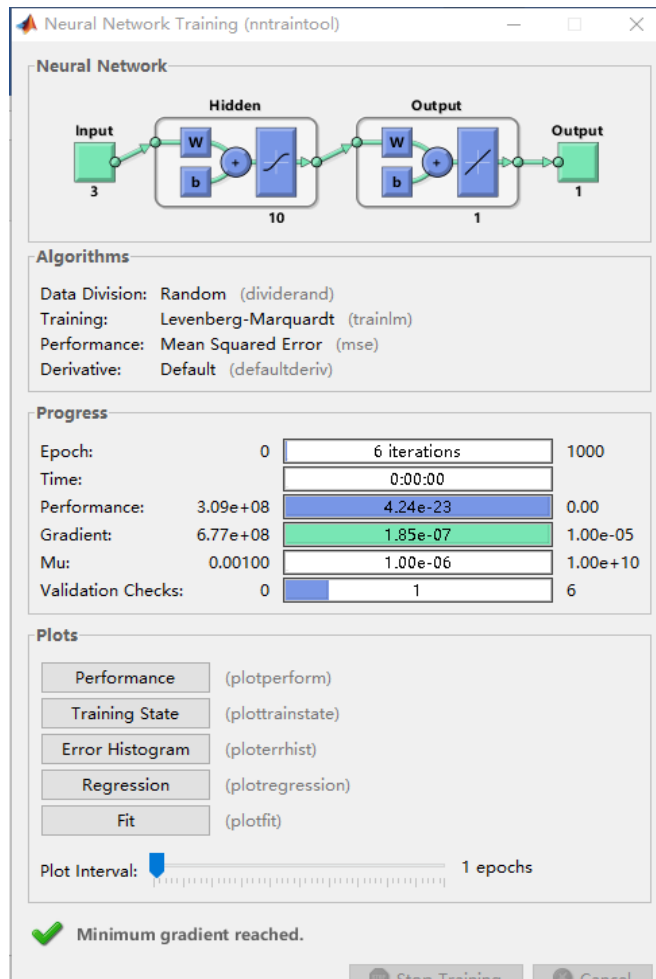


Fig. 2.15 The forecasting setting interface of non-EBs

Table 2.6 The EB forecasting result residual error of NAR

Year	Actual EB number	Forecasted EB number	residual error e	relative error %
2009	1700	1697	3	0.2
2010	2100	2098	2	0.1
2011	2500	2470	30	1.2
2012	3100	3108	-8	0.3
2013	4200	4221	-21	0.5
2014	5400	5407	-7	0.1
2015	7000	7111	-111	1.6

Table 2.7 The non EB forecasting result residual error of NAR

Year	Actual non-EB number	Forecasted non-EB number	residual error e	relative error %
2009	6200	8323	-2123	34
2010	7320	7320	0	0
2011	9300	9300	0	0
2012	10800	10800	0	0
2013	13500	13500	0	0
2014	19000	19118	-118	1
2015	27500	27500	0	0

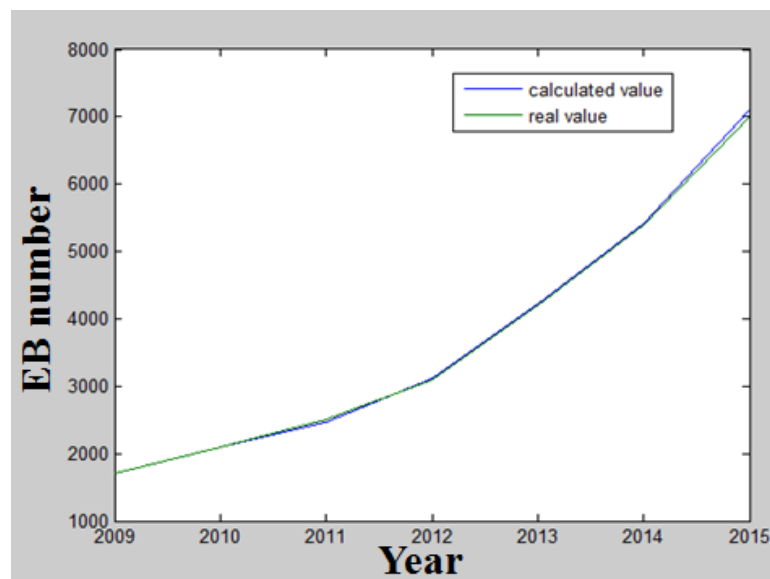


Fig. 2.16 The forecasted results of EBs by NAR

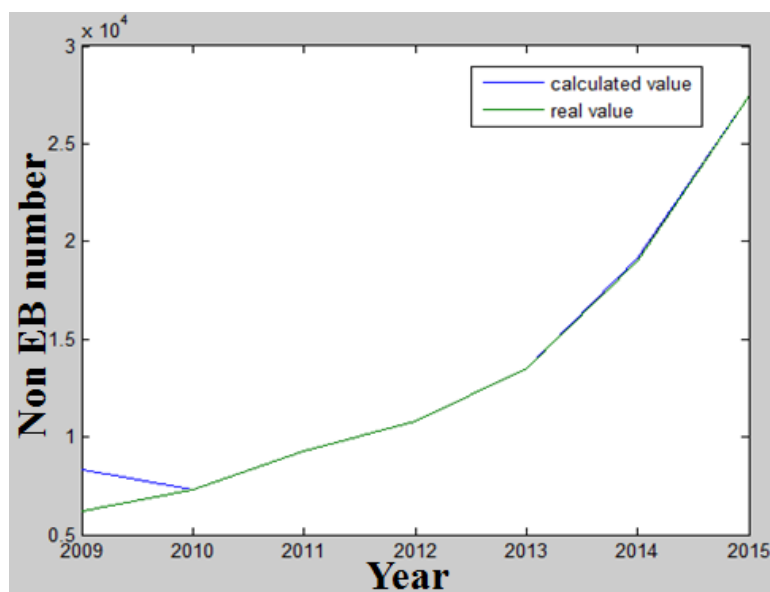


Fig. 2.17 The forecasted results of non EBs by NAR

2.5.3 DBN method Forecasting Results Analysis

As shown in Fig. 2.18, an urban area in UK coupled distribution and transportation system is employed to demonstrate the effectiveness of the DBN forecasting model. This frequently used 11-kV 38-node system represents a typical UK DS, the load of which is proportional (0.01%) to that of the UK [169]. The traffic flow on the roads of the system could be obtained from the official website of Highways England [167-168]. The traffic flow on nodes 33-37 in 2022 should be forecasted because they are candidate locations for the constructions of CSes.

The data for DBN based forecasting is classified as monthly data and hourly TF data. The monthly data comprises aggregated TF of each calendar month, and the monthly data from 2015 to 2018 is obtained in [168] for growth trends forecasting. The utilized hourly TF data is sampled in 15-min intervals and is distributed in the period from May 2016 to May 2018 [167]. The number of total data points used for training is around 350,000. Four 15-min intervals over 1 hour are averaged to get the hourly TF data used in this work. The TF data in the past 3 years is divided into a training dataset and a testing dataset. The training dataset covers the first 2 years. The data of the rest 1 year comprises the testing dataset.

The TF passing by the candidate CSes in the planning horizon has first to be forecasted as an important precondition for the EV CS planning. Table 2.8 firstly verifies the performance of the DBN based TF forecasting on node 33 and 37 compared with the Back Propagation Neural Network (BPNN), Support Vector Machine (SVM), Auto-Regressive and Moving Average Model (ARMA), and Morlet Wavelet Neural Network (MWNN). It is clear that the DBN method has lower MAE, MAPE and RMSE values than other methods, which indicates that the DBN method has a better performance in forecasting the TFs. Fig. 2.19 demonstrates the forecasting curves of different methods on node 37. It could be found that the forecasted result by the DBN method is closest to the actual data among the 4 methods, which verifies its good performance.

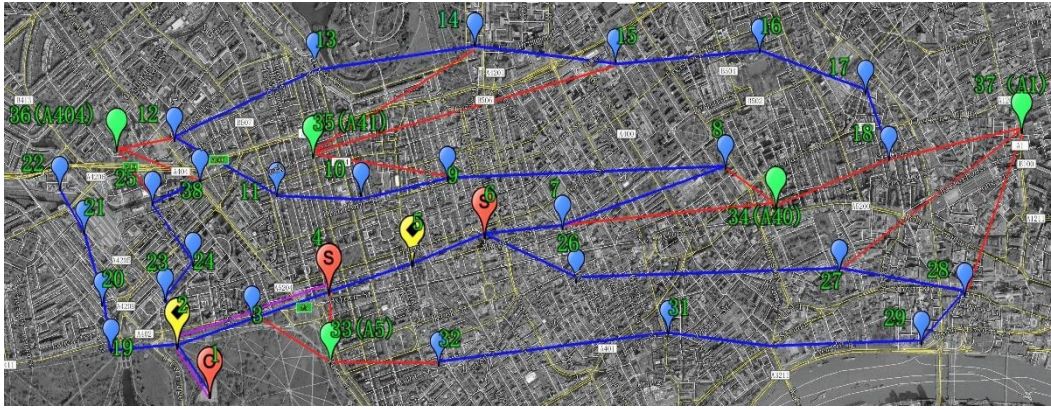


Fig. 2.18 The graphic display of the test system (green node: candidate CS, red node: existing substation (O) and candidate substation (S), blue node: existing node, yellow node: wind power, red line: candidate feeder, blue line: existing feeder, yellow line: major roads).

Table 2.8 TF Forecasting Error Comparison at Node 33 and 37

Location	Error	BPNN	SVM	ARMA	MWNN	DBN
Node 37	MAE	114.63	107.48	122.07	122.72	106.81
	RMSE	151.21	150.83	165.58	162.69	144.61
	MAPE(%)	11.88	11.14	12.65	12.72	11.07
Node 33	MAE	53.89	39.61	45.18	52.09	37.29
	RMSE	93.70	54.64	71.86	68.12	48.47
	MAPE(%)	14.45	10.62	12.11	13.96	10.00

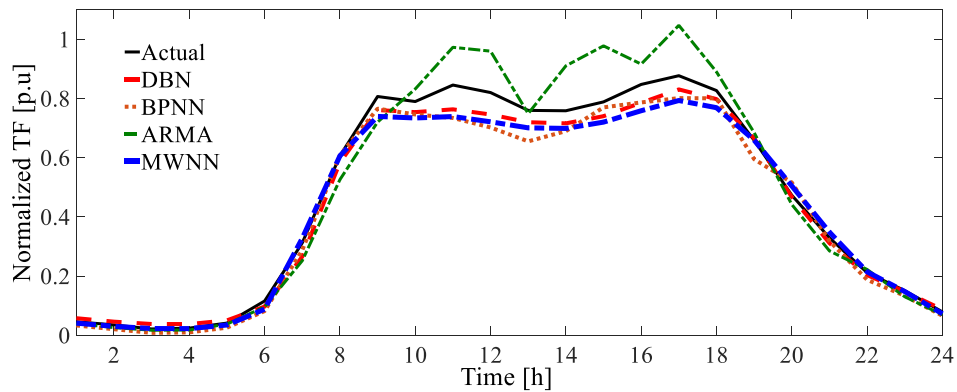


Fig. 2.19 Forecasting results by different methods on node 37

2.5.4 DCNN TF Forecasting Results Analysis

The proposed deep learning method is tested using TF data from the M42 motorway between sites J5 and J6 (GPS Ref: 417049:278576-419805:283048) in England, UK [120]. The TF data with 15 minute temporal resolutions from Jan to

Dec 2014 are analyzed. Factors such as weather conditions and travel purposes vary significantly during different days or seasons and lead to prominent uncertainties in TF. By considering the seasonal and weekly differences and diversity, the proposed approach is tested using TF data from weekdays and weekends during the 4 different seasons. The data for the first 2 months of each season are chosen as the training dataset, and the remaining 1 month of data are chosen as the testing dataset. The input data are decomposed using the WT method into 1 approximation frequency and 3 detail frequencies. The building blocks consisted of 4 convolution layers and 4 pooling layers for each frequency. The obtained results are compared using the back-propagation neural network (BPNN), support vector machine (SVM), SAE, time-delayed neural network (TDNN), and recurrent neural network (RNN) methods.

Parameters and hyper parameters of different methods should be properly set to obtain good forecasting results for comparison. These parameters are chosen by the validation test in a trail-and-error manner. For example, as shown in Fig. 2.20 and Fig. 2.21, the performance of BPNN and SAE is assessed by the MAPE. 41 hidden neurons are chosen by the BPNN to reach the smallest MAPE, and the SAE with 5 hidden layers can ensure the optimal MAPE. Kernel function type is critical for the performance of SVM, and it can be seen in Table 2.9 the SVM with radial basis function (RBF) will have the best MAE, RMSE and MAPE compared with other typical kernel functions.

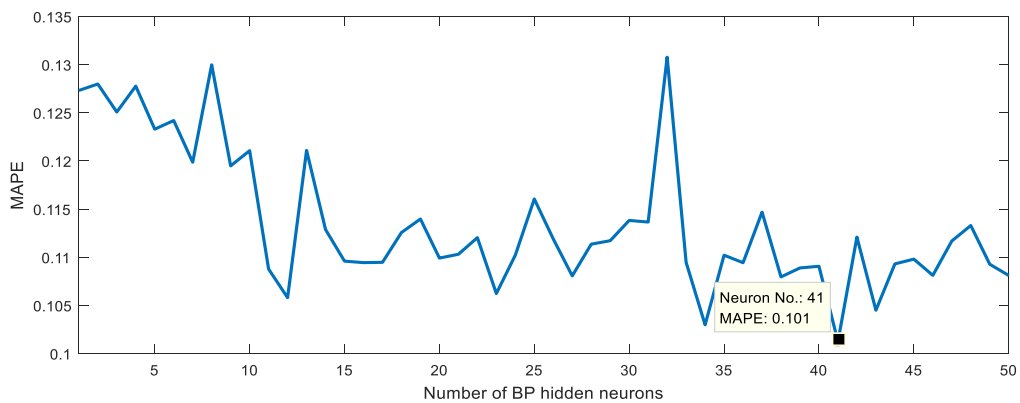


Fig. 2.20 Validation test for BPNN with different number of hidden neurons

The seasonal deterministic 1-hour ahead forecast absolute residuals of the different methods are shown in Fig 2.22 and Fig 2.23. *Residual* is the difference between the actual value and the forecasted value. It can be observed from the two

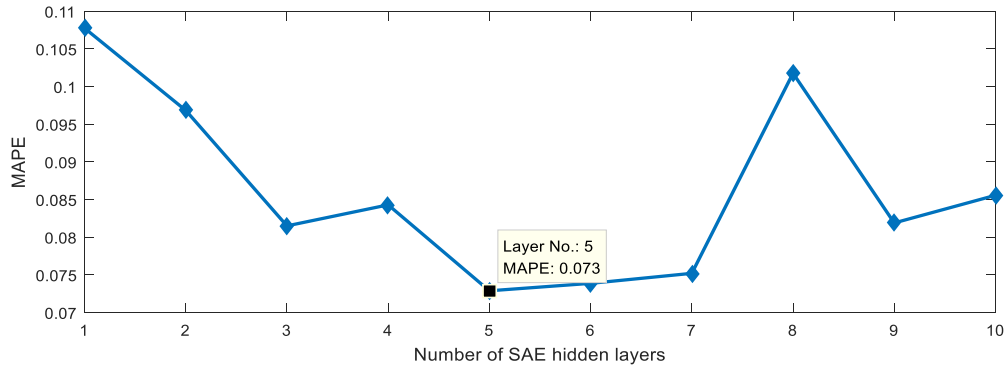


Fig. 2.21 Validation test for SAE with different number of hidden layers

Table 2.9 Validation Test for SVM with Different Kernel Function Types

Kernel function type	MAE	RMSE	MAPE
Linear	363.7714	506.7461	13.29%
Polynomial	534.6109	739.4766	19.21%
RBF	228.1530	348.2298	8.20%
Sigmoid	272.3463	360.3255	9.45%

figures that the forecasted results of the proposed method have the smallest residuals, indicating that, among the 6 methods, the forecasted TF curve is closest to the actual TF curve. Therefore, the comparative results visually demonstrate the effective forecast capability of the proposed approach. The results can be explained by the greater ability of the DCNN method to extract the complexity and non-smoothness of the TF series. Forecast performance evaluation indices are illustrated in Table 2.10. The indices of MAE, RMSE and MAPE during the different seasons in Table 2.10 also show that the errors of the proposed method are approximately half those obtained using other methods, indicating that the DCNN provided the best point forecast performance over the benchmarks.

Table 2.10 Deterministic One-hour Ahead TF Forecasting Error

Season	Error	BPNN	SVM	SAE
Spring	MAE	296.5926	229.8162	265.6717
	RMSE	416.6938	341.5507	382.4075
	MAPE	10.56%	8.18%	9.46%
Summer	MAE	291.2690	238.1329	271.2713
	RMSE	398.1834	369.2117	382.9356
	MAPE	10.08%	8.24%	9.39%
Fall	MAE	337.7184	263.1371	312.5201
	RMSE	482.9903	412.7680	464.0448
	MAPE	12.61%	9.83%	11.67%
Winter	MAE	273.3713	181.5259	258.1541
	RMSE	372.9150	269.3890	351.7644
	MAPE	9.88%	6.56%	9.33%
Average	MAE	299.7378	228.1530	276.9043
	RMSE	417.6956	348.2298	395.2880
	MAPE	10.78%	8.20%	9.96%
Season	Error	TDNN	RNN	DCNN
Spring	MAE	359.9786	260.8728	93.4223
	RMSE	535.3427	331.3600	118.3225
	MAPE	12.87%	9.23%	3.29%
Summer	MAE	291.2655	267.3694	94.2701
	RMSE	433.1820	324.6583	120.6187
	MAPE	10.14%	9.20%	3.26%
Fall	MAE	336.8291	307.9589	107.1443
	RMSE	498.2443	371.3890	140.9987
	MAPE	12.63%	11.46%	3.97%
Winter	MAE	291.2980	232.2863	83.3157
	RMSE	392.0209	297.3276	110.2241
	MAPE	10.61%	8.33%	3.05%
Average	MAE	319.8428	267.1219	94.5381
	RMSE	464.6975	331.1837	122.5410
	MAPE	11.56%	9.56%	3.39%

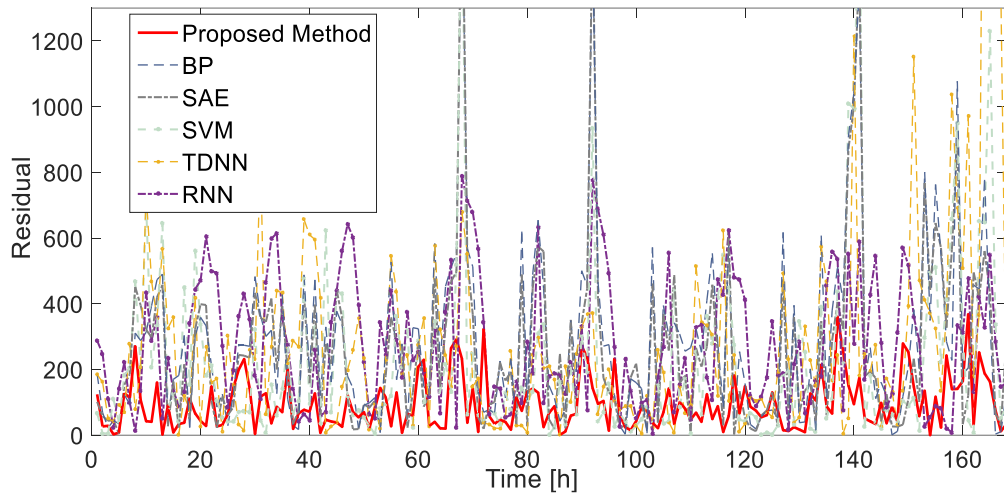


Fig. 2.22 Deterministic TF forecast absolute residual in summer at J5-J6 M42

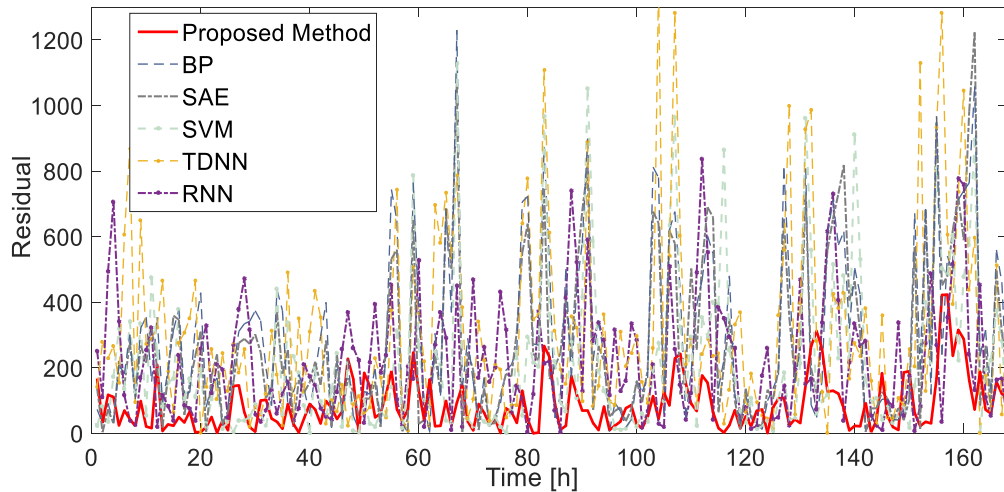


Fig. 2.23 Deterministic TF forecast absolute residual in winter at J5-J6 M42

Compared with the deterministic forecast, probabilistic forecast evaluates the impacts of data uncertainty and model uncertainty in the forecast procedures. PICP, ACE, and IS, as shown in Table 2.11, are used as the indices to evaluate the probabilistic performance. PI nominal confidence (PINC) levels of 90%, 95% and 99% are used since high reliability is desired for FCS operation and control. The PICP is supposed to be the closest to PINC for reliable PIs. Meanwhile, the difference between the PICP and PINC, which is defined as ACE, is supposed to be as close to zero as possible. It can be seen from the PICP index that the proposed method has the most reliable PIs of the measured TF. For example, at the confidence level with $PINC = 95\%$, the DCNN approach generates PICPs of

Table 2.11 Probabilistic One-hour Ahead Forecasting Error

Season		Spring			Summer		
	PINC	90%	95%	99%	90%	95%	99%
BPNN	PICP	87.50%	91.11%	94.44%	87.50%	92.22%	96.11%
	ACE	-2.50%	-3.89%	-4.56%	-2.50%	-2.78%	-2.89%
	IS	-392.53	-254.72	-94.43	-353.59	-233.02	-96.97
SVM	PICP	97.50%	98.61%	99.72%	96.11%	97.78%	99.44%
	ACE	7.50%	3.61%	0.72%	6.11%	2.78%	0.44%
	IS	-391.40	-242.33	-63.37	-429.39	-252.26	-65.27
SAE	PICP	88.89%	93.06%	96.67%	90.83%	94.17%	96.94%
	ACE	-1.11%	-1.94%	-2.33%	0.83%	-0.83%	-2.06%
	IS	-383.54	-240.65	-87.73	-345.91	-215.25	-70.13
TDNN	PICP	92.72%	94.40%	97.48%	91.04%	94.40%	96.64%
	ACE	2.72%	-0.60%	-1.52%	1.04%	-0.60%	-2.36
	IS	-526.28	-322.06	-89.36	-353.28	-212.99	-63.12
RNN	PICP	93.06%	96.39%	97.78%	86.11%	91.67%	95.83%
	ACE	3.06%	1.39%	-1.22%	-3.89%	-3.33%	-3.17%
	IS	-226.49	-140.14	-44.03	-232.61	-148.19	-60.35
DCNN	PICP	90.48%	95.49%	99.25%	90.48%	95.24%	98.25%
	ACE	0.48%	0.49%	0.25%	0.48%	0.24%	-0.75%
	IS	-176.06	-102.68	-28.64	-191.72	-108.51	-23.91
Season		Fall			Winter		
	PINC	90%	95%	99%	90%	95%	99%
BPNN	PICP	88.61%	92.22%	96.11%	88.06%	92.50%	95.83%
	ACE	-1.39%	-2.78%	-2.89%	-1.94%	-2.50%	-3.17%
	IS	-412.37	-266.90	-104.85	-557.25	-340.52	-109.12
SVM	PICP	90.56%	94.44%	97.22%	99.44%	100%	100%
	ACE	0.56%	0.56%	1.78%	9.44%	5.00%	1.00%
	IS	-398.32	-241.41	-72.52	-404.19	-239.13	-62.95
SAE	PICP	89.17%	92.50%	96.11%	85.00%	90.56%	96.94%
	ACE	-0.83%	-2.50%	-2.89%	-5.00%	-4.44%	-2.06%
	IS	-449.23	-286.78	-108.37	-341.63	-199.79	-58.14
TDNN	PICP	91.88%	93.00%	96.36%	91.32%	94.68%	96.36%
	ACE	1.88%	-2.00%	-2.64%	1.32%	-0.32%	-2.64%
	IS	-421.49	-264.43	-89.70	-360.11	-232.58	-91.14
RNN	PICP	86.67%	90.83%	96.67%	88.61%	93.89%	98.61%
	ACE	-3.33%	-4.17%	-2.33%	-1.39%	-1.11%	-0.39%
	IS	-248.07	-154.94	-46.74	-209.69	-123.70	-33.97
DCNN	PICP	90.40%	95.47%	99.20%	89.72%	95.24%	98.75%
	ACE	0.40%	0.47%	0.20%	-0.28%	0.24%	-0.25%
	IS	-170.34	-99.94	-27.05	-201.04	-121.04	-30.64

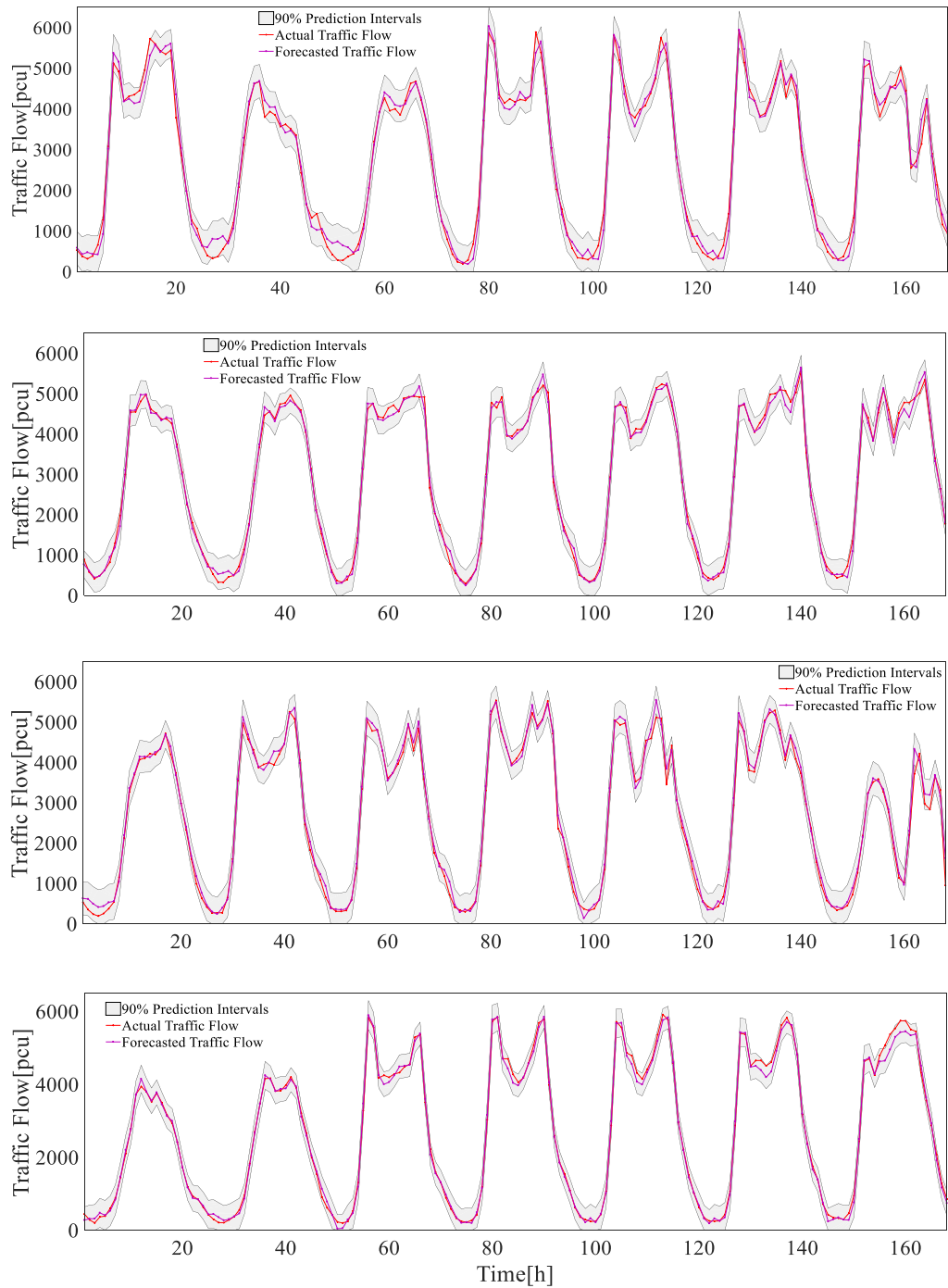


Fig. 2.24 Probabilistic one-hour ahead TF forecast results during the spring, summer, fall, and winter of 2014.

95.49%, 95.24%, 95.47% and 95.24% for 4 seasons, and outperform all other approaches. Although the PICP is only a bit better than that of other methods, the indices of ACE and IS are only half those of the other methods, and the improvements are significant. In all 4 seasons, the ACEs of the proposed method

are smaller than 1%, showing the lowest deviations from the nominal confidence levels, and prove the least reliability errors and highest forecast reliability among the benchmarks. A small absolute IS means higher interval sharpness, and the IS index in Table 2.11 also indicates that the proposed approach outperformed the other 5 methods from the perspective of interval sharpness. E.g., the DCNN approach generates PIs with absolute IS index of 28.64 and 23.91 in spring and summer at the confidence level 99%, which are the smallest compared to all other methods.

Fig. 2.24 shows the actual TF, the forecasted TF, as well as the established PIs with PINC 90% for the 4 seasons. It is obvious that the curves in the 4 graphs fluctuate widely, indicating the nonlinear and non-stationary features of TF data during the 4 seasons. It can be seen that in each graph, the shapes of the lower and upper bounds, as well as the actual and forecasted TF curves, are very similar to each other. This shows that the actual and forecasted TF are perfectly enclosed by the constructed upper and lower bound, indicating that the probabilistic performance of the proposed approach is satisfactory for the construction of high-performance PIs.

2.5.5 Charging Load Forecasting Results Analysis

In the simulation, the FCS has the rated power of $P_r^{FCS} = 0.88$ MW combined with $C = 22$ chargers of $EV = 40$ KW, and could accommodate a maximum of $K=30$ EVs. The average charging duration time is $t_c=20$ minutes. The default parameters of EVs are set to be $\zeta=20\%$, $\sigma=1$ and $\delta=1$.

The distribution of EV daily travel distances are estimated using the mixture model, in which the normal distributions are chosen as the selected PDFs; and the results are shown in Fig. 2.25. It is clear that the curve estimated using the mixture model closely follows the trend of the actual data, which graphically confirms the effectiveness of the proposed model. Based on the TF forecast results and the established model in Section. 2.4, the forecasted charging load and the 90%

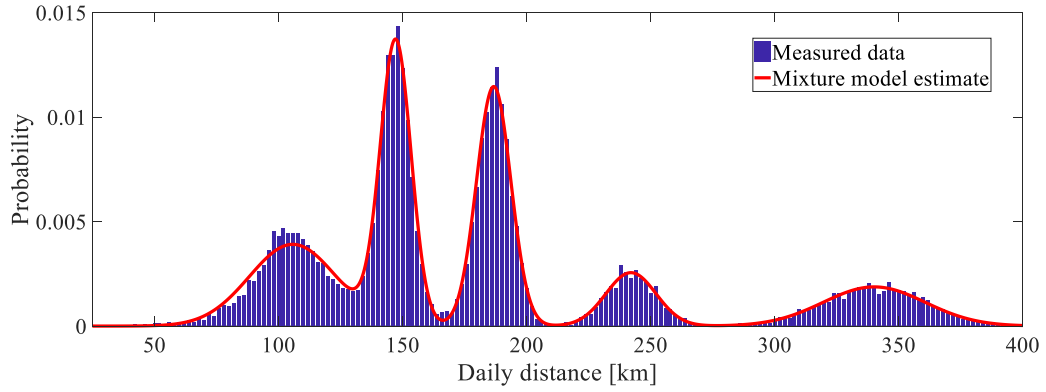


Fig. 2.25 The PDF of EV daily travel distance estimated using the mixture model

Table 2.12 Correlation coefficients of TF and charging demand

Season	Pearson	Kendall	Spearman
Spring	0.9414	0.8041	0.9490
Summer	0.9321	0.8298	0.9373
Fall	0.9274	0.8303	0.9504
Winter	0.9533	0.8455	0.9584

confidence PIs during the different seasons are visually presented in Fig. 2.26, which demonstrates that the trend of the charging load curve is not the same as the TF and fluctuates more significantly. This is due to the significant stochasticity of EV charging behavior, as well as the nonlinearity and complexity of the charging load dataset. It is also found that the PI of charging load is much narrower than that of the TF. This is due to the FCS parameters, as well as to the nonlinear relationship of charging load and the influence of TF on the construction of charging load PIs. However, the forecasted curve is still within the constructed PIs by a large percentage. Therefore, it can be concluded the probabilistic performance of the proposed approach is satisfactory for the operation and control of FCS. To further explore the trend differences between TF curve and charging load curve as shown in Fig. 2.24 and Fig. 2.26, their correlations are studied. Table 2.12 gives the Pearson (linear), Kendall, and Spearman correlation coefficients [120] of TF and charging load during the different seasons. All the coefficients range between 0.8 to 1 and show that, although there is a strong relationship between the 2 time series, the trend differences should not be neglected. Fig. 2.27 further clarifies the

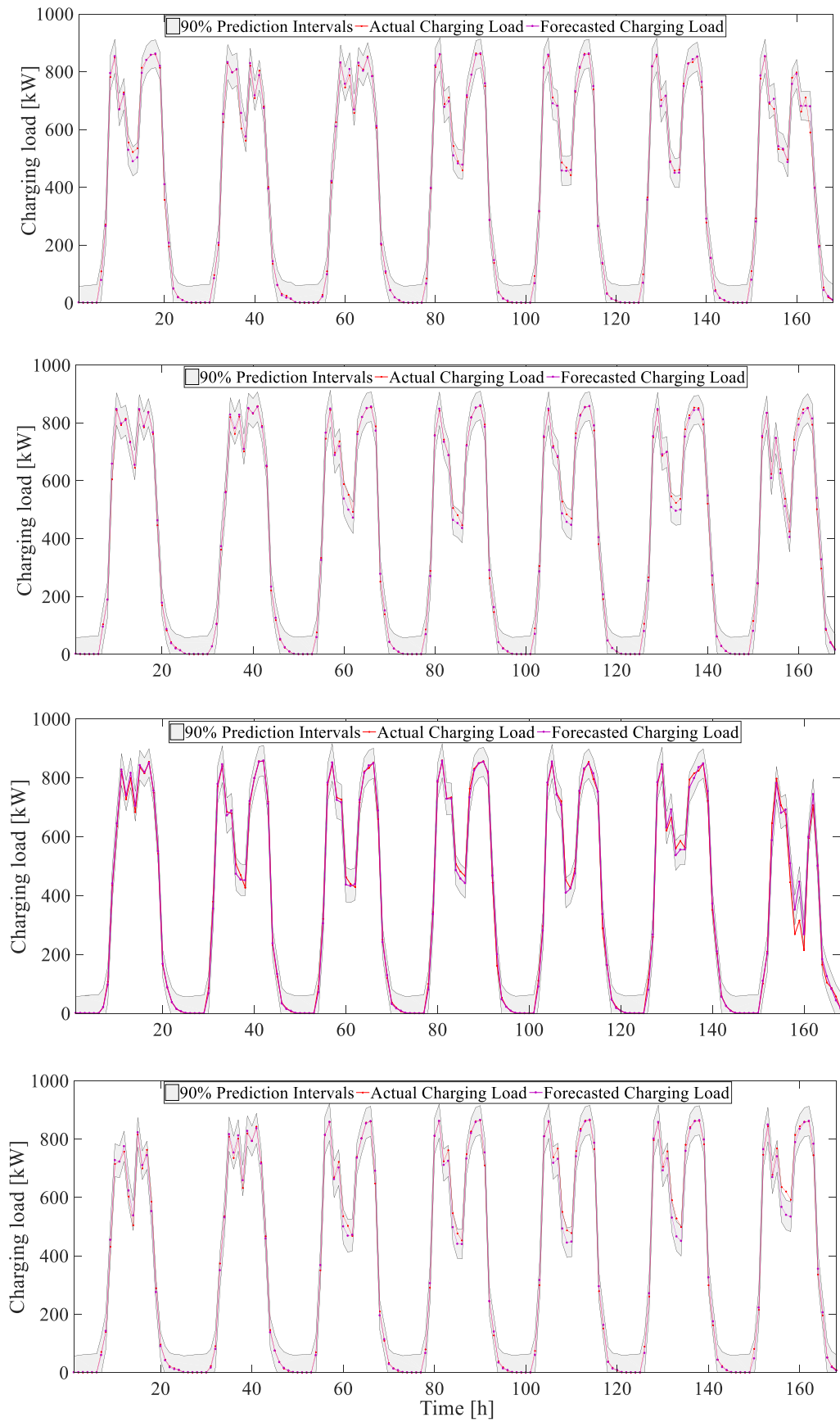


Fig. 2.26 Probabilistic one-hour ahead charging load forecast results during the spring, summer, fall, and winter of 2014

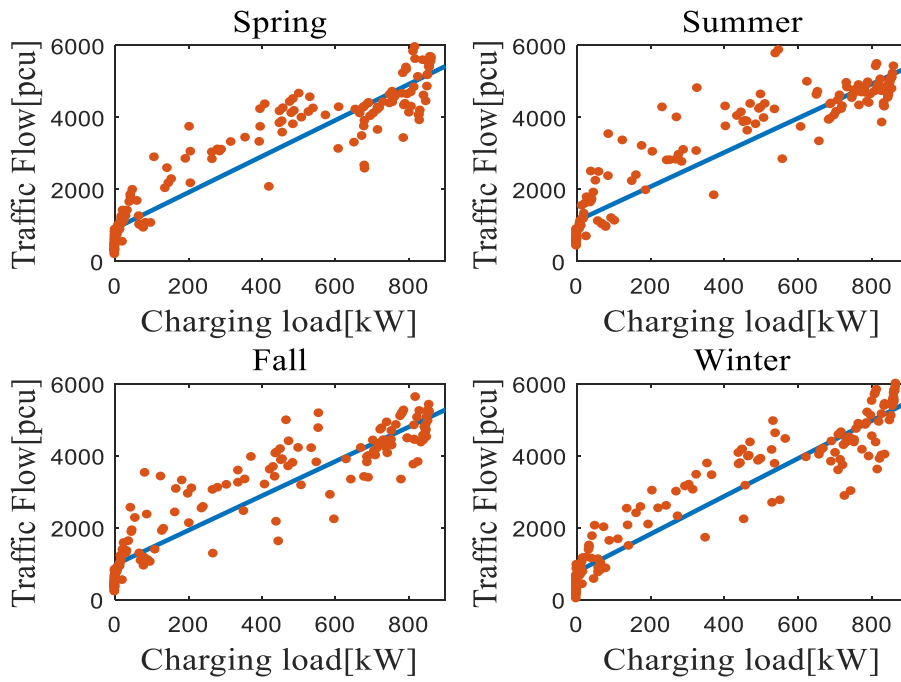


Fig. 2.27 The Pearson (linear) correlation between TF and charging load in different seasons

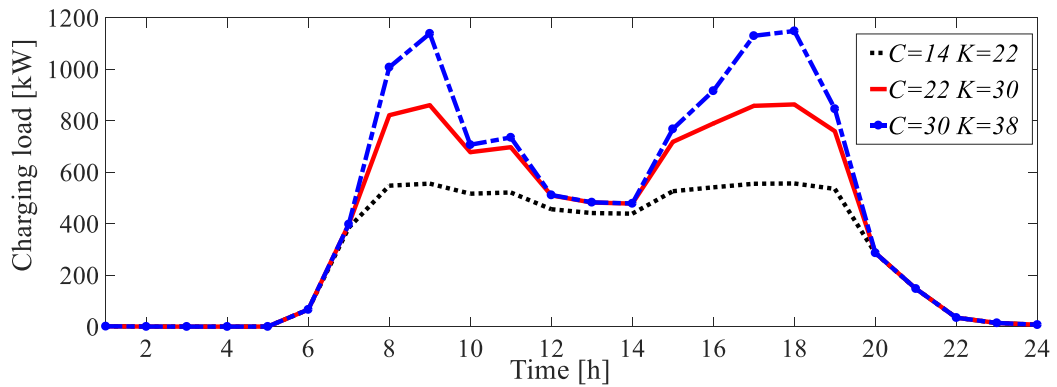


Fig. 2.28 The charging load for different values of C or K

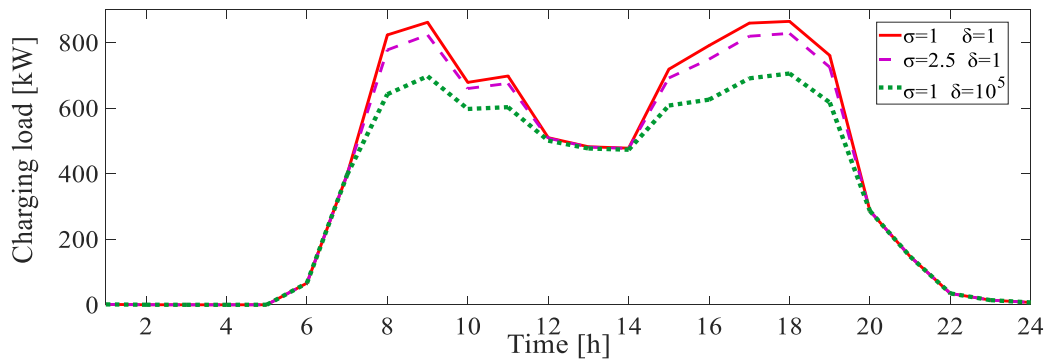


Fig. 2.29 Forecasted charging load for different values of σ or δ

increasing monotonic trend between TF and charging load. This relationship is not strictly linear, however, due to the complicated nonlinear transformation associated with the proposed queuing model.

It is assumed in this study that driver behaviors have a significant influence on the charging load forecast results, and are classified roughly as forced leave, refuse to join, and impatient leave. Fig. 2.28 shows that the charging load becomes larger when the charging post number, C , or capacity, K , of the FCS increases, since fewer EVs will be forced to leave due to limitations of FCS service capability. Clearly, the shortages of charging posts and charging capacity impose restrictions on the wide use of EVs, and the installation of enough charging facilities, which can effectively enhance EV driver charging convenience, will make EVs more popular. Driver sensitivity to charging wait time is another factor that can influence the charging load. Fig. 2.28 demonstrates that if drivers are more sensitive to waiting time, which translates to a larger “refuse to join” probability parameter, σ , or a larger “impatient leave” probability parameter, δ , the charging load decreases accordingly. From the curves shown in Fig. 2.29, it can also be seen that the charging load reduction becomes particularly evident during rush hour, when there is higher charging demand. This indicates that flexible strategies should be taken in the FCS operation process in order to promote service capabilities, such as the establishment of appropriate time-of-use (TOU) prices for charging power and other strategies.

2.6 Summary

In this chapter, both long-term forecasting and short-term forecasting of EV charging demand are studied. For long-term prediction, the grey system forecasting theory and the NAR neural network are applied to the forecasting of EV charging demand. The simulation results show that the prediction accuracy of the grey system forecasting model is high only when the original EV demand data

increases exponentially. Otherwise, the prediction appears a larger deviation. In comparison to the grey system forecasting theory, it is shown that the NAR neural network model has a good performance in future practical application. Additionally, the DBN method is firstly used to predict TF in CS construction planning horizon and case studies show that it outperforms other four typical algorithms which are BPNN, SVM, ARMA and MWNN.

For short-term prediction, a probabilistic deep learning forecast model, that considered FCS service limitations and driver behaviors is developed for the prediction of EV charging loads. In the established model, the TF is forecasted using the DCNN approach, while the model and data uncertainties are considered when constructing the forecast PIs. To obtain the EV charging load forecast results, mixture models are used to analyze the historic data and a novel MMCK queuing model is proposed. Simulation results are presented to demonstrate the effectiveness of the employed method and model. The proposed approach will be beneficial for the future planning and operation of FCSes.

Chapter III

Negotiated Planning of Distribution System and EV Charging Stations in Deregulated Electricity Markets

3.1 Introduction

According to the forecasting results, sufficient number of CSes should then be planned to meet the increasing charging demand of EVs. Further DS should be expanded to supply the required energy to the CSes. This chapter therefore would focus on the negotiated planning of CSes and DS in deregulated electricity markets based on the forecasting results of DBN method mentioned in Chapter 2.

In this chapter, a locational marginal pricing model capable of alleviating distribution system congestion and promoting the response of electric demands is utilized to simulate the deregulated market environment of the future smart grid, and the charging stations are considered as market bidder to maximize their operation profits. Additionally, a cooperative game-theory based planning strategy is proposed to assist the distribution and charging station planners to reach a negotiated planning solution for profit sharing and cost recovery of new distribution feeders and charging stations to guarantee the service of EV charging.

3.2 Framework of the Proposed Model

Accurate EV demand forecasting is the precondition of CS and charging network planning, and it is important to select a suitable method and an appropriate model to simulate and predict the EV demand. Meanwhile, the operation costs and the incomes are the most concerns of both CS and network planning operators and

should therefore be considered in the planning procedures. As a result, the proposed planning model is composed of three phases, corresponding to forecasting, construction and operation, respectively.

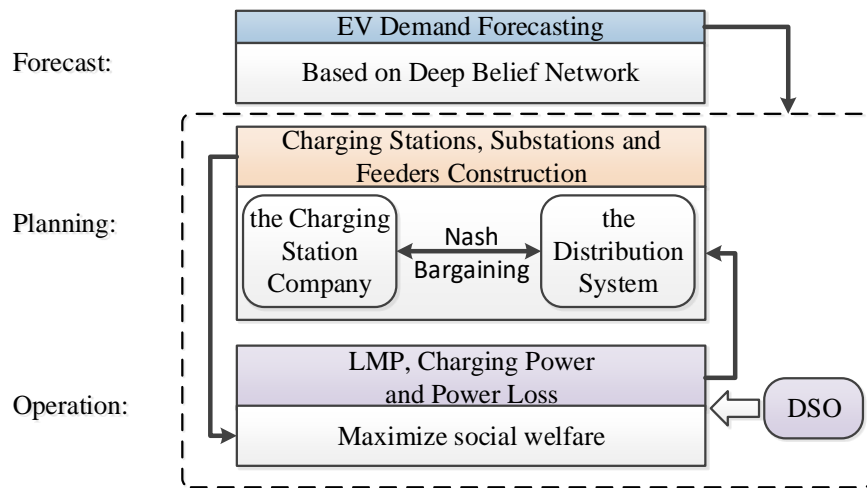


Fig. 3.1 Framework of the proposed model

As shown in Fig. 3.1, the EV demand in the planning horizon is obtained from the forecasting phase based on Deep Belief Network and then transferred to the planning and operation phases. The planning module implements the Nash bargaining process between the CS company and the DS to determine the decision variables of CSes construction plan and DS extension scheme simultaneously, which considers the impacts of LMPs and flexible demands provided by the operation phase. Based on the network topology generated from the planning phase, the operation module solves the electricity price model based on market mechanism and offers decision variables of distribution LMPs as well as flexible loads including charging demands to the planning phase. The decision variables of the operation phase will iteratively update the planning scheme results until the optimal solution achieved.

3.3 The Mathematical Model

3.3.1 Nash Bargaining Model: General Formulation

The Nash bargaining game between two players is in essence a jointly generated surplus sharing problem used to model bargaining interactions. Research on bargaining game has found extensive real applications, such as contract negotiation [126], social justice allocation [127], and risk aversion [128].

In the Nash bargaining game, two players demand a portion of surplus they jointly created, which could only be obtained if the negotiation satisfying both players could be reached. This could be modeled that game players are in a negotiation to identify an agreement outcome (u, v) from the payoff possibility set χ . (u^0, v^0) is called the players' disagreement point, which is the outcome the players can expect to receive if negotiations break down. The problem has solutions if agreements in χ are better for both players than the disagreement point. A Nash bargaining solution (u^*, v^*) should satisfy four axioms, which reflects its fairness and efficiency properties: Pareto efficiency, symmetry, independence of irrelevant alternatives, and invariance under positive linear-affine transformation [129]. It is proved by John Nash that under mild conditions, the payoff (u^*, v^*) is exactly a Nash bargaining solution (NBS) if it solves the following optimization problem [129][130]:

$$\max \quad (u - u^0)(v - v^0) \quad (3.1)$$

$$\text{subject to} \quad (u, v) \in \chi \quad (u^0, v^0) \in \chi^0 \quad (3.2)$$

$$(u, v) \geq (u^0, v^0) \quad (3.3)$$

where χ and χ^0 are the set of possible payoffs and the set of disagreement outcome, respectively. The optimization (3.1)-(3.3) makes the acquisition process of the NBS very simple, intuitive, and efficient. Moreover, the details of bargaining process could be ignored and the four axioms will be satisfied automatically by solving the proposed optimization model. Therefore, it is widely applied in solving the cooperative gaming problems.

3.3.2 Nash Bargaining of the Cooperative Planning

The DS planning encounters new challenges due to the fast development of EVs. EV CSEs and DS are required to be planned simultaneously to meet the rapidly growing EV charging demand, but research on this is still limited [59][131] and mainly under the simplified assumption that the planning is managed by a single utility. This is in fact contrary to the reality of deregulated market environment. Uncertainties such as price volatility and renewable energy intermittency in the market environment make the financial recovery for the CS and DS planning no longer guaranteed and discourage planners' investment willingness. However, CS and DS are rational independent decision makers, which are self-operated with self-interests such as cost minimization. Without properly designed negotiating mechanism, they will interact with each other only if more benefits could be obtained as a result, and this leads to difficulties to the cooperative planning of the CS and DS. Therefore, an incentive mechanism should be designed to encourage proactive interactions and fair profit sharing between CS and DS in the planning. In such mechanism, a "win-win" cooperative planning is still feasible, which makes the DS obtain more profits by providing transmission service, and the CS operators provide required charging service to EVs and recover their investments. Therefore, a Nash bargaining based cooperative planning model is proposed here for the first time to analyze the possible realistic planning procedures of CSEs and DS. In the proposed model, the tightly coupled planning variables of CS and DS are jointly scheduled and optimized simultaneously to take the advantages of diverse profits obtained by both participants.

According to the general model (3.1)-(3.3) proposed in Section III-B, the cooperative planning results are the NBS obtained by solving the following optimization problem:

$$\max [u^{\text{CS}}(Y_i) - u_0^{\text{CS}}(Y_i)][v^{\text{DC}}(Y_m^{\text{SE}}, Y_m^{\text{SN}}, X_{mn}^{\text{LN}}) - v_0^{\text{DC}}(Y_m^{\text{SE}}, Y_m^{\text{SN}}, X_{mn}^{\text{LN}})] \quad (3.4)$$

$$\text{where } u^{\text{CS}}(Y_i) = d^{\text{year}} \left(\sum_{t \in \Omega^{\text{T}}} \sum_{i \in \Omega^{\text{CS}}} D_t p_{i,t} P_{i,t} Y_i - \sum_{t \in \Omega^{\text{T}}} \sum_{i \in \Omega^{\text{CS}}} D_t p_{i,t}^{\text{LMP}} P_{i,t} Y_i \right)$$

$$- \sum_{i \in \Omega^{CS}} (c_i^{CSOM} + c_i^{CSC}) Y_i \quad (3.5)$$

$$\begin{aligned} v^{DC}(Y_m^{SE}, Y_m^{SN}, X_{mm}^{LN}) = & d^{year} \sum_{t \in \Omega^T} D_t [\sum_{i \in \Omega^{CS}} (P_{i,t}^{LMP} - p_t^S) P_{i,t} Y_i \\ & + \sum_{m \in \Omega^{noCS}} (P_{m,t}^{LMP} - p_t^S) P_{m,t}^{noCS}] \\ & - d^{year} c^E \sum_{mm \in \Omega^L} \sum_{t \in \Omega^T} D_t [G_{mm} X_{mm}^{OP} (U_{m,t}^2 + U_{n,t}^2 \\ & - 2U_{m,t} U_{n,t} \cos \theta_{mm,t})] \\ & - \sum_{m \in \Omega^{SN}} (c^{SOM} + c^{SN}) Y_m^{SN} \\ & - \sum_{m \in \Omega^{SE}} (c^{SOM} + c^{SE}) Y_m^{SE} \\ & - \sum_{mm \in \Omega^{LN}} (c^{BOM} + c^{LN}) d_{mm} X_{mm}^{LN} \end{aligned} \quad (3.6)$$

$$\text{subject to } u^{CS}(Y_i) \geq u_0^{CS}(Y_i) \quad (3.7)$$

$$v^{DC}(Y_m^{SE}, Y_m^{SN}, X_{mm}^{LN}) \geq v_0^{DC}(Y_m^{SE}, Y_m^{SN}, X_{mm}^{LN}) \quad (3.8)$$

$$\sum_{mm \in \Omega^L} X_{mm}^{OP} = n^B - n^{SE} - n^{SN} \quad (3.9)$$

$$\sum_{i \in \Omega^{CS}} Y_i = n^{CS} \quad (3.10)$$

$$\sum_{m \in \Omega^{SN}} Y_m^{SN} = n^{SN} \quad (3.11)$$

In the Nash bargaining between the CS company and the DS, the threatening point is assumed to be $(u_0^{CS}, v_0^{DC}) = (0, 0)$, which means that if the payoffs of two participants are less than zero, no negotiate settlement would be reached. Based on (3.1), (3.4) can be easily concluded and further explained in (3.5) and (3.6), which represent the expected payoffs of the CS company and the DS, respectively. Furthermore, the payoff of the CS company in (3.5) is composed of three components, namely earnings from EVs charging, electricity bills paying to the DS, and the investment, operation and maintenance cost of CSes. As shown in (3.6), v^{DC} represents the payoff of the DS, where the first and second terms denote

its net profits by selling electricity to CSes and other customers, and the cost of energy losses. The next two terms are the investment, operation and maintenance cost of reinforcing existing substations and constructing new substations. The last term indicates the investment, operation and maintenance cost of new feeders. The service price EV owners paid to CSes for charging is defined by the weighed electricity and gasoline price and could be defined as $p_{i,t} = (1+\omega_c) \cdot p_{i,t}^{\text{LMP}} + \zeta_c \cdot p^{\text{GAS}}$.

Y_i represents decision variable for candidate CS at node i . Y_m^{SN} is decision variable for candidate substation at node m . Y_m^{SE} is decision variable for the existing substation at node m with reinforcement of high capacity. X_{mn}^{LN} is the decision variable to invest a new feeder mn . d^{year} accounts for days in the planning horizon. Ω^{T} is set of all time subperiods. Ω^{CS} is set of candidates CSes. D_t is duration of subperiod t (h). $p_{i,t}$ is electricity price customers pay for EV charging in CS i at time t . $P_{i,t}$ is active power CS i offered to EVs at time t (MW). $p_{i,t}^{\text{LMP}}$ is distribution locational marginal price (LMP) of the node where CS i locates at time t (US\$/MWh). c_i^{CSOM} is operation and maintenance (O&M) costs of the CS i per year. c_i^{CSC} is investment cost for the CS i . $p_{m,t}^{\text{LMP}}$ is distribution LMP of node m at time t . p_t^{S} is electricity price of the balance bus at time t (US\$/MWh). Ω^{noCS} is Set of system nodes except the nodes of Ω^{CS} . $P_{m,t}^{\text{noCS}}$ is active power demand at node m of Ω^{noCS} at time t . c^{E} is electricity energy cost. c^{SE} is costs to reinforce a substation with high capacity (US\$). c^{SN} is costs to invest a new substation (US\$). $p_{m,t}^{\text{L}}$ is offer/bid price of node m at time t . Ω^{L} is set of feeders. G_{mn} is conductance and susceptance of feeder mn . X_{mn}^{OP} is variable indicates the feeder mn operates or not. $U_{m,t}$ and $U_{n,t}$ are Voltage magnitude at node m and n at time t . $\theta_{mn,t}$ is deviation of phase angle between node m and n at time t . Ω^{SE} and Ω^{SN} are set of existing and candidate substations (SS). c^{SOM} is operation and maintenance fee of a substation. c^{SE} and c^{SN} are costs to reinforce a substation with high capacity and invest a new substation. Ω^{LN} are set of existing and candidate feeders. c^{LN} are costs to invest a new feeder, respectively. c^{BOM} is operation and maintenance fee of a feeder per year. d_{mn} is length of feeder mn . n^{B} is the number of nodes in a DS. n^{CS} is the

number of CSEs to be built. n^{SN} and n^{SE} are the number of substations to be built and the number of existing substations, respectively.

(3.7) and (3.8) ensure if any payoff of these two participants is less than the threat point, the negotiation fails. Based on the graph theory, in order to guarantee that a sub-graph is a tree, it must fulfil two conditions: 1) there are n^B-1 edges in this sub-graph while the number of nodes of this sub-graph is n^B , and 2) n^B nodes are connected. The first condition is implicitly ensured by (3.9) while (3.17) and (3.18) guarantee the second condition [132]. At last, the constraints of CS and new SS number are determined by (3.10) and (3.11), respectively. It is also worthwhile to point out that the time granularity for all the time dependent parameters and variables with subscript t is $D_t = 1h$ in this work.

3.3.3 EV Participated Market Mechanism

Well-designed market mechanism in the DS has many advantages in the planning and operation of the smart grid, including but not limited to congestion alleviation, fairness promotion, and cost reduction [133]. Nowadays, certain kinds of loads, such as demands in households controlled by temperature, are flexible and dispatchable. Moreover, batteries of EVs are also controllable to achieve smart charging. There is potential for these dispatchable loads to respond to energy market signals.

The dispatch of CS demand is simulated in a discrete-state, discrete-time fashion at each time interval of one hour. The dispatchable demand in the CS is dynamic during a day and highly dependent on the TF passing by the CS, the temporal distribution of which is forecasted by the proposed DBN method. The EV's charging in the CS is a typical probabilistic queuing process, which assumes the arrival EV number n of each time step follows a Poisson process:

$$P(n) = e^{-\lambda} (\lambda^n / (n!)) \quad n=0,1,2... \quad (3.12)$$

where λ is the average arrival EV number at each time step. The charging duration

t_c follows a negative exponential distribution.

$$f(t_c) = \mu e^{-\mu t_c} \quad (3.13)$$

where μ is average number of EVs that finish charging and leave the CS at each time step. According to the queuing theory, the dispatchable EV number is $N^{\text{avi}} = \lambda/\mu$, and the available EV power $P^{\text{FL,avi}}$ is

$$P^{\text{FL,avi}} = v N^{\text{avi}} p_r^{\text{EV}} \quad (3.14)$$

where EV_r is the rated power of chargers in the CS, and v is a coefficient less than 1 that ensures the dispatched EV's charging requirement could be satisfied.

On the other hand, load ramps exist extensively in the DS [160], which could drive the DS into balance violations and price spikes if not properly handled [161]. Due to the good controllability and fast responsive characteristics, EVs in the CS have the potential to eliminate the impacts of load ramps [162] to provide the ramp reserve $R_{i,t}$, which is taken into the consideration in the proposed model.

Based on the available EV power, the market mechanism problem consists of (3.15) - (3.27), and the overall electricity purchasing cost is minimized for social welfare maximization [134]:

$$\min \sum_{m \in \Omega^{\text{SE}} \cup \Omega^{\text{SN}}} p_{m,t}^{\text{L}} P_{m,t}^{\text{S}} - \sum_{m \in \Omega^{\text{noCS}}} p_{m,t}^{\text{L}} P_{m,t}^{\text{noCS}} - \sum_{i \in \Omega^{\text{CS}}} p_{i,t}^{\text{L}} P_{i,t} \quad (3.15)$$

$$\text{subject to} \quad U_m^{\min} \leq U_{m,t} \leq U_m^{\max}, \forall m \in \Omega^{\text{B}} \quad (3.16)$$

$$P_{m,t}^{\text{S}} = P_{m,t}^{\text{L}} + U_{m,t} \sum_{m,n \in \Omega^{\text{B}}} U_{n,t} (G_{mn} \cos \theta_{mn,t} + B_{mn} \sin \theta_{mn,t}) \quad \forall m, n \in \Omega^{\text{B}} \quad (3.17)$$

$$Q_{m,t}^{\text{S}} = Q_{m,t}^{\text{L}} + U_{m,t} \sum_{m,n \in \Omega^{\text{B}}} U_{n,t} (G_{mn} \sin \theta_{mn,t} - B_{mn} \cos \theta_{mn,t}) \quad \forall m, n \in \Omega^{\text{B}} \quad (3.18)$$

$$(P_{m,t}^{\text{S}})^2 + (Q_{m,t}^{\text{S}})^2 \leq (S_m^0 + Y_m^{\text{SE}} S_m^{\text{SE}} + Y_m^{\text{SN}} S_m^{\text{SN}})^2 \quad \forall m \in \Omega^{\text{SE}} \cup \Omega^{\text{SN}} \quad (3.19)$$

$$P_{m,t}^{\text{L}} = \begin{cases} P_{m,t}^{\text{noCS}}, & \forall m \in \Omega^{\text{noCS}} \\ P_{i,t}, & \forall m \in (\Omega^{\text{B}} - \Omega^{\text{noCS}}), \forall i \in \Omega^{\text{CS}} \end{cases} \quad (3.20)$$

$$P_{m,t}^{\text{noCS}} = \begin{cases} P_{m,t}^{\text{U}} + P_{m,t}^{\text{F}}, \forall m \in \Omega^{\text{F}} \\ P_{m,t}^{\text{U}}, \forall m \in (\Omega^{\text{noCS}} - \Omega^{\text{F}}) \end{cases} \quad (3.21)$$

$$P_{i,t} = P_{i,t}^{\text{U}} + P_{i,t}^{\text{FL}}, \forall i \in \Omega^{\text{CS}} \quad (3.22)$$

$$P_{m,t}^{\text{F,min}} \leq P_{m,t}^{\text{F}} \leq P_{m,t}^{\text{F,max}}, \forall m \in \Omega^{\text{F}} \quad (3.23)$$

$$P_{i,t}^{\text{FL,min}} \leq P_{i,t}^{\text{FL}} + R_{i,t} \leq P_{i,t}^{\text{FL,avi}}, \forall i \in \Omega^{\text{CS}} \quad (3.24)$$

$$I_{mn,t} \leq I_{mn}^{\text{max}} \cdot X_{mn}^{\text{OP}}, \forall mn \in \Omega^{\text{L}} \quad (3.25)$$

$$0 \leq |R_{i,t}| \leq \min(R_{i,t}^{\text{max}}, \Delta_i), \forall i \in \Omega^{\text{CS}} \quad (3.26)$$

$$\sum_{i \in \Omega^{\text{CS}}} R_{i,t} \geq |R_t^{\text{SYS}}| \quad (3.27)$$

Inequality (3.16) is the voltage magnitude constraint. (3.17) and (3.18) denote the typical AC power flow equality constraints. (3.19) compactly gives the capacity constraints for substations. (3.20) assumes that there are no other loads except CS demand on nodes where new CSes are located. As shown in (3.21) and (3.22), parts of loads are dispatchable. (3.23) denotes the upper and lower limits of dispatchable load on nodes where no CSes are located. Inequality (3.24) denotes the sum of dispatched power and ramp reserve does not exceed the maximum available power. Inequality (3.25) enforces feeder capacity constraints. (3.26) indicates that the reserve provided by the CS are limited by the maximum reserve as well as their physical ramp rates Δ_i . (3.27) requires that the sum of the reserve should meet the system requirements.

In this optimization model, network parameters, power flow limits and output limits are known data for the optimization. Some required data such as load demand and TF levels are forecasted by the market operators to solve this DS market optimization model. The control variables include $P_{m,t}^{\text{F}}$ and $P_{i,t}^{\text{FL}}$ et al, while the state variables include $U_{m,t}$ and $\theta_{mn,t}$. Those variables could be obtained by solving this social welfare maximization problem with their initial values being assumed in the beginning of the solving process. According to the classical LMP

theory [162-164], the LMPs equal to the Lagrangian multipliers ($p_{i,t}^{\text{LMP}}$ and $p_{m,t}^{\text{LMP}}$) obtained by solving the proposed market mechanism optimization (3.15)-(3.27).

$p_{m,t}^{\text{L}}$ is offer/bid price of node m at time t . $P_{m,t}^{\text{noCS}}$ is active power demand at node m of Ω^{noCS} at time t . U_m^{max} and U_m^{min} are maximum and minimum acceptable voltage magnitude of node m . Ω^{B} is set of all system nodes. $P_{m,t}^{\text{S}}$, $Q_{m,t}^{\text{S}}$ are active and reactive power provided by the substation at node m at time t . $P_{m,t}^{\text{L}}$, $Q_{m,t}^{\text{L}}$ are active and reactive power demand at node m at time t . S_m^0 is apparent power capacity of the existing substation at node m . S_m^{SE} is added apparent power capacity of the existing substation at node m . S_m^{SN} is apparent power capacity of the candidate substation at node m . $P_{m,t}^{\text{U}}$ is fixed active power demand at node m of Ω^{noCS} at time t . Ω^{F} is set of nodes with dispatchable demands in Ω^{noCS} . $P_{m,t}^{\text{F}}$ is dispatched active power demand at node m of Ω^{F} at time t . $P_{i,t}^{\text{FL}}$ is dispatched power CS i offered to EVs at time t . $P_{i,t}^{\text{U}}$ is Fixed power the CS i offers to EVs at time t . $P_{m,t}^{\text{F,max}}$ and $P_{m,t}^{\text{FL,min}}$ are maximum and minimum demand of $P_{m,t}^{\text{F}}$. $P_{i,t}^{\text{FL,min}}$ is minimum demand of $P_{i,t}^{\text{FL}}$. $I_{mn,t}$ is current magnitude of feeder mn at time t . I_{mn}^{max} is maximum acceptable current magnitude of feeder mn . $R_{i,t}^{\text{max}}$ is maximum reserve at the node where CS i locates at time t . R_t^{SYS} is system-wide ramping reserve requirements at time t .

3.3.4 The Centralized Planning Model for Comparison

Although it could be quite contrary to the reality, centralized planning model is still widely used in practice in some countries, even the CS company and DS have been operating independently and bears their own costs. This situation brings difficulties of the investment cost recovery for both the DS and CS companies and leads to the lack of incentives for constructing enough CSes and DS to facilitate the EV popularization. To simulate this situation, the centralized planning to maximize the expected system net benefits is therefore briefly introduced here as the comparison benchmark.

Planning Phase:

$$\begin{aligned}
W(Y_i, Y_m^{SN}, Y_m^{SE}, X_{mn}^{LN}) = & d^{year} \sum_{t \in \Omega^T} D_t [\sum_{m \in \Omega^{noCS}} P_{m,t}^{LMP} P_{m,t}^{noCS} + \\
& + \sum_{i \in \Omega^{CS}} p_{i,t} P_{i,t} Y_i - \sum_{m \in \Omega^{noCS}, i \in \Omega^{CS}} p_t^S (P_{m,t}^{noCS} + P_{i,t} Y_i)] \\
& - d^{year} c^E \sum_{mn \in \Omega^L} \sum_{t \in \Omega^T} D_t [G_{mn} X_{mn}^{OP} (U_{m,t}^2 + U_{n,t}^2 \\
& - 2U_{m,t} U_{n,t} \cos \theta_{mn,t})] - \sum_{i \in \Omega^{CS}} (c_i^{CSOM} + c_i^{CSC}) Y_i \\
& - \sum_{m \in \Omega^{SN}} (c^{SOM} + c^{SN}) Y_m^{SN} \\
& - \sum_{m \in \Omega^{SE}} (c^{SOM} + c^{SE}) Y_m^{SE} \tag{3.28}
\end{aligned}$$

subject to (3.9) and (3.11)

Operation Phase: (3.15) - (3.27)

(3.33) summarizes the overall net benefits, which consists of 5 terms: the first term is the income of electricity sales; the second term is the cost of power loss; and the last 3 terms are the construction, operation and maintenance cost of CSes, substations and feeders. The constraints of the planning model are the same as (3.9) - (3.11). The objective functions of operation model and constraints are the same as (3.15)-(3.27). u^{CS} and v^{DC} of the bargaining model for comparison are calculated based on the centralized planning situation according to the objectives (3.5) and (3.6).

3.3.5 Scenario-based Approach for Uncertainty Consideration

Various uncertainties exist in the future CS and DS planning, which should be properly considered to minimize risk, avoid unpredicted losses and minimize operational problems. Load demand levels, TF levels, penetration levels of renewable energy sources, and penetration levels of EVs are the four uncertainties studied in this work. Chance constrained optimization and robust optimization are frequently used to cope with uncertainties, but such methods have drawbacks such as not able to economically quantify the risks bought by uncertainties. Therefore, scenario-based approach is utilized in this thesis to deal with uncertainties involved

in the planning and operation processes, and the mentioned four uncertainties are stated by the vector as

$$\Phi_s = [\mathbf{P}_s^D, \mathbf{TF}_s, \beta_s^{\text{EV}}, \gamma_s^{\text{RE}}] \quad \forall s \in \Omega^s \quad (3.29)$$

where Φ_s represents scenario s ; \mathbf{P}_s^D is the load demand vector (including demands of all nodes) in scenario k ; \mathbf{TF}_s is the TF vector (including TF passing by all nodes) in scenario k ; β_s^{EV} and γ_s^{RE} are the penetration levels of EVs and renewable energy sources in scenario k , respectively. In general, the uncertainties of penetrations of EVs and renewables can hardly be derived from the historical data and are categorized into nonrandom uncertainties. Typical scenarios of this kind of uncertainties could be predefined in line according to the factors such as subsidy policies, battery performance and renewable purchasing cost. On the other hand, as described in Section III.A, the load and TF levels could be predicted by the historical data and are categorized into random uncertainties. Deviation strategy is applied to the predicted results of this kind of uncertainties [18][58], and the typical scenarios are generated. For example, if 3 typical scenarios for TF levels are needed, they could be assumed as $(1-\alpha\%) \times$ forecasted value, forecasted value, and $(1+\alpha\%) \times$ forecasted value.

Based on the generated scenarios, the mathematical model considering uncertainties is summarized as

$$\text{Objective} \quad \sum_{s \in \Omega^s} \pi_s f_s(\mathbf{X}_s, \Phi_s) \quad (3.30)$$

$$\text{subject to} \quad \mathbf{H}_s^{\min} \leq \mathbf{H}_s(\mathbf{X}_s, \Phi_s) \leq \mathbf{H}_s^{\max} \quad \forall s \in \Omega^s \quad (3.31)$$

$$\mathbf{G}_s(\mathbf{X}_s, \Phi_s) = \mathbf{0} \quad \forall s \in \Omega^s \quad (3.32)$$

$$\sum_{s \in \Omega^s} \pi_s = 1 \quad (3.33)$$

where f_s is the objective function of the planning or operation phases in different scenarios, including the cooperative planning model, centralized planning model, and the market operation model aforementioned. \mathbf{X}_s is the decision variable vector;

(3.31) and (3.32) represent the inequality and equality constraints of different scenarios. π_s is scenario occurrence probability of scenario s , and (3.33) ensures the total probability equals to 1.

3.4 Solution Methodology

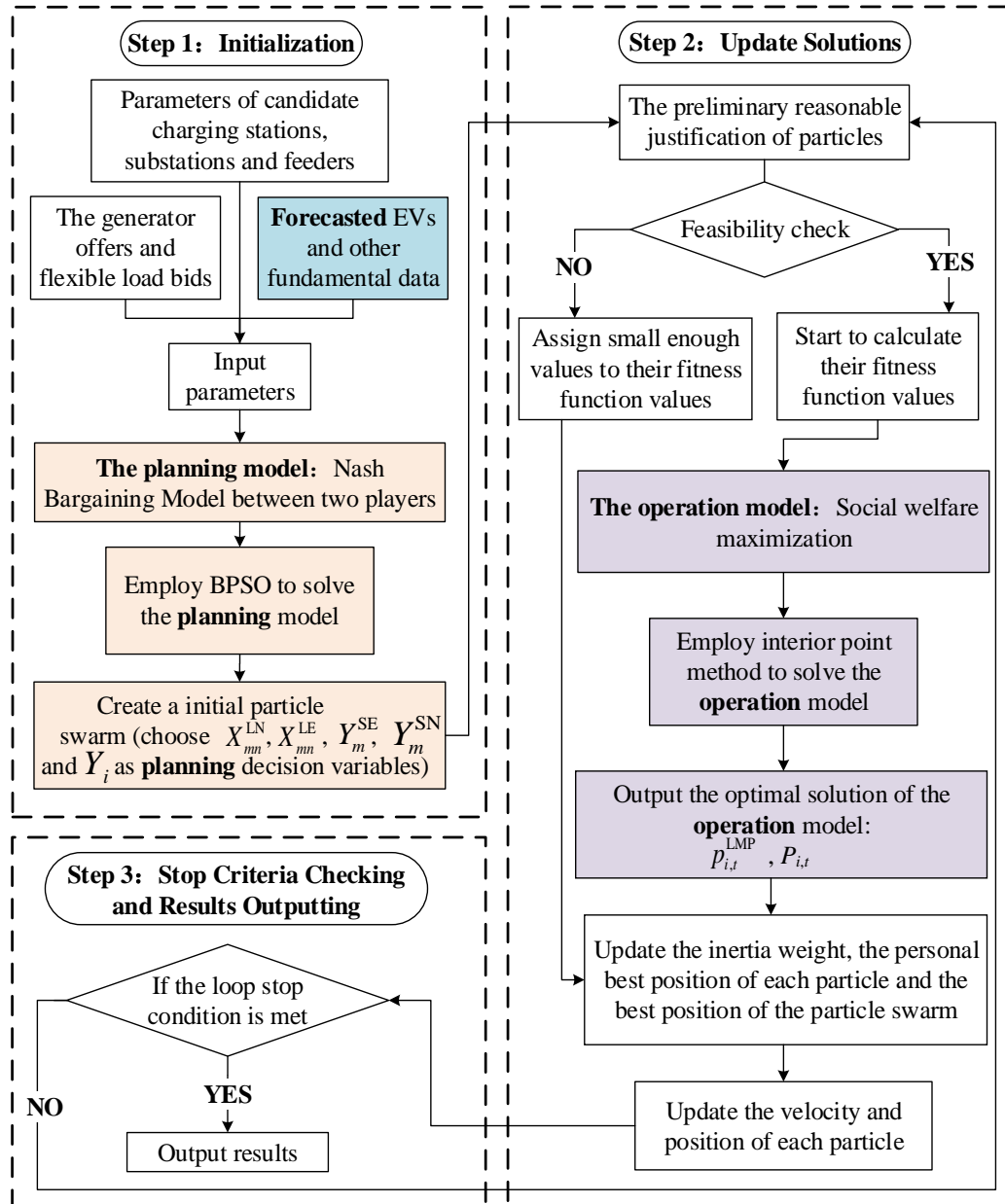


Fig. 3.2 The programming flow chart

Fig. 3.2 illustrates the programming flow chart of the planning and operation

of CS and DS corresponding to the model in Fig. 3.1. In the planning phase, locations of CSEs, constructions of substations and cable selections of feeders are regarded as decision variables. It is a typical mixed integer nonlinear optimization and cannot be easily solved by conventional solution methods, thus the binary particle swarm optimization algorithm (BPSO), which is a population-based stochastic optimization algorithm inspired by bird flocking or fish schooling [135], is applied to solve this problem.

An initial swarm composed of n^P D -dimension particles according to decision variables is created. Two formulas are used to describe the particle's behaviors. Formula (3.39) defines the velocity of the particle, and formula (3.40) denotes the location of the particle. On each dimension d :

$$v_{id}^{k+1} = \omega v_{id}^k + c_1 \zeta (p_{id}^k - x_{id}^k) + c_2 \eta (p_{gd}^k - x_{id}^k) \quad (3.34)$$

$$x_{id}^{k+1} = \begin{cases} 1 & \text{rand}(\cdot) < S(v_{id}^{k+1}) \\ 0 & \text{rand}(\cdot) > S(v_{id}^{k+1}) \end{cases} \quad (3.35)$$

where v_{id}^k and x_{id}^k are the velocity and the position on d th dimension of i th particle in k th iteration. p_{id}^k represents the d th dimension of the best solution of each particle in k th iteration. p_{gd}^k denotes the d th dimension of the best location searched by all particles in the particle swarm in k th iteration. ω represents the inertia weight:

$$\omega = \omega^{\max} - (\omega^{\max} - \omega^{\min}) \times k / k^{\max} \quad (3.36)$$

where ω^{\max} and ω^{\min} are the maximum and minimum values of the inertia weigh. k^{\max} is the total number of iteration. c_1 and c_2 are acceleration constants. ζ and η denote random numbers between 0 and 1. The $S(v_{id}^{k+1})$ in (3.35) could be expressed as $S(v_{id}^{k+1}) = 1 / (1 + \exp(-v_{id}^{k+1}))$, which produces a value between 0 and 1. As shown in (3.35), a number is generated randomly in (0, 1) and compared with $S(v_{id}^{k+1})$ to determine whether x_{id}^{k+1} equals to 0 or 1. Before transferring data to the operation phase, each particle will be screened for its validity, for any invalid particle that does not satisfy constraints (3.9)-(3.11), a small enough value is assigned to the fitness function value to avoid unnecessary calculation and reduce the run time of

the program. This process is denoted as the “Feasibility check” in Fig. 3.2.

The solution obtained by the BPSO cannot be guaranteed to be the global optima because the algorithm is essentially a heuristic evolutionary method, but BPSO could be repeated for multiple times to avoid the randomness of the results. Besides, the global convergence of this algorithm could be verified by the method of exhaustion because the planning problem has a finite total number of feasible solutions. Moreover, despite that the implementation of BPSO may have heavy computational burden, the proposed planning model is not time critical, and hybrid technologies or parallel strategies [166] could effectively improve the computation efficiency.

For each valid particle in the planning phase, results of distribution LMPs and dispatchable loads of nodes (including dispatchable CS demand) can be obtained from the computation in the operation phase. The proposed market participation model is a complicated nonlinear programming (NLP) problem with a large number of constraints, which is solved by the primary-dual interior point method to improve the computing efficiency. Then the fitness function value of each valid particle will be calculated based on the results of the two phases. In each loop, the optimal position of each particle and the best position of the particle swarm are found according to values of the fitness function. Finally, the optimal position of the particle swarm in the last step is selected as the best plan to achieve the negotiation.

3.5 Case Studies

In this section, results of the centralized planning are first obtained for benchmarking with the NBS. In addition, Nash bargaining planning with fixed electricity prices is studied and compared with the planning considering LMP model. The robustness of the Nash bargaining model is also verified with various disagreement points.

3.5.1 Test System and Experiment Data Description

As shown in Fig. 2.18, an urban area in UK with coupled distribution and transportation system is employed to demonstrate the effectiveness of the proposed methodology. In the planning process, it is necessary to consider the nature of load and factor in annual load increment [170], because the loads do not grow uniformly in the whole area. Therefore, as shown by the Lateral 1-3 in Fig. 3.4(a), the loads are divided into 3 categories: commercial, industrial, and residential, while the Lateral 4 composites loads of the 3 kinds. The annual load increment factors for the Lateral 1-4 are set to be 3%, 4%, 5% and 4%. The normalized load patterns of the 3 kinds of loads in UK are shown in Fig. 3.3. Detailed description of the DS system parameters and load data natures could be found in [167-168].

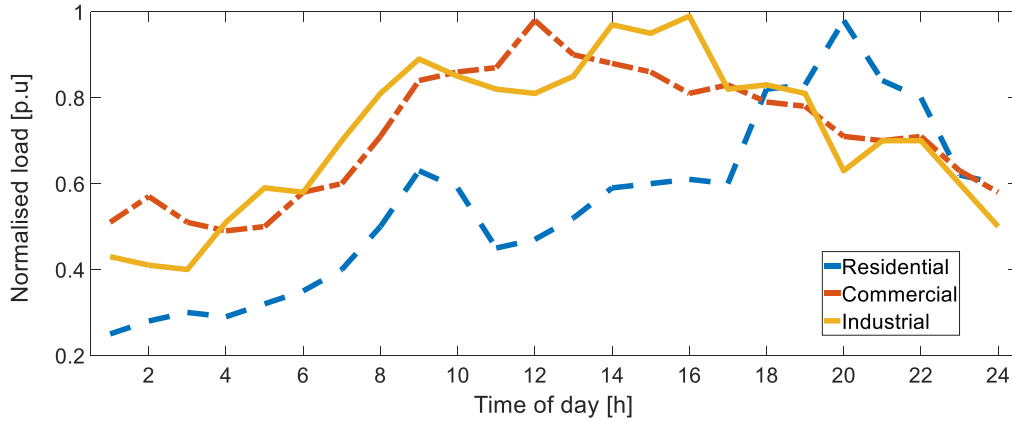


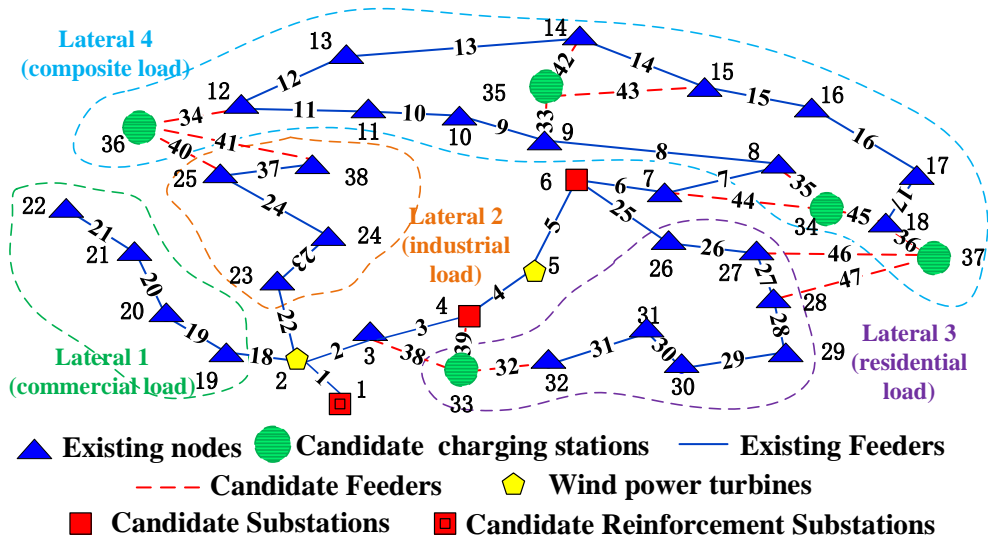
Fig. 3.3 Normalized load patterns of different load categories in the UK [169]

The candidate sets for CSes, SSs and feeders should be predefined for the planning. There are 2 major principles influencing the selection of CS candidates [46]: The service radius of each CS, R_{CS} , should not exceed the EV's driving range d_{EV}^E ; The shortest distance of 2 neighboring CSes, D_{CS} should be neither too close nor exceed their total service radius. The principles are mathematically described as

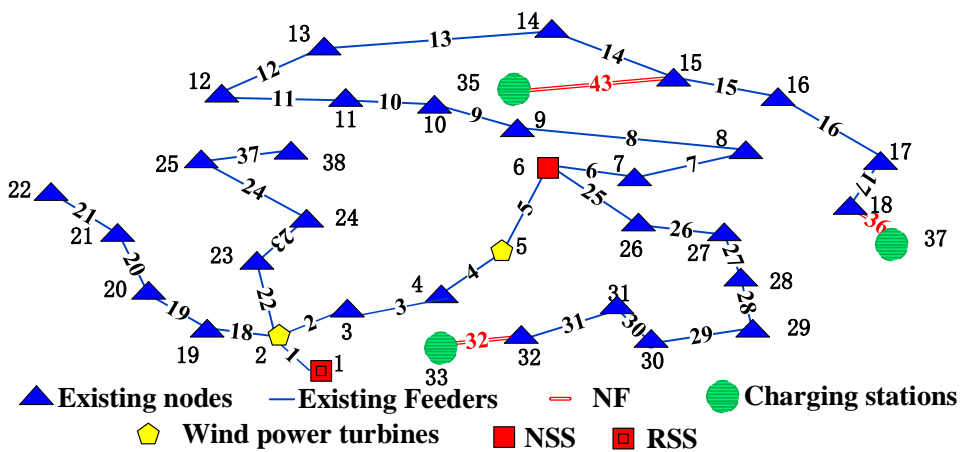
$$R_{CS} \leq d_{EV}^E \quad (3.37)$$

$$R_{CS} \leq D_{CS} \leq 2R_{CS} \quad (3.38)$$

where D_{CS} could be calculated by Dijkstra or Floyd shortest path algorithms. Other perspectives such as location adaptability and environmental friendliness should also be considered to choose the proper locations into the CS candidate sets. The feeders should be correspondingly planned to match the development of CSEs. For each candidate CS, 3 possible feeders which connect the CS and CS's neighboring nodes with relatively short length are chosen as the candidate feeders. Based on the proposed principles, there are five candidate locations (node 33-37) for the construction of three CSEs (CS1, CS2, and CS3), which are on the roads of A5, A40, A41, A404 and A1, respectively [167]. The capacity of the CS is 0.5 MW.



(a) 38-bus DS



(b) The centralized plan

Fig. 3.4 The 38-bus DS and the centralized planning result (NF: new feeder; NSS: new substations; RSS: reinforced substations)

Table 3.1 Reinforcement/Construction Costs for Substations

Substations	S1	S2	S3
Locations	Node 1	Node 4	Node 6
Initial capacity (MW)	2	--	--
Reinforcement (MW)	2	--	--
Reinforcement Cost (10 ³ US\$)	140	--	--
Planned (MW)	--	2	1.5
Construction Cost (10 ³ US\$)	--	300	250

Lengths of candidate feeders connecting the CS and the DS node are summarized in Table 3.4 with the impedance of $0.2359 + j0.2402 \Omega/\text{km}$. Loads of CSEs are assumed dispatchable and be able to provide ramp reserve. The reserve requirement for this system is 0.45 MW. The max reserve quantity for each charging station is 0.25 MW and the max ramp rate for each CS is 0.24 MW/h. Fig. 3.4(a) is the corresponding distribution network of the test system. The time horizon for the planning considered here is 5 years. Loads in node 13, 20, and 23 are set to be controllable. On nodes with both flexible and inflexible loads, the proportion of its inflexible loads and the maximum of its flexible loads are 70% and 30%, respectively. 2 wind power turbines are located at node 2 and node 5. An existing substation S1 is located in node 1 with reinforcement options. Two new candidate substations (S2 and S3) are located at node 4 and node 6. The reinforcement or construction costs for substations are described in Table 3.1. The generator offers and controllable load bids are listed in Table 3.2 [137], the parameters of construction, operation, and maintenance costs of CSEs are detailed in Table 3.3 [77] with the operation and maintenance cost of each CS estimated as 5% of its construction cost. The service charge coefficient ω_c and ζ_c are assumed 20% and 15%, respectively. For simplicity, the petrol price is assumed constant.

For the BPSO, $\omega^{\max}=0.9$, $\omega^{\min}=0.4$, $k^{\max}=1000$, $c_1=2$, $c_2=2$, n^P is 50, $D=23$. The initial particle position and velocity are randomly generated.

Table 3.2 the SS Offers and Load/CS Bids (US\$/MWh)

SS	CS1	CS2	CS3	Node13	Node20	Node23
100	150	150	150	120	120	120

Table 3.3 Costs of CSes

Candidate CSes	Locations	c_i^{csc} ($10^3\text{US}\$$)	C_i^{CSOM} ($10^3\text{US}\$$)
1	33	650	162.5
2	34	260	65
3	35	350	87.5
4	36	420	105
5	37	530	132.5

Table 3.4 Lengths of Candidate Feeders

Feeder Number	Lengths (m)	Feeder Number	Lengths (m)	Feeder Number	Lengths (m)
32	624	38	436	43	693
33	500	39	780	44	580
34	562	40	690	45	532
35	686	41	770	46	498
36	562	42	596	47	800

3.5.2 Scenarios Description

Based on the DBN forecasted results in Chapter 2, 3 scenarios, $0.9 \times$ forecasted value, forecasted value, and $1.1 \times$ forecasted value, are constructed for the TF levels and load levels respectively. Scenarios for the penetration levels of EVs and renewables are assigned in a similar way, setting the penetration values with 0.2 and 0.4 (proportions in all vehicles or total power). For example, the vector [1.1, 0.9, 0.4, 0.2] stands for the scenario that the TF is 1.1 times of the forecasted value, load level is 0.9 times of the forecasted value, the penetration of EV is 0.4 and the penetration of renewables is 0.2. Besides, the occurrence probability is set to be the same for each scenario.

3.5.3 Results of the Centralized Planning Benchmark

The centralized plan is put forward with the goal of maximizing the net benefits carried out by a single payoff. As shown in Fig. 3.4(b), the solution for the centralized planning is to have the three CSes constructed on node 33, 35, and 37 via new Feeder 32, 43, and 36, respectively, with substation S1 upgraded to higher capacity (4 MW), substation S3 constructed and no upgraded feeders. The total net benefit is US\$12,836,870 with the benefits of CSes and DS being US\$9,726,360 and US\$3,110,510, respectively.

3.5.4 The Nash Bargaining Solution

Aiming to have a fair plan to both the DS and CSes, the proposed Nash bargaining approach is used instead with its solution shown in the Fig. 3.5(a). The locations of CSes are node 33, 34 and 37 via new Feeder 32, 45 and 36, respectively. Again, Substation S1 need to be reinforced with higher capacity and no feeders should be upgraded. Substation S3 needs to be constructed. Meanwhile, the benefits of CSes and DS are US\$9,271,810 and US\$3,365,920.

3.5.5 Discussion: A Comparison between the two Schemes

In the deregulated environment, the centralized mode itself, which assumes both the DS and CSes belonging to one entity, is contrary to the facts and its solution is therefore inappropriate for the real world. Compared to the centralized program, Nash bargaining tries to achieve the most fair and Pareto-efficient payoff allocation for the two independent participants by choosing suitable CS locations and new feeders. The outcomes of the proposed centralized and negotiated schemes, including the benefits and the construction plans, are summarized in Table 3.5.

to support the development of EVs. The payoff gap between DS and CS (defined as $u^{\text{CS}} - v^{\text{DC}}$) is also 10.73% smaller in the case of Nash bargaining (US\$5,905,890 vs US\$6,615,850), which indicates a more fair solution for the DS and CS could be achieved by the proposed negotiated model.

3.5.6 Nash Solutions with Fixed Electricity Prices

In the traditional DS, usually the electricity prices on all nodes are set to a fixed value decided by the DSO. This widely used fixed electricity price mechanism may lead to congestion, voltage collapse, and other problems in the DS [59]. To show the advantage of the proposed LMP model, the traditional DS price mechanism with fixed electricity price values is utilized as the *benchmark case* and compared with the proposed novel LMP model. It is assumed that in the benchmark case, the electricity price of all loads is set to a fixed average value over the entire timespan. Results with different fixed electricity prices are detailed in Table 3.6. It can be observed that the Nash solution cannot be obtained until the price increases to 111 US\$/MWh. The planning solution with fixed electricity price of 111 and 112 US\$/MWh is demonstrated in Fig. 3.5(b). When the price is below 111 US\$/MWh, Nash bargaining fails, and no agreement is achieved between the CS company and the DS. This is because the benefit of the DS is less than zero when the price is not high enough, and the negotiation result is below its threatening point.

Table 3.7 shows the electricity prices of the CSes in the LMP model. It is clear that the electricity price obtained via the market mechanism is significantly higher than the minimum found using the fixed electricity price model in Table 3.6. The DS would therefore make more profits by providing electricity service to the CSes as well as EV users, and the risks of Nash bargaining failure could be avoided with acceptable electricity prices for both DS and CSes by using the LMP model. It could therefore be concluded that well-designed market mechanism, as described in this work, will effectively help the participants reach the planning bargaining

solutions, and facilitate the development of EV CSEs as well as the popularization of EVs.

Table 3.6 Nash Solutions with fixed electricity prices

Electricity Price(US\$/MWh)	u^{CS} (US\$)	v^{DC} (US\$)	Construction Plan			
			CS	NF	NSS	RSS
108	--	--	--	--	--	--
109	--	--	--	--	--	--
110	--	--	--	--	--	--
111	9344270	43542	33, 36, 37	38, 40, 46	S3	S1
112	9356880	229819	33, 36, 37	38, 40, 46	S3	S1

CS: the location of CS; NF: new feeder; NSS: new substations; RSS: reinforced substations

Table 3.7 Electricity prices in the LMP model

Node Number	Electricity Price(US\$/MWh)
34	116.734
35	149.934
37	149.958

3.5.7 Nash Solutions with Different Disagreement Points

To test the robustness of the proposed Nash bargaining model, results are obtained by choosing different disagreement points. Except the disagreement point (0, 0), another 5 disagreement points are selected as benchmarks, the results of which are shown in Table 3.8. It can be seen that Nash solutions remain stable although disagreement points vary in a certain range. The planning result changes only when the disagreement point of one participant becomes very large, for example, US\$6×10⁶ required by the CS. The results demonstrate that the proposed model is promising for practical application.

Table 3.8 Nash Solutions with Different Disagreement Points

Disagreement Point (10 ⁶ US\$)	u^{CS} (US\$)	v^{DC} (US\$)	Construction Plan			
			CS	NF	NSS	RSS
(0, 0)	9271810	3365920	33, 34, 37	32, 45, 36	S3	S1
(2, 2)	9271810	3365920	33, 34, 37	32, 45, 36	S3	S1
(3, 1)	9271810	3365920	33, 34, 37	32, 45, 36	S3	S1
(3, 3)	9271810	3365920	33, 34, 37	32, 45, 36	S3	S1
(4, 3)	9271810	3365920	33, 34, 37	32, 45, 36	S3	S1
(6, 1)	9726360	3110510	33, 35, 37	32, 43, 36	S3	S1

CS: the location of CS; NF: new feeder; NSS: new substations; RSS: reinforced substations

3.6 Summary

This chapter focuses on the cooperative planning of CSEs and DS. The proposed Nash bargaining strategy is a joint program to plan for the future development of EV CSEs and DS. Different from most existing research, this work considers the practical situation that CSEs and the DS do not belong to one entity and operate in a deregulated market environment. The obtained Nash bargaining solution is an agreement achieved between both participants to ensure players are treated fairly. Moreover, a new EV participated LMP model is applied in this chapter to realistically simulate the impact of electricity market environment on the planning results, which is proved for its immediate and far-reaching significance to promote the development of CSEs as well as EVs.

Chapter IV

Multiple Group Search Optimization based on Decomposition for Multi-Objective Dispatch with Electric Vehicle and Wind Power Uncertainties

4.1 Introduction

Once CSes are constructed according to the planning results, the operation of CSes should be investigated to ensure the high efficiency and reliability of CSes and DS. Electric power dispatch is an essential function required to determine the optimal steady-state operation of dispatchable generating plants. While the number of EVs increases rapidly, the application potential of EVs should be accounted in electric power dispatch with several conflicting and competing objectives such as providing V2G service or coordinating with wind power. Moreover, the uncertainties of wind power and EVs should be properly handled while the power dispatch involves both wind power and EVs. Nevertheless, research considering these aspects is rarely conducted in the literature yet.

In this chapter, an innovative highly constrained multi-objective dispatch model considering the uncertainties of EVs and wind power is set up. Furthermore, a multiple group search optimization based on decomposition (MGSO/D) is proposed to solve this multi-objective optimization problem (MOOP). Specifically, the decomposition approach aims to reduce the computational complexity, and the innovatively incorporated producer-scrounger model aims to improve the diversity and spanning of the Pareto-optimal front (PF). Meanwhile, the estimation error punishment is utilized to take account of the uncertainties. The performance of MGSO/D and the effectiveness of the uncertainty model are investigated on the

IEEE 30-bus system (2 wind farms and 2 CSes) and 118-bus system (6 wind farms and 5 CSes).

4.2 Formulation of the Multi-objective Power Dispatch Problem

4.2.1 Optimization Objectives Considering Uncertainties

Extensively existed uncertainties in the power system operation with a high penetration of EVs and wind power should be properly tackled. Here, the estimation error punishment method [98][138] are utilized to coordinate the stochastic availability of V2G and wind power, and reduce the loss resulted from uncertainties. In addition, the objective functions involved REs or EVs are derived according to the probability density functions (PDFs) to account their randomness. Meanwhile, operations of the smart grids usually have conflicting multi-objectives, and a family of Pareto-optimal solutions that are the acceptable tradeoffs among the objectives should be found. In this work, reducing generation cost, emissions and power loss are chosen as the most important objectives of the system operators.

(1) Generation Cost Objective:

Because of the energy storage ability of EV batteries, it is widely believed that EVs could be coordinated dispatched to provide the V2G power to the power system [92][98]. Due to the length limitation, this work only focuses on EV power dispatch in the system operation and omits the EV information interaction or market participation problems. All EVs charged on the same bus are modeled as an aggregator and provides V2G power as a virtual power plant (VPP). On this premise, the uncertainties of V2G power as well as wind power are considered, and the battery degradation resulted by V2G is accounted.

Therefore, the economic objective f_1 is formulated in (4.1) to minimize the expected total generation cost, which is consisted of 3 components: The first component denotes the cost summation of thermal generators. The second and third parts represent the cost of EVs V2G power and the cost of wind power

generators respectively. EVs and wind power uncertainties are incorporated to this objective function.

$$\begin{aligned}
f_1 = & \sum_{k=1}^{N^T} C_k^T(T_k) \\
& + \sum_{n=1}^{N^E} \left[C_n^E(E_n) + C_n^{E,p}(E_n^{AV}, E_n) + C_n^{E,r}(E_n^{AV}, E_n) + C_n^B(E_n) \right] \\
& + \sum_{m=1}^{N^W} \left[C_m^W(W_m) + C_m^{W,p}(W_m^{AV}, W_m) + C_m^{W,r}(W_m^{AV}, W_m) \right] \quad (4.1)
\end{aligned}$$

where N^W , N^T and N^E are the numbers of wind power generators, thermal generators, and nodes with V2G facilities installed; T_k is the active power generation of the k th thermal generator; C_k^T is the cost of the conventional generator; E_n and E_n^{AV} denotes the scheduled V2G power and actual available V2G output on node n ; C_n^E , $C_n^{E,p}$ and $C_n^{E,r}$ are the V2G direct operation cost, underestimated penalty cost and overestimated penalty cost; C_n^B is the battery degradation cost; W_m and W_m^{AV} are the scheduled and the actual available output of wind generator m ; C_m^W , $C_m^{W,p}$ and $C_m^{W,r}$ are the direct cost, underestimated penalty cost and overestimated penalty cost of the m th wind generator, respectively.

The first component (thermal generation cost) is non-convex because of the valve-point effects, which could be modeled by ripple curves [139]. Therefore, the cost function for a conventional generator is represented as a combination of a quadratic function and a sine component term:

$$C_k^T(T_k) = a_k T_k^2 + b_k T_k + c_k + |d_k \sin[e_k (T_k^{\min} - T_k)]| \quad (4.2)$$

where a_k , b_k , c_k , d_k and e_k are cost coefficients for the k th conventional generator. T_k^{\min} is the minimum active power output of the k th thermal generator.

The second component (cost of V2G power) is divided into four parts, including $C_n^E(E_n)$, $C_n^{E,p}(E_n^{AV}, E_n)$, $C_n^{E,r}(E_n^{AV}, E_n)$ and $C_n^B(E_n)$ [92][140][141]. The first part is the scheduled power direct cost $C_n^E(E_n)$, which comes from the electricity purchasing cost to charge the batteries of EVs:

$$C_n^E(E_n) = g_n^E E_n \quad (4.3)$$

where g_n^E represents coefficients of direct operation cost.

Based on the conclusion of [99], the PDF of the actual V2G power $f_P(E_n^{AV})$ is assumed a normal distribution:

$$f_P(E_n^{AV}) = (1/\sqrt{2\pi\phi^2}) \cdot \exp[-(E_n^{AV} - \mu)^2 / (2\phi^2)] \quad (4.4)$$

where μ and ϕ are the mean and standard deviation of the normal distribution respectively. Because the outputs of EVs are highly stochastic, the system power dispatch based on the forecasted data will have deviations. If the scheduled power is less than the available power, surplus power has to be wasted. In the other aspect, if the scheduled power is more than the available power, reserve service is needed to compensate this imbalance. According to the PDF in (4.4) and this estimation error punishment principle, the second and third parts, underestimated penalty cost $C_n^{E,p}(E_n^{AV}, E_n)$ and overestimated penalty cost $C_n^{E,r}(E_n^{AV}, E_n)$, are derived as

$$\begin{aligned} C_n^{E,p}(E_n^{AV}, E_n) &= \varepsilon_n^{E,p} \int_{E_n}^{+\infty} (E_n^{AV} - E_n) f_P(E_n^{AV}) dE_n^{AV} \\ &= \frac{\varepsilon_n^{E,p}}{2} (\mu - E_n) \left[1 + \operatorname{erf}\left(\frac{\mu - E_n}{\sqrt{2}\phi}\right) + \frac{\varepsilon_n^{E,p} \cdot \phi}{\sqrt{2\pi}} e^{-\frac{(\mu - E_n)^2}{2\phi^2}} \right] \end{aligned} \quad (4.5)$$

$$\begin{aligned} C_n^{E,r}(E_n^{AV}, E_n) &= \varepsilon_n^{E,r} \int_0^{E_n} (E_n^{AV} - E_n) f_P(E_n^{AV}) dE_n^{AV} \\ &= (\varepsilon_n^{E,r} \cdot \phi / \sqrt{2\pi}) \left\{ \exp\left(\frac{-\mu^2}{2\phi^2}\right) - \exp\left[\frac{-(\mu - E_n)^2}{2\phi^2}\right] \right\} \\ &\quad + (\varepsilon_n^{E,r} / 2) (\mu - E_n) \left\{ \operatorname{erf}\left[\mu / (\sqrt{2}\phi)\right] - \operatorname{erf}\left[(\mu - E_n) / (\sqrt{2}\phi)\right] \right\} \end{aligned} \quad (4.6)$$

where $\operatorname{erf}(\bullet)$ represents the Gauss error function, which could be calculated with numerical integration; $\varepsilon_n^{E,p}$ and $\varepsilon_n^{E,r}$ represent coefficients of underestimated penalty and overestimated penalty cost of the V2G power on node n , respectively.

Providing V2G power by EVs will accelerate the battery degradation, the cost of which could be calculated in proportion to the V2G power. Besides, additional compensation should be paid to motivate EV owners to participate in the V2G service. Hence the fourth part, total degradation cost $C_n^B(E_n)$, should be set higher

than the direct battery degradation cost:

$$C_n^B(E_n) = (1+r)[C^{BI}/(1000L^C E^B d^{DOD})]E_n \quad (4.7)$$

where r is the EV aggregator operation cost coefficient for additional compensation; C^{BI} denotes the battery investment cost; L^C corresponds to EV's battery cycle life at a certain depth of discharge (DoD); E^B represents EV's battery capacity; d^{DOD} is the DoD to determine L^C ; the number 1000 is applied to convert the kWh to MWh.

Similarly, the cost of a wind power generator consists of 3 parts, C_m^W , $C_m^{W,p}$ and $C_m^{W,r}$. The direct cost C_m^W is:

$$C_m^W(W_m) = g_m^W W_m \quad (4.8)$$

where g_m^W denotes the coefficient of direct cost. C_m^W accounts the cost paid by system operator to the wind power owners. It should be noted that C_m^W is 0 if the generators are owned by the system operator because the incremental cost of wind power is 0. As stated before, the underestimation and overestimation of wind power will lead to additional losses. Considering this uncertainty, the expectations of the underestimated penalty cost $C_m^{W,p}(W_m^{AV}, W_m)$ and overestimated penalty cost $C_m^{W,r}(W_m^{AV}, W_m)$ are derived as [138]:

$$C_m^{W,p}(W_m^{AV}, W_m) = \varepsilon_m^{W,p} \int_{w_m}^{w_m^r} (W_m^{AV} - W_m) f_W(W_m^{AV}) dW_m^{AV} \quad (4.9)$$

$$C_m^{W,r}(W_m^{AV}, W_m) = \varepsilon_m^{W,r} \int_0^{w_m} (W_m^{AV} - W_m) f_W(W_m^{AV}) dW_m^{AV} \quad (4.10)$$

where $\varepsilon_m^{W,p}$ and $\varepsilon_m^{W,r}$ denote coefficients of underestimated penalty and overestimated penalty cost for the m th wind generator. w_m^r is the rated wind power of the m th wind generator and $f_W(W_m^{AV})$ corresponds to the PDF of wind power, which can be described as follows [138]:

$$f_W(W_m^{AV}) = \frac{\gamma l v_m}{h} \left[\frac{(1+\rho l)v_m}{h} \right]^{\gamma-1} \exp\left\{-\left[\frac{(1+\rho l)v_m}{h}\right]^\gamma\right\} \quad (4.11)$$

where v_m is the wind speed of the m th wind generator, h and γ accounts for the scale factor and sharp factor at a given location, l denotes the ratio of linear range of wind speed to cut-in wind speed and ρ represents the ratio of wind power output

to the rated wind power. It should be noted that the integration results could be easily obtained by the quadrature methods.

(2) Emission Objective

The second objective aims to reduce emissions from thermal power plants [154]. The overall emission in ton/h could be formulated as

$$f_2 = \sum_{k=1}^{N^T} 10^{-2} (\alpha_k T_k^2 + \beta_k T_k + \zeta_k + \chi_k \exp(\lambda_k T_k)) \quad (4.12)$$

where $\alpha_k, \beta_k, \zeta_k, \chi_k$ and λ_k are the emission coefficients of the k th thermal generator.

(3) Power Loss Objective

The third objective is to reduce the system power loss. The goal is to minimize the network transmission loss with several operating constraints, which could be solved using Newton-Raphson method and derived as follows:

$$f_3 = P^{\text{LOSS}} = \sum_{ij=1}^{N^L} (G_{ij} V_i^2 + V_j^2 - 2V_i V_j \cos(\delta_i - \delta_j)) \quad (4.13)$$

where N^L represents the number of transmission lines. V_i, V_j are respectively the voltage magnitude of bus i and bus j . δ_i and δ_j denote the voltage angle of node i and node j , and G_{ij} corresponds to the conductance of the line between node i and j .

4.2.2 MOOP Constraints

(1) Power Balance Constraints:

Power balance equality constraint indicates that the total electric power generation from thermal units, wind power and V2G power should be equal to the total power loss P^{LOSS} plus the total load P^{D} :

$$\sum_{k=1}^{N^T} T_k + \sum_{m=1}^{N^W} W_m + \sum_{n=1}^{N^E} E_n - P^{\text{D}} - P^{\text{LOSS}} = 0 \quad (4.14)$$

This constraint could be satisfied by redistributing the total active power output after the power flow calculation.

(2) Transmission Line Apparent Power Constraints:

This constraint is to guarantee that the apparent power of the transmission line from bus i to j (and j to i) S_{ij} (and S_{ji}) should be limited within its maximum loading capacity $S_{ij,max}$ for secure operation of transmission system. It can be formulated as:

$$\max[|S_{ij}|, |S_{ji}|] \leq S_{ij,max} \quad ij = 1, 2, \dots, N^L \quad (4.15)$$

(3) Generation Capacity Constraints :

In practice, thermal generators have prohibited operating zones (POZs) because of the physical constraints of power plant components (e.g. shaft bearing tremor is magnified in some operating zones) [142]. For a POZ, the generator could only operate below or above this zone. These disconnected sub-zones form a non-convex decision space and make the proposed MOOP highly nonsmoothed, non-continuous and nonlinear. The output delivered by the k th generator while considering POZ is given in (4.16).

$$\begin{cases} T_k^{\min} \leq T_k \leq T_{k,1}^{lb} \\ T_{k,u-1}^{ub} \leq T_k \leq T_{k,u}^{lb}, u = 2, 3, \dots, NP_s \\ T_{k,u}^{ub} \leq T_k \leq T_k^{\max}, u = NP_s \end{cases} \quad (4.16)$$

where T_k^{\min} , T_k^{\max} are the minimum and maximum active output power of k th generator. $T_{k,u}^{lb}$ and $T_{k,u}^{ub}$ represent the lower and upper limits of the k th generator with u th POZ, and NP_s corresponds to the number of POZ of k th generator.

Besides, the generation capacity limits of the scheduled V2G power and wind power are stated as:

$$E_n^{\min} \leq E_n \leq E_n^{\max} \quad (4.17)$$

$$W_m^{\min} \leq W_m \leq W_m^{\max} \quad (4.18)$$

where E_n^{\min} and E_n^{\max} account for the lower and upper bound of the scheduled V2G power n while W_m^{\min} and W_m^{\max} account for the lower and upper limits of the scheduled wind power m .

4.3 Multiple Group Search Optimization based on Decomposition

4.3.1 General Framework

The proposed MOOP is very hard to solve and easily trapped by local optima due to its complicated nonconvex and nonlinear nature. To overcome this obstacle, a novel MGSO/D method, which combines 2 powerful optimization tools, is applied in this work. Firstly, decomposition strategy is used to divide the MOOP into a few subproblems to optimize simultaneously and reduce the computational complexity [143]. Secondly, the producer-scrounger model is innovatively incorporated as the main population generation methodology [104] in each subproblem to enhance the population diversity. Under this mechanism, the population is no longer evaluated iteratively like GSO, thus the efficiency of the proposed method is improved. To the best of authors' knowledge, it is the first time to employ the combination of advantages of decomposition and producer-scrounger mechanism to solve the proposed MOOP considering EVs and wind power uncertainties.

4.3.2 Decomposition of the Proposed MOOP

The Tchebycheff approach [143] is employed to decompose the MOOP with N^{OBJ} objectives into C scalar optimization subproblems by adjusting the j th subproblem's weight vector $\boldsymbol{\lambda}^j = (\lambda_1^j, \dots, \lambda_{N^{\text{OBJ}}}^j)^T$, and the objective function of the j th subproblem is

$$\min_{\mathbf{x} \in \Omega} g^{te}(\mathbf{x} | \boldsymbol{\lambda}^j, \mathbf{z}) = \max_{1 \leq i \leq N^{\text{OBJ}}} \{ \lambda_i^j | f_i(\mathbf{x}) - z_i | \} \quad (4.19)$$

where Ω is the decision (variable) space. $\mathbf{z} = (z_1, \dots, z_{N^{\text{OBJ}}})^T$ is the reference point vector and z_i is to store the best i th single objective fitness value for each $i=1, \dots, N^{\text{OBJ}}$. At each run, MGSO/D will minimize all these C subproblems simultaneously, and the best solutions obtained so far for every subproblem constitute the population. The j th subproblem is optimized by using only the

current solutions of its neighborhood subproblems because it is believed that the neighboring subproblems' optimal solutions should be close to each other and be helpful for the optimization.

4.3.3 Innovatively Incorporated Producer-Scrounger Model

Producer-scrounger model of GSO is an efficient framework inspired by the animal searching behavior. It is innovatively incorporated in the proposed algorithm for its merit of providing diverse and well-scattered population, which contributes to the resulted PF's performance. The population of the GSO is defined as a *group* and individuals in the population are defined as *members*. GSO group consists of *producers* for resource searching, *scroungers* for joining resources uncovered by others, and *rangers* for performing random walks to avoid local optimum [104]. If the optimal solution is in an N -dimensional search space, each member has a current position $\mathbf{x} \in \mathbf{R}^N$ and a head angle $\boldsymbol{\varphi} = (\varphi_1, \dots, \varphi_{N-1}) \in \mathbf{R}^{N-1}$. The search direction of each member is a unit vector $\mathbf{D}(\boldsymbol{\varphi}) = (d_1, \dots, d_N) \in \mathbf{R}^N$, which can be solved from $\boldsymbol{\varphi}$ by a polar to Cartesian coordinate transformation [155]:

$$d_1 = \prod_{q=1}^{N-1} \cos(\varphi_q) \quad (4.20)$$

$$d_j = \sin(\varphi_{j-1}) \cdot \prod_{q=j}^{N-1} \cos(\varphi_q) \quad (j = 2, \dots, N-1) \quad (4.21)$$

$$d_N = \sin(\varphi_{N-1}) \quad (4.22)$$

One subproblem and its $Y-1$ selected neighbor subproblem combines a searching group, and Y swarm members of each searching group are categorized into producers, scroungers and rangers to carry out different searching strategies:

(1) *Producer:*

The producer uses the food searching mechanism inspired from animals to find new optimal results. The member with the best single objective fitness is designated to be the producer. The solution of the chosen objective has the greatest

orders of magnitude among all objectives. The producer will scan the vision field, which is distinguished by the current position \mathbf{x}_p , maximum pursuit angle $\theta_{\max} \in \mathbb{R}^1$, and maximum pursuit distance $l_{\max} \in \mathbb{R}^1$, by randomly sampling 3 points [104]: a point at zero degree:

$$\mathbf{x}_z = \mathbf{x}_p + r_1 l_{\max} \mathbf{D}_p(\boldsymbol{\varphi}) \quad (4.23)$$

a point in the left-hand side hypercube:

$$\mathbf{x}_l = \mathbf{x}_p + r_1 l_{\max} \mathbf{D}_p(\boldsymbol{\varphi} - \mathbf{r}_2 \theta_{\max} / 2) \quad (4.24)$$

and a point in the right-hand side hypercube:

$$\mathbf{x}_r = \mathbf{x}_p + r_1 l_{\max} \mathbf{D}_p(\boldsymbol{\varphi} + \mathbf{r}_2 \theta_{\max} / 2) \quad (4.25)$$

where $r_1 \in \mathbb{R}^1$ represents a normal distributed random number with average 0 and standard deviation 1; $\mathbf{r}_2 \in \mathbb{R}^{N-1}$ denotes a uniformly distributed random sequence in the range (0,1).

The producer tries to search the best point, and if there is a point in these 3 points with better resource (better fitness value) than the current position, the producer will move to the point. If not, it will not change its position and update its head to a new angle $\boldsymbol{\varphi}^{new}$:

$$\boldsymbol{\varphi}^{new} = \boldsymbol{\varphi} + \mathbf{r}_2 \alpha_{\max} \quad (4.26)$$

where $\alpha_{\max} \in \mathbb{R}^1$ is the maximum turning angle.

(2) Scroungers:

Part of group members are chosen as scroungers to join the resources found by the producer, whose behavior is to move across for searching in the immediate area around the producer. This behavior of random walking toward the producer could be expressed as:

$$\mathbf{x}^{new} = \mathbf{x} + \mathbf{r}_3 \circ (\mathbf{x}_p - \mathbf{x}) \quad (4.27)$$

where \mathbf{x}^{new} is the new position; $\mathbf{r}_3 \in \mathbb{R}^N$ is a uniform random vector in the range (0, 1); Operator “ \circ ” figures the entry-wise product of 2 matrices. During this

scrounging, the scrounger will go on searching for other chances to join [104], and the scrounger's head angle is updated by (4.26).

(3) *Rangers*:

Other group members are rangers, which employ random walks to perform efficient searching that starts without cues leading to randomly distributed resources and benefits the population diversity. Ranger's head angle is updated in the similar way of (4.26) but the α_{\max} is set to be 2π to improve its searching ability:

$$\boldsymbol{\varphi}^{new} = \boldsymbol{\varphi} + 2\pi\mathbf{r}_4 \quad (4.28)$$

where $\mathbf{r}_4 \in \mathbb{R}^{N-1}$ represents a uniform distributed random sequence in the range (0,1), and then the ranger selects a random distance $a \cdot l_{\max}$ and moves to the new position:

$$\mathbf{x}^{new} = \mathbf{x} + a \cdot r_5 l_{\max} \mathbf{D}(\boldsymbol{\varphi}^{new}) \quad (4.29)$$

where $r_5 \in \mathbb{R}^1$ denotes a normal distributed random number with mean 0 and standard deviation 1 and $a \in \mathbb{R}^1$ is a constant.

4.3.4 Solving Process

The major steps of the framework are demonstrated below and depicted in Fig. 4.1.

Step 1) Initialization.

Step 1.1) Set $ER = \emptyset$, where ER is the external repository [143] to preserve the nondominated solutions found during the search process.

Step 1.2) Generate C evenly spread weight vectors $\boldsymbol{\lambda}^1, \dots, \boldsymbol{\lambda}^C$ related to the C subproblems respectively.

Step 1.3) Calculate the *Euclidean* distance between any 2 weight vectors and then figure out the B nearest weight vectors of each weight vector. For each $j=1, \dots, C$, define its neighborhood set to be $NE(j)=\{j_1, \dots, j_B\}$, where $\{\boldsymbol{\lambda}^{j_1}, \dots, \boldsymbol{\lambda}^{j_B}\}$ are the B nearest weight vectors of $\boldsymbol{\lambda}^j$.

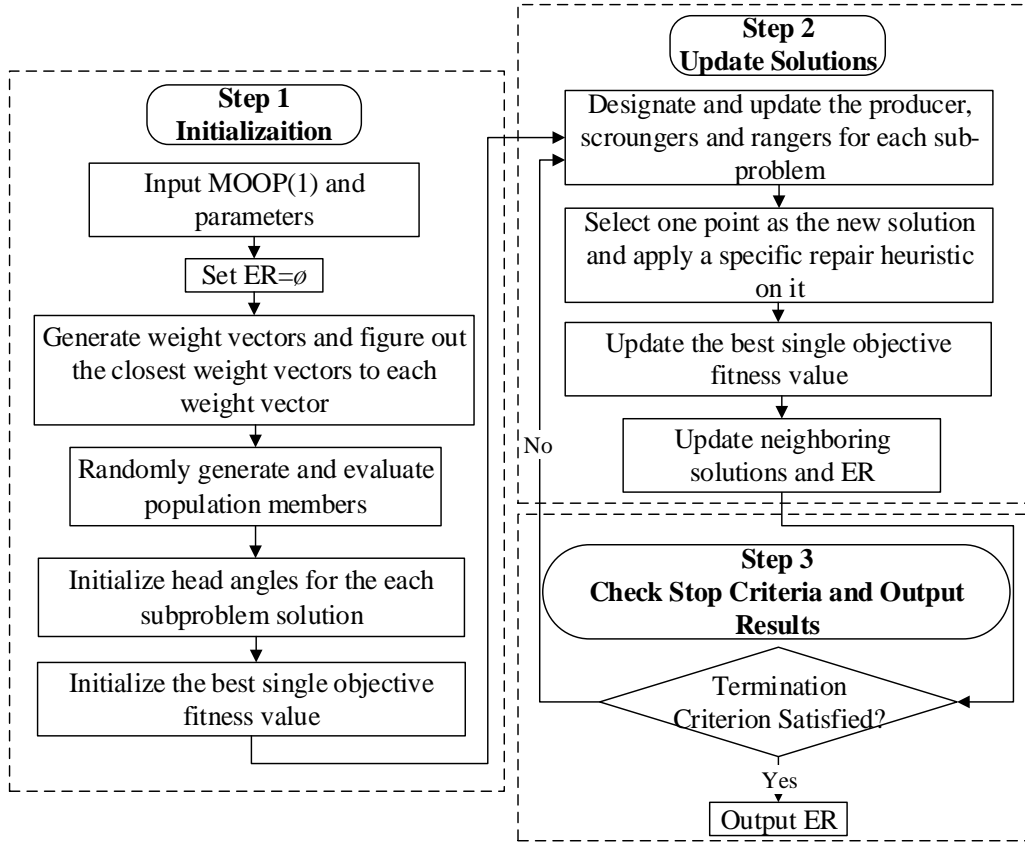


Fig. 4.1 Flowchart of MGSO/D to solve the proposed problem

Step 1.4) Randomly generate an initial population $\mathbf{x}^1, \dots, \mathbf{x}^C$. For the j th subproblem, calculate its fitness function value vector $\mathbf{FV}^j = F(\mathbf{x}^j)$. Randomly initialize head angles ϕ for the solution of each subproblem. Initialize \mathbf{z} randomly.

Step 2) Updating subproblem solutions.

For $j=1, \dots, C$, perform steps as follows:

Step 2.1) Reproduction:

(1) Producer Designate the best individual in B group members as the producer $x^w(\phi^w)$ with the index w .

(2) Producing The producer makes producing by (4.23)-(4.26).

(3) Scrounging Except the producer, randomly choose $[80\% \cdot (Y-1)]$ members from $B-1$ group members as scroungers and carry out scrounging using (4.26)-(4.27).

(4) Ranging Except the producer and scroungers, other members are rangers

and carry out ranging using (4.28)-(4.29). Then randomly select one point from the Y points as the new solution \mathbf{y} .

Step 2.2) Improvement: apply the greedy repair producer [144] on \mathbf{y} to produce \mathbf{y}' to eliminate the infeasible solutions and improve the efficiency of the solving process.

Step 2.3) The updating of \mathbf{z} : for every $i=1, \dots, N^{\text{OBJ}}$, when $z_i > f_i(\mathbf{y}')$, set $z_i = f_i(\mathbf{y}')$.

Step 2.4) The updating of Neighboring Solutions: For every index $i \in NE(j)$, if $g^{te}(\mathbf{y}' / \lambda^i, \mathbf{z}) \leq g^{te}(\mathbf{x}^i / \lambda^i, \mathbf{z})$, set $\mathbf{x}^i = \mathbf{y}'$ and $FV^i = F(\mathbf{y}')$.

Step 2.5) The updating of ER: Omit all the vectors dominated by $F(\mathbf{y}')$ from ER, and add $F(\mathbf{y}')$ to ER otherwise.

Step 3) Termination.

If stopping criteria is met, terminate and export ER. If not, go back to **Step 2)**.

4.3.5 Performance Metrics of the Proposed MGSO/D Method

It is hoped that the obtained PF by the MGSO/D could be close enough to the true PF. However, the true PF is very hard to figure out and guarantee, and the reference PF [145] is used instead. Here the PF solutions obtained by the NSGA-II [146], MGSO [147], MOEA/D [143] and MGSO/D are ranked by dominance comparisons to select the reference PF. Afterwards, 4 indices are utilized to compare the PF solution quality of MGSO/D with other typical algorithms. 1) *Convergence metric*: measuring the closeness degree from the reference PF to the obtained PF. For each obtained PF, the minimum Euclidean distance between each solution on the obtained PF and solutions on the reference PF is computed, and the mean of these distances is defined as the convergence metric [146]. 2) *Span metric*: measuring the normalized Euclidean distance of the boundary solutions [148] for MOOP objectives, which estimates the spread of the PFs. 3) *Spacing metric* [149]: calculating the relative crowding distance between adjacent solutions on the obtained PF. This metric is adopted to evaluate the distribution uniformity of the

resulting PF. 4) l_{\max}/l_{\min} *metric* [150]: It is the ratio of maximum distance of consecutive Pareto points to the minimum distance, which is an indicator to measure the spatial distribution of PF solutions and can be the supplement of the spacing metric.

4.4 Numerical Results and Analysis

4.4.1 Investigation on the Modified IEEE 30-Bus System

A modified IEEE 30-bus system is considered to evaluate the proposed model and algorithm for dual-objective dispatch. The topology and parameters including the thermal generation cost and emission coefficients can be found in [151]. 2 wind farms are located on node 10 and 15, while 2 EV CSes are located on node 3 and 18. Their relevant information is respectively depicted in Table 4.1 [98][138] and Table 4.2 [98]. For fair comparisons, the maximum numbers of generations in 4 benchmarks are equal to 200. To determine the optimum settings for each algorithm, 20 independent runs of each algorithm are carried out. The key settings for the algorithm are: $Y=3$, $C=33$, $B=20$.

(1) Case 1:

A dual-objective dispatch is studied to optimize the generation cost f_1 and emission f_2 in this case. The averages of 4 performance metrics on convergence, span, l_{\max}/l_{\min} and spacing measures over the 20 optimization runs for different algorithms are tabulated in Table 4.3.

In this case, the reference PF used for computing the convergence metric consists of 257 nondominated solutions, in which 48.63% and 51.37% of the solutions are offered by MOEA/D and MGSO/D, respectively. It reveals that all of the solutions obtained by NSGA-II and MGSO are dominated by those obtained by MOEA/D and MGSO/D, and MGSO/D has contributed more to form the reference PF solutions than MOEA/D. It can also be observed that the solutions obtained by the proposed algorithm are closer to the true PF.

Table 4.1 Parameter setting

Parameters	Value	Parameters	Value
γ	2,4	C^{BI}/E^B	100\$/kWh
l	2	L^C	1000
v_m	5m/s	d^{DOD}	0.8
h	5,10	μ	1
r	0.2	ϕ	6

Table 4.2 Cost coefficients of wind and V2G power

Wind Generator	Value	V2G Power	Value
g_m^W	10\$/MWh	g_n^E	65\$/MWh
$\varepsilon_m^{W,p}$	30\$/MWh	$\varepsilon_n^{E,p}$	30\$/MWh
$\varepsilon_m^{W,r}$	70\$/MWh	$\varepsilon_n^{E,r}$	70\$/MWh

Table 4.3 Resulting statistics of performance metrics in Case 1

Case 1	NSGA-II	MGSO	MOEA/D	MGSO/D
Convergence	0.040145	0.047759	0.017542	0.013515
Span	0.457428	0.913644	1.052471	1.309735
l_{\max}/l_{\min}	64.20240	58.00052	10.31539	7.460752
Spacing	0.106931	0.219106	0.018393	0.017782

It could be pointed out from Table 4.3 that the convergence metric of the proposed algorithm is much lower than those of other benchmarks, which means MGSO/D can most effectively obtain the non-dominated solutions in the separated feasible islands. Besides, the maximum normalized span indicates MGSO/D has a more powerful global exploratory capability than other algorithms. Furthermore, the proposed algorithm performs best in the l_{\max}/l_{\min} and spacing metric, and it illustrates that the PF outlines of proposed algorithm are more uniformly-distributed. Therefore, it can be concluded the proposed algorithm can markedly outperform other 3 methods, and provides satisfactory performance on these 4 indices.

Table 4.4 listed the best solutions for emission and generation cost obtained by the boundary solutions in the PFs of the best runs of all algorithms and the corresponding PF solutions are plotted in Fig. 4.2. The results indicate that the best run of MGSO/D achieves outstanding diversity with 2 better boundary solutions

compared with other 3 algorithms. Meanwhile, the best PF with MGSO/D could find solutions with much better fitness on the objectives of the generation cost and the emission compared to other 3 algorithms. The decomposition approach helps MGSO/D have higher exploratory capability than MGSO. Meanwhile, the producer- scrounger model also enhances its searching ability than MOEA/D.

Table 4.4 Comparison of best solutions in Case 1

Case 1	Best generation cost				Best emission			
	A	B	C	D	A	B	C	D
W_1	0.6012	0.5345	0.9047	0.9635	0.6009	0.5837	0.2351	0.3076
W_2	0.4080	0.4399	0.6281	0.7434	0.8074	0.3430	0.0901	0.1709
E_1	0.4587	0.2839	0.7785	0.4487	0.5431	0.4262	0.0084	0.0436
E_2	0.1379	0.2580	0.0176	0.1578	0.0399	0.5514	0.0771	0.0090
T_1	0.1351	0.1380	0.0500	0.0627	0.0928	0.0386	0.0620	0.3510
T_2	0.1789	0.2679	0.1215	0.0680	0.0894	0.2669	0.4014	0.3937
T_3	0.1989	0.2618	0.0588	0.1566	0.0947	0.3227	0.4991	0.4330
T_4	0.2362	0.2205	0.1936	0.1971	0.3113	0.2602	0.3093	0.3204
T_5	0.2612	0.3053	0.0539	0.0566	0.1617	0.3268	0.4604	0.5274
T_6	0.2179	0.1731	0.0905	0.0639	0.0927	0.2111	0.3908	0.5107
f_1	590.26	623.65	538.81	521.55	831.93	895.72	877.48	897.52
f_2	0.2360	0.2273	0.2448	0.2468	0.2001	0.1962	0.1962	0.1956

A: NSGA-II; B: MGSO; C: MOEA/D; D: MGSO/D ; W: wind power;
E: V2G power; T: thermal generator power; f : fitness value

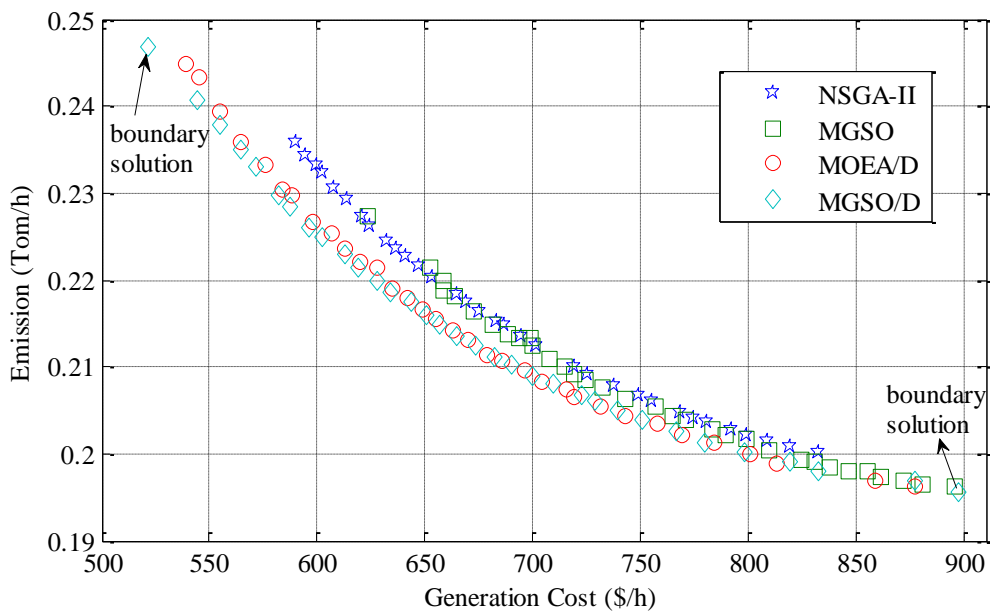


Fig. 4.2 The best PFs obtained for Case 1

(2) Case 2:

This case is to test the overall performance of MGSO/D when the MOOD has two competing objectives of the emission f_2 and power loss f_3 . Here there are 273 points on the reference Pareto Front. Among 273 points, none is contributed by NSGA-II, and only 2 solutions are from MGSO. However, MOEA/D and MGSO/D offers 120 points (43.95%) and 151 points (55.32%). In 4 benchmarks, MGSO/D has contributed most of reference PF solutions.

From the results presented in Table 4.5, MGSO/D again performs well on convergence, span, l_{\max}/l_{\min} and spacing metrics. The best convergence and span metrics verify its outstanding searching ability to find solutions covering the entire true PF and the diversity of its PF. In addition, the smallest l_{\max}/l_{\min} and spacing metrics confirm that the Pareto solution set formed by MGSO/D is most evenly distributed among these four benchmarks.

Table 4.5 Resulting statistics of performance metrics in Case 2

Case 2	NSGA-II	MGSO	MOEA/D	MGSO/D
convergence	0.121255	0.034027	0.007484	0.005917
span metric	0.818879	1.079506	1.094476	1.226634
l_{\max}/l_{\min}	74.29048	63.58833	18.93584	14.30798
spacing metric	0.201233	0.261979	0.037620	0.036508

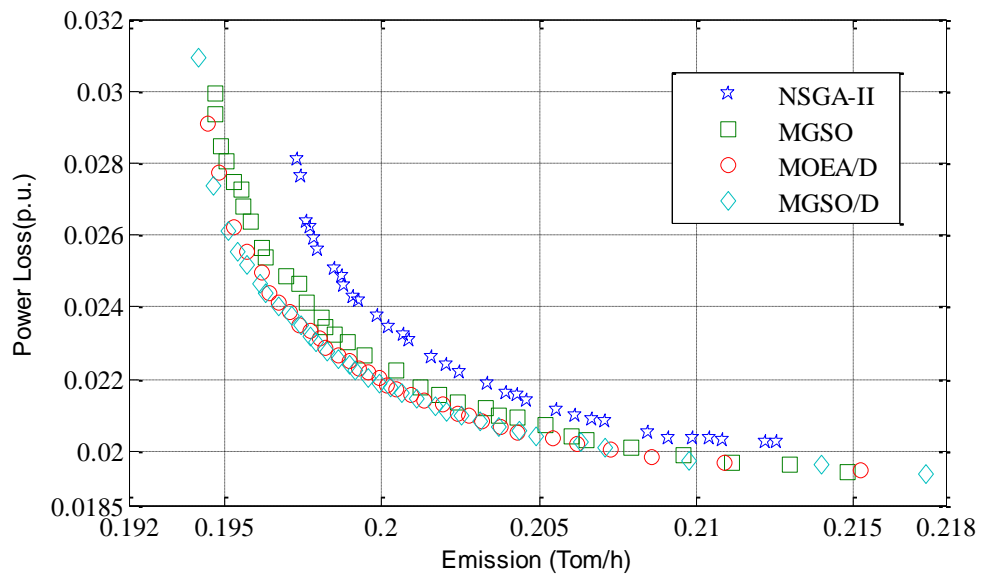


Fig. 4.3 The best PFs obtained for Case 2

Fig. 4.3 shows the best Pareto Fronts obtained from four algorithms, which again proves the outstanding spanning of the PF of MGSO/D and the Pareto optimality of the proposed algorithm.

(3) *Case 3:*

The third case is to investigate a dual-objective MOOP with the objectives of the generation cost f_1 and power loss f_3 . The components of the reference PF of case 3 is shown in Table 4.6 Again, solutions from MGSO/D are closer to the true Pareto set than those of other algorithms.

Table 4.6 The components of the reference PF in Case 3

PF	MOEA/D	MGSO/D
points	120	128
percentage	48.39%	51.51%

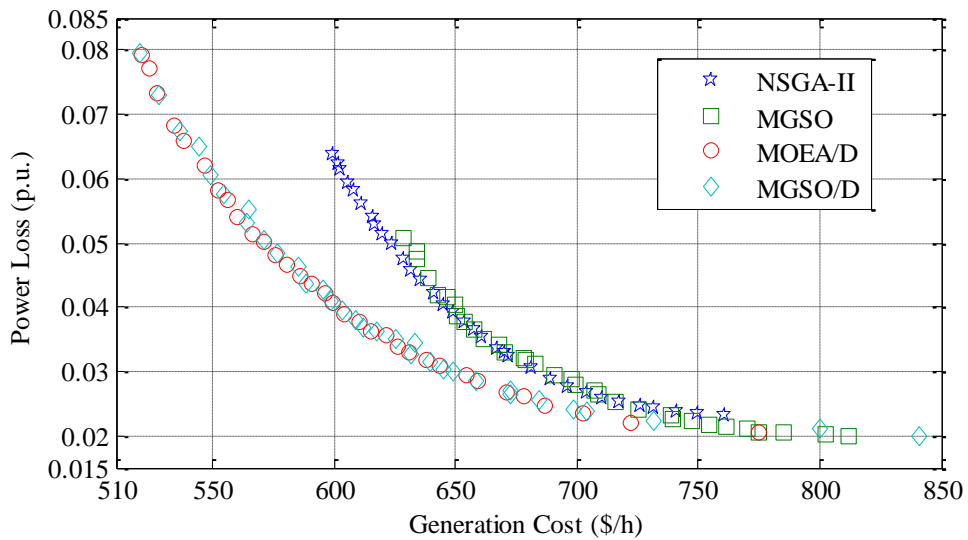


Fig. 4.4 The best PFs obtained for Case 3

Table 4.7 lists resulting statistics of performance metrics obtained by MGSO/D and other algorithms, and the corresponding PF solutions of the best run of each benchmark are plotted in Fig. 4.4. Among all algorithms, the developed algorithm performs best in the metrics of convergence, span and l_{max}/l_{min} , which indicates good overall performance of MGSO/D. Besides, it can be seen in Tab. VII the PFs of MOEA/D have slightly smaller spacing metric, which means PF points from MOEA/D are more uniformly-spaced, but only by a very small margin.

Additionally, MOEA/D performs worse than MGSO/D in other 3 metrics. Therefore, for this dual-objective MOPD, the proposed algorithm can give the best performance among 4 benchmarks.

Table 4.7 Resulting statistics of performance metrics in Case 3

Case 3	NSGA-II	MGSO	MOEA/D	MGSO/D
convergence	0.123154	0.104922	0.011829	0.011321
span metric	0.739562	0.736552	1.228029	1.409085
I_{\max}/I_{\min}	68.48074	106.59971	20.16012	15.92876
spacing metric	0.182097	0.171581	0.031338	0.033932

It can be observed from Fig. 4.4 that the best run of MGSO/D obtained 2 better outer solutions than other 3 benchmarks. Meanwhile, the best PF with MGSO/D could find solutions with much better fitness on the objectives of the generation cost and power loss compared to other 3 algorithms.

(3) *Uncertainty Discussion:*

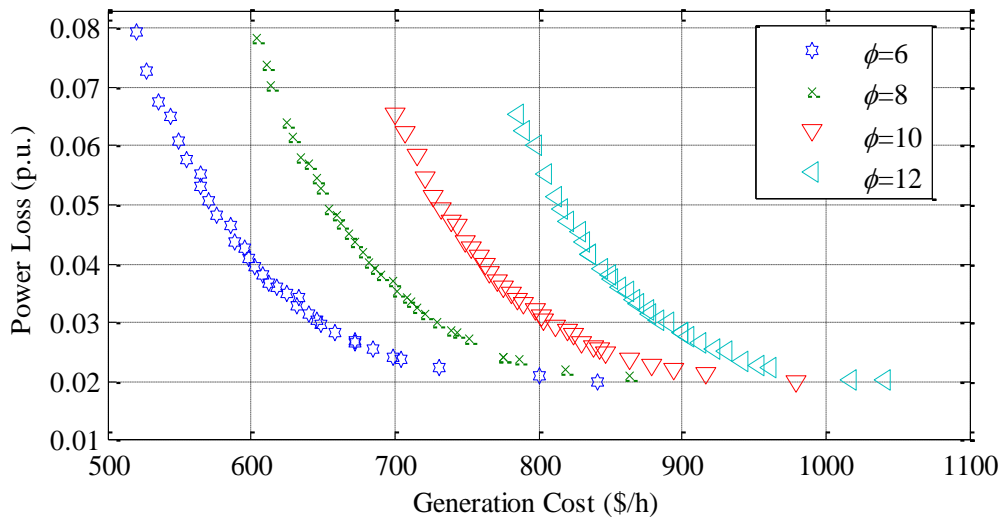


Fig. 4.5 PFs for different uncertain parameter ϕ of V2G power in Case 4

To investigate the uncertainties of V2G and wind power, the impacts of PDF parameters of h and ϕ in Case 3 are studied. At the same power loss level, it could be observed in Fig. 4.5 that the generation cost increases when the standard deviation ϕ of V2G PDF grows. Different values of wind power PDF h will also

lead to different Pareto curves as shown in Fig. 4.6. Generally, at the same generation cost level, power loss becomes smaller when the parameter h gets larger. These results clearly indicate the uncertainties significantly influences the Pareto solutions of the optimization. Therefore, it is important to account the uncertainties during the power system dispatch for better utilization of the V2G and wind power.

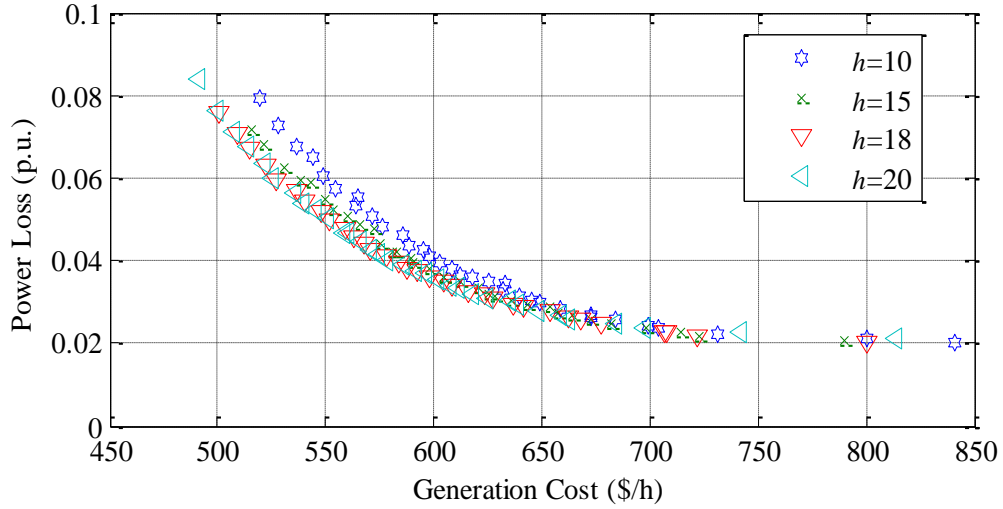


Fig. 4.6 PFs for different uncertain parameter h of wind power in Case 4

4.4.2 Investigation on the Modified IEEE 118-Bus System

Case 5: To investigate the performance of MGSO/D on large-scale power systems, a modified 118-bus system [152] consisting of 54 generators and 186 branches is used for a 3-objective optimization to reduce generation cost, emission and power loss. 6 wind farms are installed on node 11, 23, 45, 60, 82 and 106. In addition, 5 EV CSEs are constructed on node 2, 18, 44, 75 and 102. The parameters of wind farms and EV CSEs are the same with the former cases. To make it a fair comparison, the size of the PFs and the iteration number of each algorithm are all set to 45 and 200, respectively. The settings for MGSO/D are: $Y=3$, $C=45$, $B=15$. For MOEA/D, subproblem number is equal to 45 the same as MGSO/D. Additionally, M_p of MGSO and the population size of NSGA-II are set to 283 and 855, respectively to make their number of function evaluations be equal to MGSO/D. 20 independent runs of all comparative algorithms are carried out.

The reference PF for computing the convergence reference consists of 135 solutions, 38.52% of which (52 solutions) is obtained by MOEA/D and the rest of the reference PF containing 83 points is found with MGSO/D. It can be observed that all solutions obtained from NSGA-II and MGSO are covered by those of MOEA/D and MGSO/D. It again confirms the great ability of MGSO/D to obtain a set of solutions closer to the true Pareto set and its high potential to find Pareto optimality.

Table 4.8 Resulting statistics of performance metrics in Case 5

Case 5		Best	Worst	Average	Variance
convergence	NSGA-II	0.390974	0.840298	0.596639	0.008647
	MGSO	0.154348	0.337800	0.232941	0.003117
	MOEA/D	0.010663	0.103243	0.044616	0.000523
	MGSO/D	0.009850	0.065725	0.037132	0.000290
span metric	NSGA-II	0.021917	0.000426	0.010284	4.43E-05
	MGSO	0.021253	0.003820	0.013042	2.01E-05
	MOEA/D	0.028060	0.003516	0.013738	4.33E-05
	MGSO/D	0.064891	0.006659	0.016972	1.67E-04
l_{\max}/l_{\min}	NSGA-II	22.25166	124.6999	79.97006	1105.110
	MGSO	38.10994	159.1815	87.44264	1382.437
	MOEA/D	22.39172	239.2425	54.84145	2574.360
	MGSO/D	20.78305	77.25710	38.17302	193.5422
spacing metric	NSGA-II	0.000601	0.009117	0.005002	5.46E-06
	MGSO	0.008498	0.077129	0.026255	3.62E-04
	MOEA/D	0.001383	0.087310	0.007464	3.37E-04
	MGSO/D	0.001367	0.003574	0.002302	3.69E-07

Furthermore, the resulting statistics of performance metrics of each algorithm are shown in Table 4.8, which demonstrate that, MGSO/D markedly outperforms the other 3 benchmarks, on the convergence, span, l_{\max}/l_{\min} and spacing metrics. These statistical comparative experiments indicate that MGSO/D has the superior ability and efficiency of solution searching to guarantee the quality of PF solutions when the proposed algorithm deals with high dimensional MOOP with complex

and nonlinear power system constraints. Moreover, the variances of the convergence, l_{\max}/l_{\min} and spacing metrics confirm the stable performance of MGSO/D for the resulting Pareto set on these 3 measures. Although the variance of span metric of MGSO/D is not the best in 4 algorithms, its worst span metric in 20 runs is much higher than other benchmarks. Overall, in dealing with large-scale MOOP, the proposed algorithm also shows its obvious advantages.

In addition, the best run of each algorithm is plotted in Fig. 4.7. It is obviously that MGSO/D shows significant superiority in the searching ability than the other algorithms, especially NSGA-II and MGSO. It can also be observed that the proposed algorithm is able to obtain solutions with superior fitness on 3 objectives compared with other 3 benchmarks.

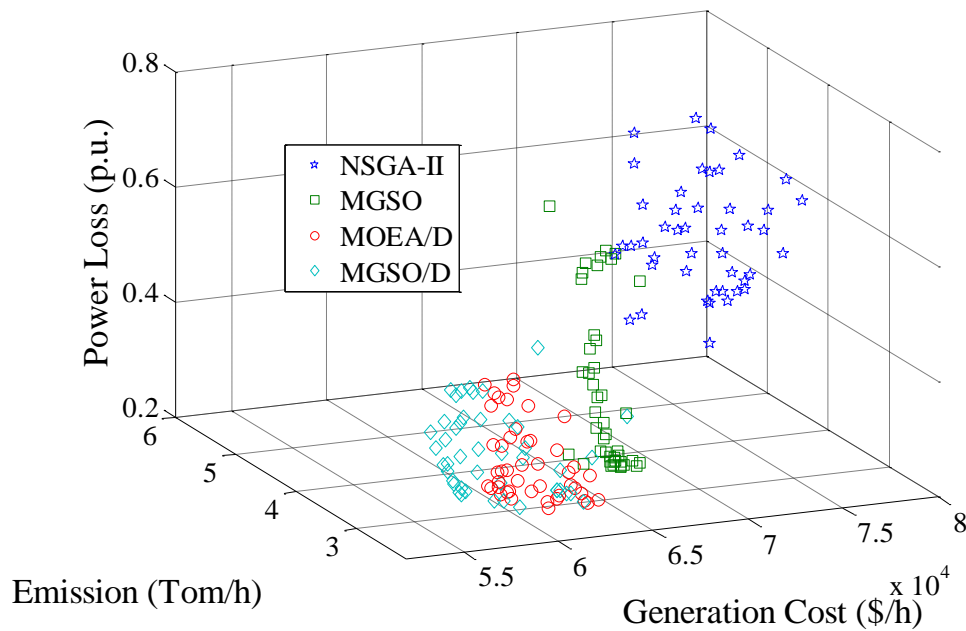


Fig. 4.7 The best PFs obtained for Case 5

4.4.3 Group Member Number Effects on MGSO/D Performance

Case 6: Group member number (Y) is a crucial parameter influencing the searching ability of MGSO/D. To investigate the effect of Y on the performance of MGSO/D, PFs are obtained as Y is 3, 10, 15 or 20 when a dual-objective MOOP with the objectives of the generation cost and emission is studied in the modified

IEEE 30-bus system in Case 6. For each Y , 10 independent runs were carried out in this case. Resulting statistics of performance metrics for $Y=3, 10, 15$ and 20 are detailed in Table 4.9. Although the spacing metric of $Y=3$ is a little worse, it can be observed the proposed algorithm performs better when $Y=3$ on convergence metric, span metric and I_{\max}/I_{\min} than those of $Y=10, 15$ and 20 , which demonstrates the best searching ability is obtained when $Y=3$. As shown in Fig. 4.8, the PFs of the best runs for $Y=3, 10, 15$ and 20 are compared. It can be found that MGSO/D ($Y=3$) can find solutions with better fitness values (emission and generation cost) than those when $Y= 10, 15$ and 20 . It is also noted that the PFs of the best run for $Y=3$ performs better with outstanding diversity and spanning.

Table 4.9 Resulting statistics of performance metrics in Case 6

Case 6	Y	Best	Worst	Average	Variance
convergence	3	0.002881	0.010480	0.005994	4.453E-06
	10	0.004331	0.024719	0.014579	3.625E-05
	15	0.005165	0.015557	0.008953	1.436E-05
	20	0.009089	0.016087	0.010991	3.932E-06
span metric	3	1.423644	1.346044	1.397212	0.000473
	10	1.044234	0.761052	0.904963	0.007660
	15	1.041209	0.668055	0.826955	0.010460
	20	0.883343	0.583129	0.762124	0.009282
I_{\max}/I_{\min}	3	3.628087	8.392825	6.168374	2.379713
	10	4.867813	14.807929	7.503204	7.247219
	15	4.164266	18.941727	8.481762	17.62801
	20	4.261702	11.807636	7.892960	6.100200
spacing metric	3	0.011898	0.024077	0.017328	1.663E-05
	10	0.011286	0.020898	0.016840	1.013E-05
	15	0.006316	0.020880	0.015017	1.825E-05
	20	0.007743	0.016995	0.011220	1.141E-05

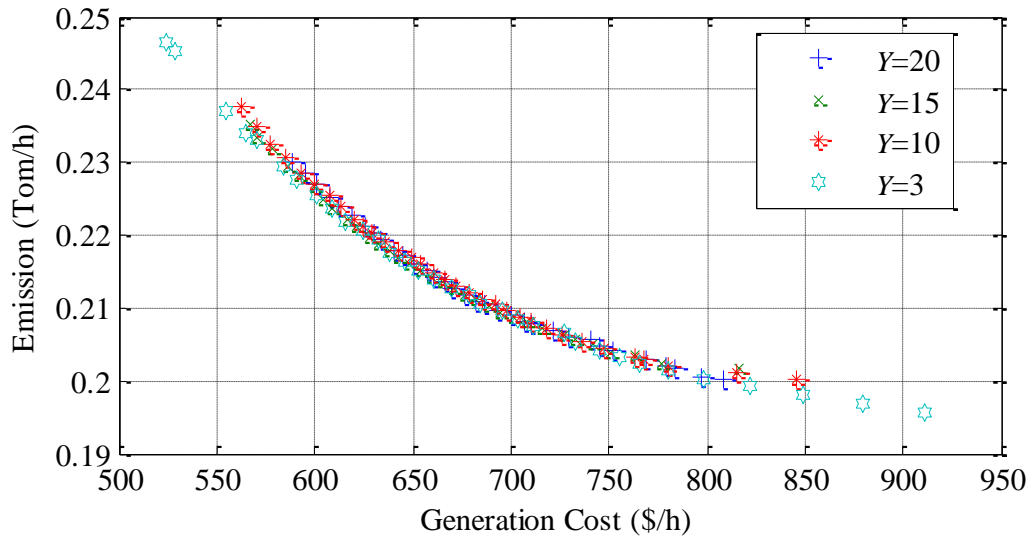


Fig. 4.8 Comparison of the PFs of the best runs for $Y=3$, 10 and 20

4.5 Summary

An efficient MGSO/D algorithm, which combines the merits of decomposition strategy and producer-scrounger model, is proposed in this chapter to solve a highly nonlinear constrained MOOP with the uncertainty of EVs and wind power being considered. It has been verified that the concerned uncertainties would have significant impacts to the simulation results, and the proposed MGSO/D has superior solution searching ability in both small-size and high-dimensional MOOPs with complex constraints and objectives, which makes it a promising framework for widely applications in solving other similar problems.

Chapter V

Optimal Dispatch of Electric Vehicle Batteries between Battery Swapping Stations and Charging Stations

5.1 Introduction

In addition to FCSes considered in previous chapters, BSSes are alternatives to provide similar services to the power system. The inconvenience of battery charging is the main barrier to the widespread use of EVs, and the EV battery-swapping technology is a promising method to assist overcoming this difficulty eventually because of its flexibility. Different from the fast charging mode, the battery charging process that would be completed in BCSes is separated from EVs in battery swapping mode. Therefore, the battery transportation between BCSes and BSSes needs to be studied.

In this chapter, a battery schedule framework is studied to dispatch batteries between BCSes and BSSes efficiently. A two-direction battery dispatch model to reduce the transportation cost is established and solved by the PSO method. Moreover, considering the serving ability limitations, the K-means clustering algorithm is utilized to pre-partition BCSes and BSSes to make the battery dispatch more efficient and effective for the large-scale system. The proposed method has been verified by an urban battery logistics case.

5.2 Assumptions and modeling

In this section, the structure of the battery swapping charging network and its

operation mechanism are firstly described. Then, the basic model and extended model of battery dispatch is established and analyzed.

5.2.1 Battery Swapping Charging Network

As shown in Fig. 5.1, in the proposed battery swapping charging mode, EVs exchange their exhausted batteries with fully charged batteries in the BSS, and the batteries exchanged from EVs in the BSS will be transferred to the BCS, where a large number of batteries could get charged uniformly. In addition, the batteries already charged are transported to BSS for the usage of other EVs. The remarkable advantage of this mode is that the BSS only exchange batteries thus does not occupy large space, and the BCS could charge batteries in a more organized way, which will greatly improve the charging efficiency and reduce the charging service cost.

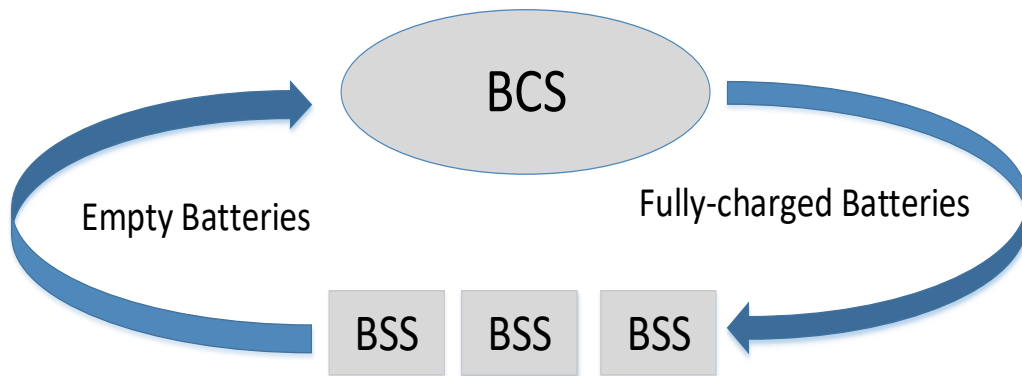


Fig. 5.1 Battery swapping charging network structure

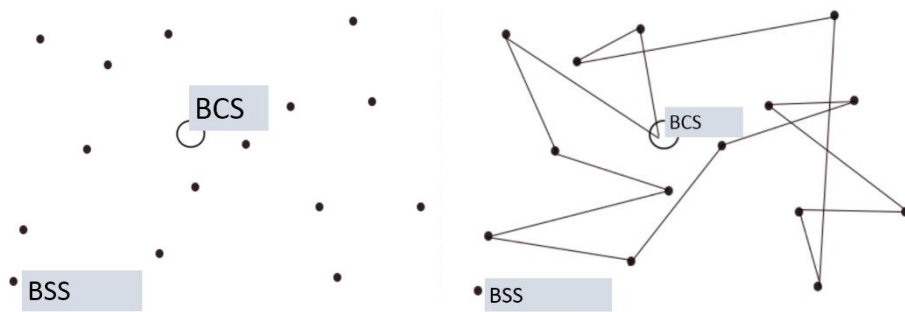


Fig. 5.2 Basic battery dispatch model

5.2.2 The Basic 2-Direction Battery Dispatch Model

Firstly the basic model of battery dispatch is illustrated in Fig. 5.2. The objective of the proposed model is to find the shortest paths to delivery full-charged batteries from BCS to BSS and get the empty batteries back from the BSS to BCS. In this model the transportation node set are $V=\{V_i | i=1,2,\dots,n-1\}$ and the path set is $E=\{(v_i,v_j) | v_i,v_j \in V, i \neq j\}$. The BSS location set are $C=\{v_1,v_2,\dots,v_{n-1}\}$ and the BCS is denoted as v_0 . $C_{ij}=C_0d_{ij}$ is the transportation cost, where C_0 is the cost per km and d_{ij} is the travel distance. $A=\{g_i | i=1,2,\dots,m\}$ is the set of delivery vehicles and the total number of which is m . The battery demand is q_i and G is the delivery vehicle capacity. The objective function and constraints are as follows:

$$\min Z = \sum_{i=0}^{n-1} \sum_{j=0}^{n-1} \sum_{k=1}^m C_{ij} X_{ijk} \quad (5.1)$$

s.t.

$$\sum_{k=1}^m \sum_{j=1}^{n-1} x_{0jk} \leq m \quad (5.2)$$

$$\sum_{k=1}^m \sum_{i=0}^{n-1} x_{ijk} = 1, \forall v_j \in C \quad (5.3)$$

$$\sum_{k=1}^m \sum_{j=0}^{n-1} x_{ijk} = 1, \forall v_i \in C \quad (5.4)$$

$$\sum_{i=1}^{n-1} x_{i0k} = 1, \forall k \in A \quad (5.5)$$

$$\sum_{i=1}^{n-1} x_{0ik} = 1, \forall k \in A \quad (5.6)$$

$$\sum_{k=1}^m \sum_{j=1}^{n-1} x_{0jk} - \sum_{k=1}^m \sum_{i=1}^{n-1} x_{i0k} = 0, \forall k \in A \quad (5.7)$$

$$\sum_{i=1}^{n-1} q_i \sum_{j=0}^{n-1} x_{ijk} \leq G, \forall k \in A \quad (5.8)$$

$$x_{ijk} = \begin{cases} 1 & \text{if the } k\text{th vehicle pass } i \text{ and } j \\ 0 & \text{otherwise} \end{cases}, \forall v_i, v_j \in V, \forall k \in A \quad (5.9)$$

where Eqn. (5.1) is the objective function to minimize the delivery cost; Eqn. (5.2) is to ensure the delivery vehicle number limitation; Eqn. (5.3) and (5.4) means every BSS's battery is provided by only 1 vehicle; Eqn. (5.5) and (5.6) means every vehicle only travel one time. Eqn. (5.7) ensures that every vehicle could go back to the BCS; Eqn. (5.8) limits the vehicle transportation capacity and the Eqn. (5.9) is the integer constraint.

5.2.3 The Extended Battery Dispatch Model by K-means Pre-partition Method

With the development of electric vehicle and battery technologies, the wide application of EVs is possible in the future. The optimal dispatch of a battery swapping charging network with a high penetration of EVs in a large area is a great challenge for the system operators. In this situation, there are more difficulties for the battery dispatch like longer travel distance, higher delivery capacity and service ability limitations, et al.

A promising way to solve this problem is pre-partition the service areas, as shown in Fig. 5.3. After the pre-partition, the battery dispatch problems could be solved separately, which will reduce the service burden and make the dispatch more efficient.

K-means clustering is popular for cluster analysis and partitions n observations into k clusters in which each observation belongs to the cluster with the nearest mean [172]. The K-means clustering could be applied into our problem as follows:

- 1) Set the c BCS locations as the initial centers;
- 2) In the k th iteration, calculate the within-cluster sum of squares (simply Euclidean distances here) of every BSS to c BCS, and partition the BSS to the nearest BCS cluster;
- 3) Update the center locations of the c BCS clusters according to least-squares estimator (arithmetic means, et. al);
- 4) Repeat step 2)-3) until the cluster assignment no longer change;
- 5) Output the cluster results.

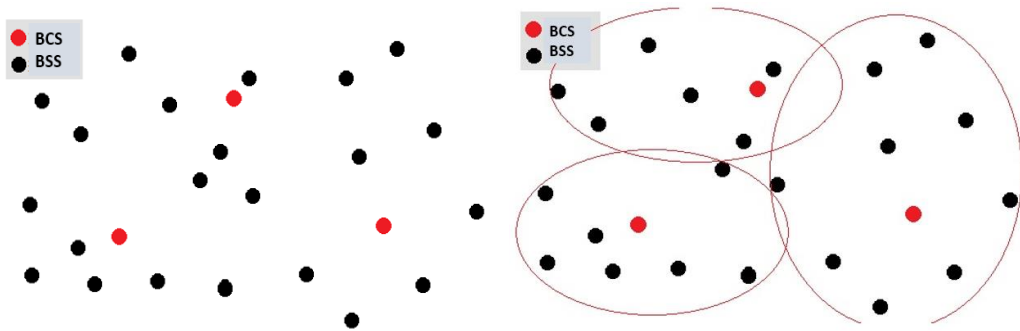


Fig. 5.3 The pre-partition step of the extended battery dispatch model

The flowchart of the K-means clustering is shown in Fig. 5.4:

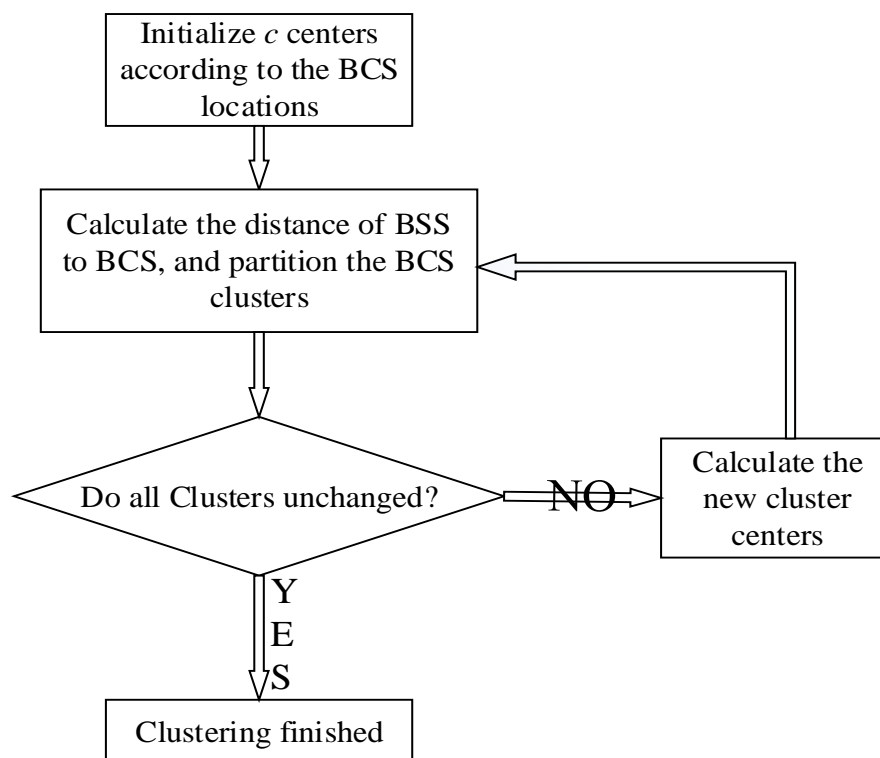


Fig.5.4 Flowchart of the BCS service K-means clustering

5.3 Solving strategies

In this thesis, PSO algorithm has been employed to solve the optimization problem described before. First, the constraints are dealt with by the penalty function method. Second, the fitness function is formed by the objective function and penalty constraints together.

5.3.1 PSO Based Optimal EV Battery Dispatch

The flowchart of the PSO procedure is shown in Fig. 5.5.

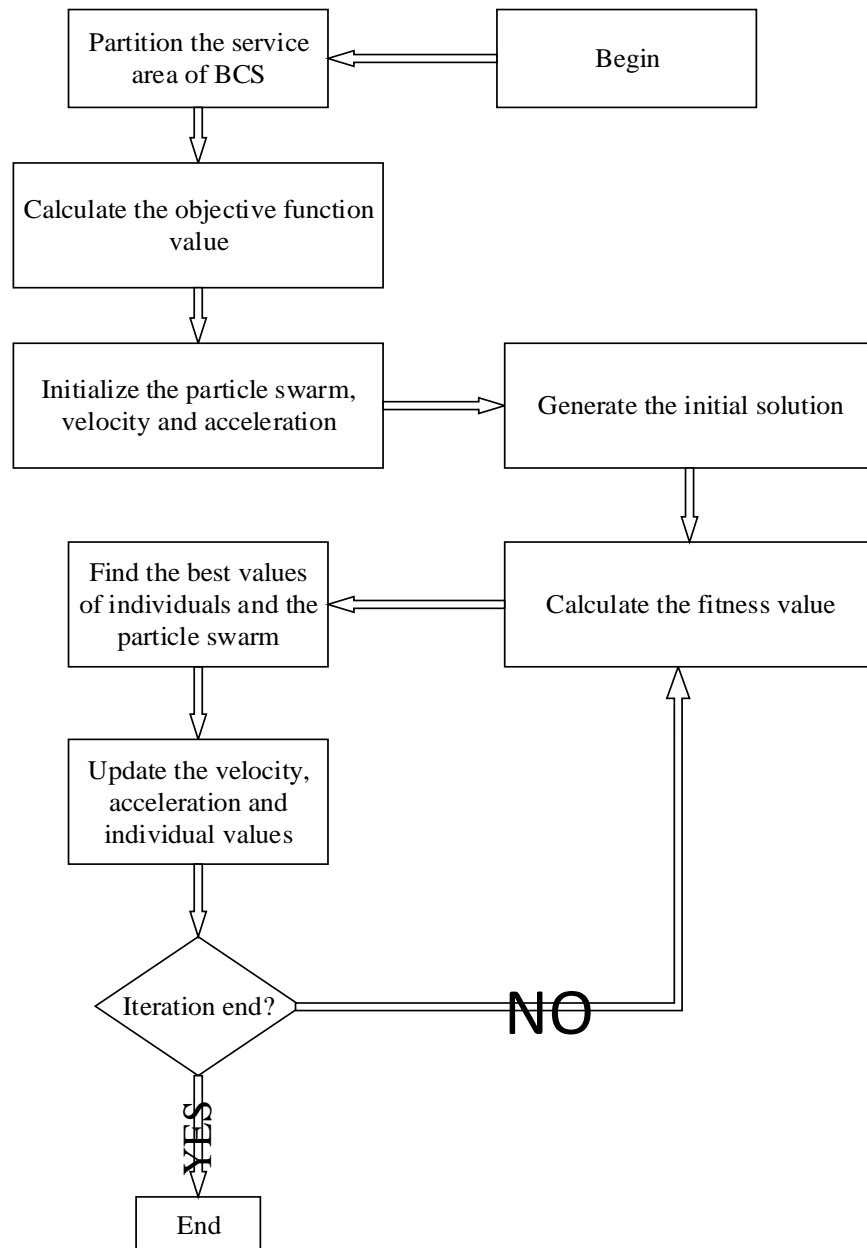


Fig. 5.5 Flowchart of the PSO based optimal EV battery dispatch

Step 1) Specify some parameters associated with PSO, such as population size

n_p , initial solution x_i , et al;

Step 2) Partition the service area of BCS by the K-means clustering method;

- Step 3) Calculate the objective function value of each cluster respectively;
- Step 4) Initialize the particle swarm, velocity and acceleration;
- Step 5) Generate the initial solution;
- Step 6) Calculate the fitness value;
- Step 7) Find the optimal values of individuals and the optimal solution of the particle swarm;
- Step 8) Update the velocity, acceleration and individual values;
- Step 9) Repeat Steps 3)-8) for N_c times.
- Step 10) Select the best individual found in the above solving procedure as the optimal solution of the BSS battery dispatch.

5.4 Case studies

5.4.1 The Basic 2-Direction Battery Dispatch Model Case

Firstly, a simple case of a 100 sq.km. area with 1 BCS and 7 BSS is studied. The BCS and BSS location is generated randomly. The transportation cost parameter $C_1=C_2=0.5$ dollar, and the PSO group size is 200. Fig. 5.6 shows the random travel path to deliver all the batteries from BCS to BSS. The total distance is 62.3024 km.

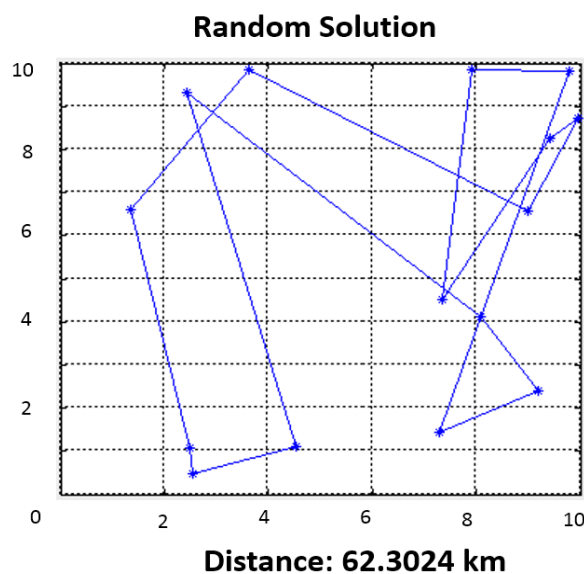


Fig. 5.6 The random travel path of the basic battery dispatch model

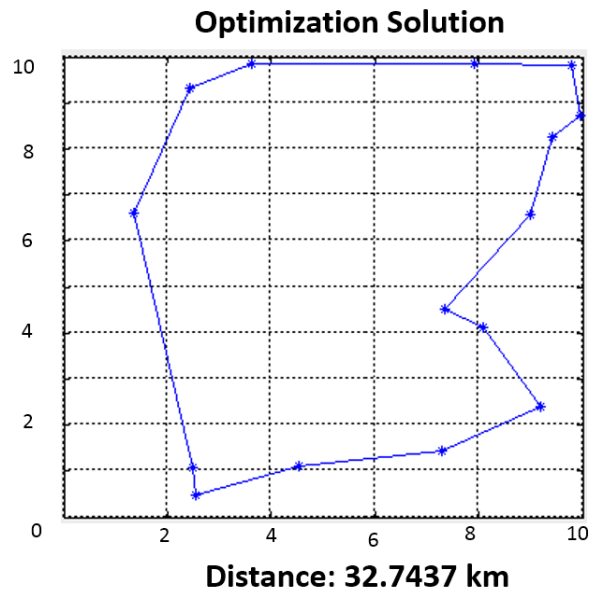


Fig. 5.7 The optimal travel path of the basic battery dispatch model

In comparison, Fig. 5.7 shows the optimal travel path of the basic model. It is clearly demonstrated that after optimization, the travel distance is greatly reduced from 62.3024 km to 32.7437 km. Therefore, the travel cost will be saved a lot.

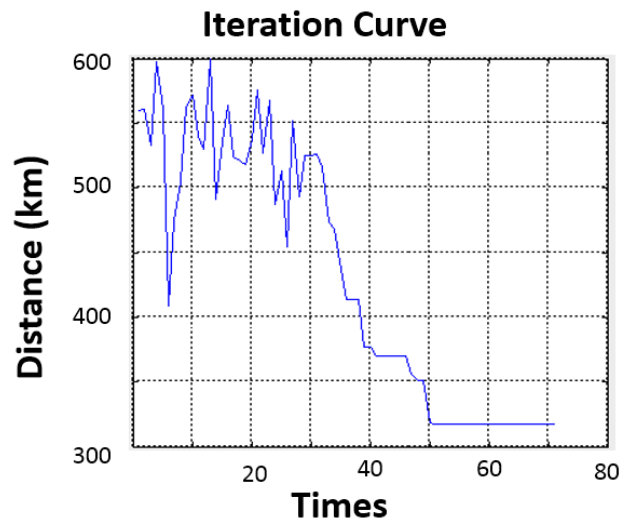


Fig. 5.8 The iteration curve of the proposed PSO method

Fig. 5.8 shows the performance of the proposed PSO solving strategy. The objective function value becomes stable after 50 iterations and the optimal solution could be obtained.

5.4.2 The Extended Battery Dispatch Model Case with K-means Clustering
Method

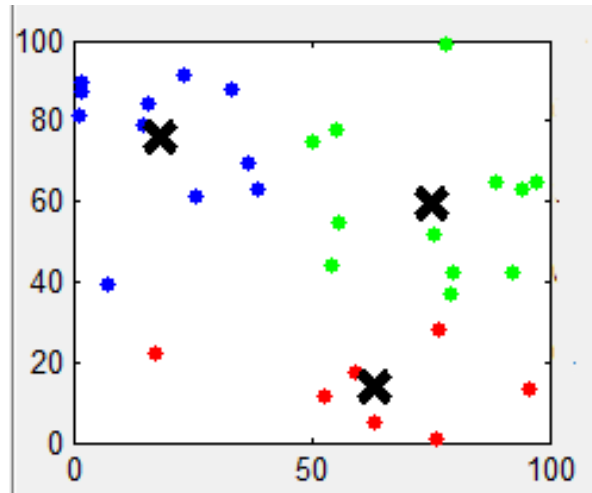


Fig. 5.9 The BSS/BCS partition results in a larger area

Table 5.1 The BSS/BCS geographic location in the extended model

No.	X	Y	No.	X	Y
1	97.43	65.07	16	59.12	17.47
2	52.85	11.29	17	25.69	61.38
3	75.88	51.62	18	1.98	89.79
4	50.28	75.07	19	54.41	44.1
5	55.67	54.74	20	63.25	5.14
6	78.49	98.9	21	55.41	77.76
7	79.33	36.69	22	23.12	91.28
8	1.89	87.43	23	14.56	79.21
9	33.02	87.59	24	94.41	62.81
10	36.77	69.51	25	17.13	22.35
11	79.72	42.43	26	76.89	28.08
12	88.51	64.62	27	15.91	84.58
13	76.14	1.05	28	38.82	62.81
14	7.03	39.09	29	95.62	13.43
15	92.41	42.34	30	1.11	81.53

It can be concluded that the basic model is very effective in the small area case. However, when the service area is large enough with high penetration of EVs in

the future (as shown in Fig. 5.9), the pre-partition is essential to solve the high-dimension problem separately. Table. 5.1 shows the geographic locations in the extended model. There are 3 BCS and 27 BSS in this model. Fig. 5.9 shows the partition results (Blue, red and green BSS means different clusters) in an area of 10000 sq.km.

After partition, the optimal battery dispatch model could be solved separately. Fig. 5.10 shows the random and optimal battery delivery path before partition. It can be observed that the shortest battery delivery path distance is 645.37 km before partition. Although it is much better result that the random solution of 1287.22 km, the distance is still a great burden for battery delivery tasks.

Fig. 5.11 shows the simulation results after partition. It clearly shows that the total battery delivery path distance is greatly reduce from 645.37 km to 524.61 km, thus the BCS and BSS service ability is improved to promote to promote the wide application of EVs in the future.

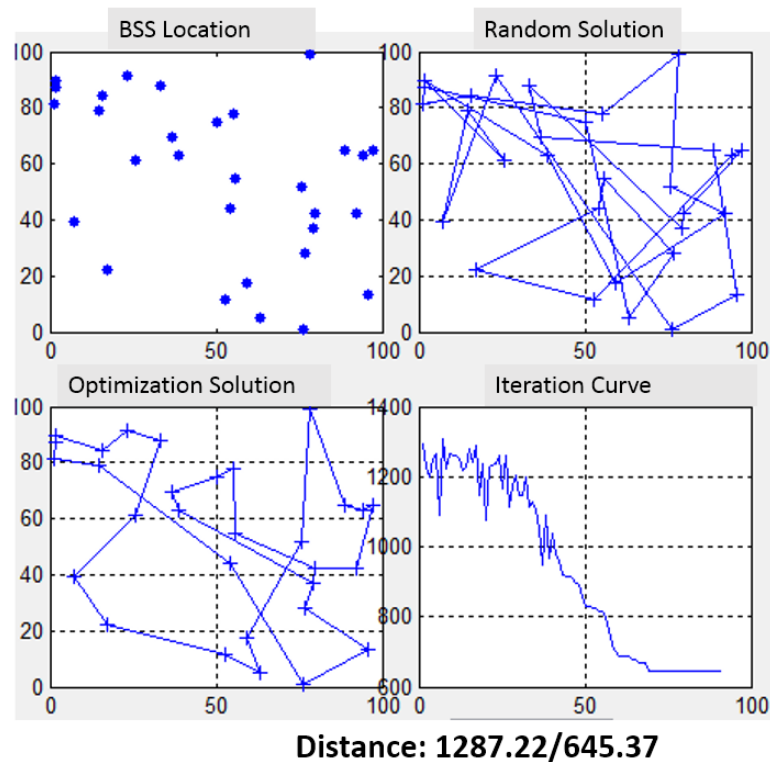


Fig. 5.10 The random path, optimal path, and iteration curve of the extended model before partition

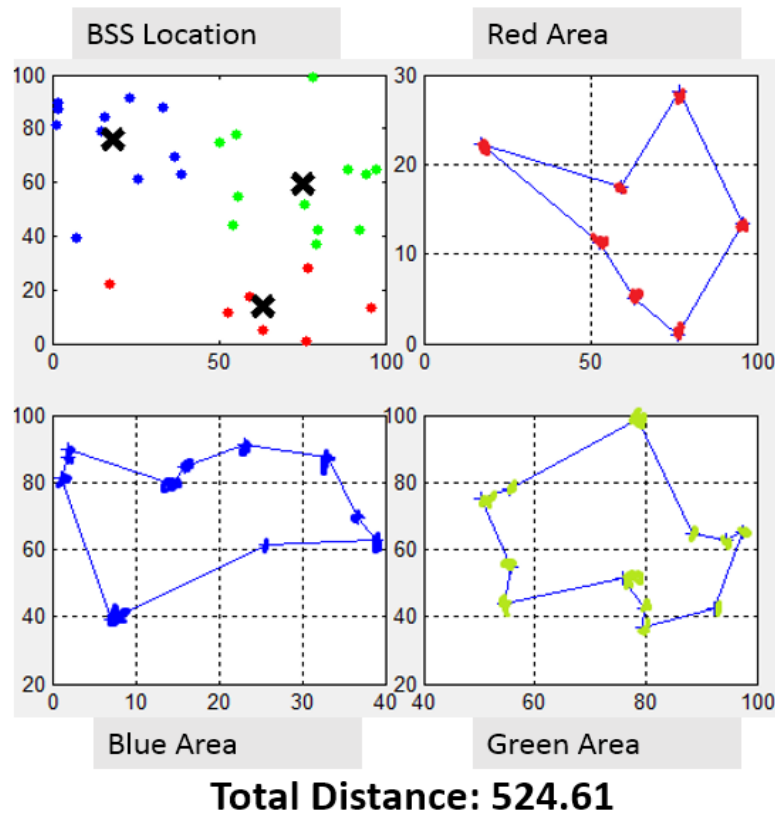


Fig. 5.11 The optimal path of the extended model after partition

5.5 Summary

This chapter has established an original battery optimal dispatch model between BSSes and BCSes to take full advantages of the battery swapping mode vehicles, which contributes to the optimal operation of the battery swapping charging network in power systems. Case studies have indicated that the optimal dispatch model based on K-means partition method can efficiently dispatch batteries by reducing the traveling distance, which largely reduces the operation costs of the existing battery swapping charging networks.

Chapter VI

Conclusions and Future Works

6.1 Conclusions

In order to reduce the adverse impact of EVs on the operation of power system and promote the integration of EVs into the modern smart grid, this thesis covers the complete picture of the forecasting of EV charging loads and the planning and the operation of EV CSEs, which can assist the traffic operator, CS companies and DSO in their decision-making processes. The EV charging load forecasting consists of investigations on both long-term forecasting and short-term forecasting. The primary conclusions and contributions of this research are summarized as follows:

- i) Comparison research on the long-term forecasting of EV charging demand based on grey system theory and the NAR neural network*

The grey system forecasting theory model and the NAR neural network model are utilized to forecast the annual growth in the number of EVs. The effectiveness, rationality, precision, and adaptability of the two models are evaluated and compared. This comparison study shows the prediction accuracy of the grey system forecasting model is high when the original EV demand data increases exponentially. Otherwise, its prediction shows a larger deviation. And compared with the grey system forecasting model, the NAR neural network model has a better performance on forecasting the EV charging demand in a long-term horizon, which is more suitable for a practical application.

- ii) The accurate TF forecasting based on the DBN method*

DBN method is firstly applied to predict EV growth in CS and DS planning horizon, which is usually used as a short-term forecasting method in the previous literatures. In this thesis, the DBN method achieves the long-term forecasting of TF by ensemble the growth trends prediction and hourly prediction together. Simulation results show that it outperforms other four typical long-term forecasting algorithms which are BPNN, SVM, ARMA and MWNN. Additionally, the forecasting results by DBN method are used as the basis of the co-planning of CSes and DS, which is also investigated in this thesis.

iii) A deep learning-based approach for probabilistic forecasting of EV charging loads

This comprehensive ensemble method is devoted to addressing complicated EV load forecasting problems, which is divided into three steps. First, TF is forecasted using a deep-learning based convolutional neural network (CNN) method in which an ensemble approach that considers both model and data uncertainty is employed to effectively formulate the TF prediction intervals (PIs). Therefore, the complicated nonlinear features of TFs are learned more effectively, and a superior forecasting performance is obtained. Second, a mixture model-based method is used to approximate the arrival rate of EVs according to historical data. Third, an advanced queuing model is formulated for the first time to predict the EV charging load in the CSes, which scientifically accounts for CS service limitations and the inherent stochasticity of EV driver behaviors. Simulation results have demonstrated that the established prediction framework for EV charging demand that has better accuracy and reliability is essential for the operation and control of FCSes, the power system, and the traffic system. Such a framework will help FCS operators determine the number of dispatchable EVs in advance in order to avoid higher costs or excessive risks. This will also assist the traffic operator in the alleviation of traffic congestion and will aid decision-making

for electricity market trading using optimized bidding when EVs participate in the ancillary service market, et al.

iv) The negotiated planning of DS and EV CSEs in deregulated electricity markets

Based on the accuracy EV growth forecasting result by DBN method, Nash bargaining theory is applied to the negotiated planning of DS and EV CSEs for the first time. Different from most existing studies, this model is the first to consider the CS company and the DS as two separate participants operating in a deregulated market environment, which corresponds to reality. Furthermore, a novel DS-based LMP model capable of alleviating congestion and promoting the response of EV charging is used to realistically simulate the impact of the environment of the electricity market on the results of planning. Case studies have demonstrated that the obtained Nash bargaining solution can achieve agreement between two players and ensures both players are treated fairly. Moreover, the proposed LMP model is proved for its immediate and far-reaching significance to promote the development of CSEs and EVs compared with models that use fixed electricity prices. The proposed Nash bargaining based framework with LMP model can encourage proactive interactions and fair profit sharing between CS and DS in the planning, which is also useful for cooperation between other participants in the deregulated market environment.

v) Multiple group search optimization based on decomposition for multi-objective dispatch that considers uncertainties of V2G power and wind power

A highly nonlinear constrained MOOP that considers the uncertainties of V2G power and wind power is proposed and solved using a novel algorithm called MGSO/D that combines the merits of the decomposition strategy and the producer-scrounger model. Simulation results have verified that the concerned uncertainties would have significant impacts to the dispatch results, which demonstrates that in the power dispatch problem, the uncertainties of V2G power and renewable

energies cannot be ignored. This is a promising framework for solving similar power dispatch problems containing V2G power and other renewable energies. Compared with three well-established Pareto heuristic methods, GSO, NSGA-II, and MOEA/D, MGSO/D has a superior solution searching ability and is able to obtain a uniformly distributed and diverse PF more effectively in both small size and high-dimensional MOOPs with complex constraints and objectives. It is also worth mentioning that MGSO/D is a useful method that cannot only solve the proposed MOOP but also solve other MOOPs with complicated and nonlinear constraints.

vi) A novel optimal dispatch of EV batteries between BSSes and BCSes

An original optimal battery dispatch model between BSSes and BCSes is established to take full advantage of battery-swapping mode vehicles. This model contributes to optimal operation of a battery swapping charging network that includes BSSes and BCSes. Moreover, the K-means partition method is applied to pre-partitioned BCSes and BSSes to make battery dispatch more efficient in a large-scale system. Case studies have demonstrated that the optimal dispatch model and K-means clustering algorithm can efficiently dispatch batteries and reduce the traveling distance, as well as significantly cut operation costs of existing battery swapping charging networks. Therefore, this model could improve the convenience of EV battery charging and promote the widespread use of EVs.

6.2 Future Works

The thesis has proposed several schemes for forecasting EV charging loads and for the cooperative planning and multi-objective operation of EV CSes. To make the current work more comprehensive, the following topics should be investigated in the future.

- (1) As increasing REs participate in power system dispatch, a negotiated planning model for DSs, EV CSes, and REs can be investigated to solve the

payoff distribution problem among these three participants. Compared with the two-player model proposed in Chapter III, the three-player model is more complicated and practical, which is worth further investigation.

- (2) Once capacities of existing CSes cannot meet the charging demand of EVs, CSes need to be expanded. Based on the CS planning results in chapter III, studies can to be performed that investigate the game-theoretical capacity expansion for EV CSes in the distribution network, assuming that each CS is a separate participant. Additionally, under the smart grid paradigm, a CS also could play the role of electric vehicle (EV) aggregation agent to participate with bids for purchasing electrical energy in the day-ahead (spot) market and selling secondary reserve in the secondary reserve markets. Therefore, the game-theoretical model for the EV CS capacity expansion considering secondary reserve sessions is worth studying.

Appendix

Obtaining Process of P_w and P_0 :

For brief expression, $\rho=\lambda/\mu$ and $\eta=\delta/\mu$ are defined at first. According to [119], the steady-state probability of the Markov chain to be at state w is defined as $P_w = \lim_{t \rightarrow \infty} P\{N(t) = w\}$, $w = 0, 1, \dots, K$. Based on (2.57) and the birth-and-death process shown in Fig. 2.7, the balance equation for each state could be elaborated as:

$$\text{State 0: } \lambda P_0 = \mu P_1 \Rightarrow P_1 = \frac{\lambda}{\mu} P_0 = \rho P_0$$

$$\text{State 1: } \lambda P_0 + 2\mu P_2 = (\lambda + \mu)P_1 \Rightarrow P_2 = \frac{\lambda}{2\mu} P_1 = \frac{\rho^2}{2!} P_0$$

$$\text{State 2: } \lambda P_1 + 3\mu P_3 = (\lambda + 2\mu)P_2 \Rightarrow P_3 = \frac{\lambda}{2\mu} P_1 = \frac{\rho^3}{3!} P_0$$

$$\text{State 3: } \lambda P_2 + 4\mu P_4 = (\lambda + 3\mu)P_3 \Rightarrow P_4 = \frac{\lambda}{4\mu} P_3 = \frac{\rho^4}{4!} P_0$$

.....

$$\text{State } C-1: \lambda P_{C-2} + C\mu P_C = [\lambda + (C-1)\mu]P_{C-1} \Rightarrow P_C = \frac{\lambda}{C\mu} P_{C-1} = \frac{\rho^C}{C!} P_0$$

State C :

$$\lambda P_{C-1} + (C\mu + \delta \ln 2)P_{C+1} = (\lambda + C\mu)P_C \Rightarrow P_{C+1} = \frac{\lambda}{C\mu + \delta \ln 2} P_C = \frac{\rho^{C+1}}{C!(C + \eta \ln 2)} P_0$$

$$\text{State } C+1: \lambda P_C + (C\mu + \delta \ln 3)P_{C+2} = (e^{-\sigma} \lambda + C\mu + \delta \ln 2)P_{C+1}$$

$$\Rightarrow P_{C+2} = \frac{\lambda e^{-\sigma}}{C\mu + \delta \ln 3} P_{C+1} = \frac{e^{-\sigma} \rho^{C+2}}{C!(C + \eta \ln 3)(C + \eta \ln 2)} P_0$$

$$\text{State } C+2: e^{-\sigma} \lambda P_{C+1} + (C\mu + \delta \ln 4)P_{C+3} = (e^{-2\sigma} \lambda + C\mu + \delta \ln 3)P_{C+2}$$

$$\Rightarrow P_{C+3} = \frac{\lambda e^{-2\sigma}}{C\mu + \delta \ln 4} P_{C+2} = \frac{e^{-2\sigma} \rho^{C+3}}{C!(C + \eta \ln 4)(C + \eta \ln 3)(C + \eta \ln 2)} P_0$$

.....

State $K-1$:

$$e^{-(K-C-2)\sigma} \lambda P_{K-2} + [C\mu + \delta \ln(K-C+1)] P_{K-1} = [\lambda e^{-(K-C-1)\sigma} + C\mu + \delta \ln(K-C)] P_{K-1}$$

$$\Rightarrow P_K = \frac{\lambda e^{-(K-C-1)\sigma}}{C\mu + \delta \ln(K-C+1)} P_{K-1} = \frac{e^{-\frac{(K-C)(K-C-1)\sigma}{2}} \rho^K}{C! [C + \eta \ln(K-C+1)] [C + \eta \ln(K-C)] \cdots (C + \eta \ln 2)} P_0$$

$$\Rightarrow P_K = \frac{e^{-\frac{(K-C)(K-C-1)\sigma}{2}} \rho^K}{C! \prod_{i=1}^{K-C} [C + \eta \ln(i+1)]} P_0$$

Therefore

$$P_w = \begin{cases} \frac{\rho^w}{w!} P_0 & 0 \leq w \leq C \\ \frac{e^{-\frac{(w-C)(w-C-1)\sigma}{2}} \rho^w}{C! \prod_{i=1}^{w-C} [C + \eta \ln(i+1)]} P_0 & C < w \leq K \end{cases}$$

Because the sum of the steady-state probabilities must be equal to one:

$$1 = \sum_{w=0}^K P_w = \sum_{w=0}^C P_w + \sum_{w=C+1}^K P_w$$

$$= \sum_{w=0}^C \frac{\rho^w}{w!} P_0 + \sum_{w=C+1}^K \frac{e^{-\frac{(w-C)(w-C-1)\sigma}{2}} \rho^w}{C! \prod_{i=1}^{w-C} [C + \eta \ln(i+1)]} P_0$$

$$= \left[\sum_{w=0}^C \frac{\rho^w}{w!} + \sum_{w=C+1}^K \frac{e^{-\frac{(w-C)(w-C-1)\sigma}{2}} \rho^w}{C! \prod_{i=1}^{w-C} [C + \eta \ln(i+1)]} \right] P_0$$

Thus

$$P_0 = \left[\sum_{w=0}^C \frac{\rho^w}{w!} + \sum_{w=C+1}^K \frac{e^{-\frac{(w-C)(w-C-1)\sigma}{2}} \rho^w}{C! \prod_{i=1}^{w-C} [C + \eta \ln(i+1)]} \right]^{-1}$$

References

- [1] W. Su, H. Tahimi-Eichi, W. Zeng, and M. Chow, "A survey on the electrification of transportation in a smart grid environment," *IEEE Transactions on Industrial Informatics*, vol. 8, no. 1, Feb. 2012.
- [2] M. Shomik, "The China New Energy Vehicles Program: Challenges and Opportunities," World Bank, Beijing, 2011.
- [3] The Internal Revenue Service, U.S.. (2013, 2 April). *New Qualified Plug-in Electric Drive Motor Vehicle Credit*. Available: https://www.irs.gov/irb/2009-48_IRB/ar09.html
- [4] Office for Low Emission Vehicles, UK Government. (2015, 4 July). *Plug-in car grant eligibility guidance*. Available: <https://www.gov.uk/government/publications/plug-in-car-grant/plug-in-car-grant-eligibility-guidance>
- [5] U. S. Department of Energy. (2015, 10 May). *Availability of Hybrid and Plug-In Electric Vehicles*. Available: http://www.afdc.energy.gov/vehicles/electric_availability.html
- [6] T. Tali and P. Telleen, "Global EV Outlook: Understanding the Electric Vehicle Landscape to 2020," International Energy Agency, April 2013.
- [7] Wikipedia. (2016, 27 January). *Electric car use by country*. Available: https://en.wikipedia.org/wiki/Electric_car_use_by_country
- [8] International Energy Agency, "Global EV Outlook 2017 Two million and counting, " pp. 1-71, 2017.
- [9] F. Lew, T. Peter, K. Tom, W. Jake, C. Pierpaolo, C. Francois, *et al.*, "Technology Roadmap-Electric and plug-in hybrid electric vehicles," in *International Energy Agency*, France, June 2011.

- [10] Chinadaily, "China to build 12,000 nev chargers by 2020." [On-line]. Available: http://www.chinadaily.com.cn/business/motoring/2015-10/13/content_22170160.htm, accessed Sep 30, 2016.
- [11] M. Duvall, E. Knipping, and M. Alexander, "Environmental Assessment of Plug-in Hybrid Electric Vehicles," *Electric Power Research Institute, U.S.*, July 2007.
- [12] D. Wu, H. Zeng, C. Lu, and B. Boulet, "Two-stage energy management for office buildings with workplace ev charging and renewable energy," *IEEE Trans. Transport. Electrific.*, vol. 3, no. 1, pp. 225–237, 2017.
- [13] M. J. E. Alam, K. M. Muttaqi, and D. Sutanto, "Effective Utilization of Available PEV Battery Capacity for Mitigation of Solar PV Impact and Grid Support with Integrated V2G Functionality," *IEEE Trans. Smart Grid*, vol. 7, no. 3, pp. 1562–1571, 2016.
- [14] M. Vasirani, R. Kota, R. L. G. Cavalcante, S. Ossowski, and N. R. Jennings, "An Agent-Based Approach to Virtual Power Plants of Wind Power Generators and Electric Vehicles," *Smart Grid, IEEE Transactions on*, vol. 4, pp. 1314-1322, 2013.
- [15] Z. Darabi and M. Fedowski, "An event-based simulation framework to examine the response of power grid to the charging demand of plug-in hybrid electric vehicles (PHEVs)," *IEEE Trans. Ind. Informat.*, vol. 10, no. 1, pp. 313-322, Feb. 2012.
- [16] J. C. Gomez and M. M. Morcos, "Impact of EV battery chargers on the power quality of distribution systems," *IEEE Trans. Power Del.*, vol. 18, no. 3, pp. 975-981, Jul. 2003.
- [17] P. T. Staats, W. M. Grady, A. Arapostathis, and R. S. Thallam, "A statistical analysis of the effect of electric vehicle battery charging on distribution system harmonic voltages," *IEEE Trans. Power Del.*, vol. 13, no.2, pp. 640-646, Apr. 1998.

- [18] G. Wang *et al.*, "Robust Planning of Electric Vehicle Charging Facilities with Advanced Evaluation Method," *IEEE Transactions on Industrial Informatics*, vol. 14, no. 3, pp. 866-876.
- [19] G. Wang, J. Zhao, F. Wen, Y. Xue and G. Ledwich, "Dispatch Strategy of PHEVs to Mitigate Selected Patterns of Seasonally Varying Outputs from Renewable Generation, " *IEEE Transactions on Smart Grid*, vol. 6, no. 2, pp. 627-639, March 2015.
- [20] LAI Hongsong, ZHU Guorui, et al, "Population forecast based on combination of grey forecast and artificial neural networks," *Economic Geography*, vol.24, no.2, pp. 197-201, Mar. 2004. (in Chinese).
- [21] SHI Deming, LI Linchuan, et al, "Power system load forecasting based upon combination of grey forecast and artificial neural network," *Power System Technology*, vol.25, no.12, pp. 14-17, Dec. 2001. (in Chinese).
- [22] WANG Xiang, HE Jixiang, et al, "Establishment of aquaculture water nitrite prediction model based on NAR neural network," *Fishery Modernization*, vol.42, no.4, pp. 30-34, Aug. 2015. (in Chinese)
- [23] WEI Duan, LU Xiangyang, "An improved BP neural networks applied to classification," *Energy Procedia*, vol.13, no.4, pp. 7065-7069, Sep.2012
- [24] Xiao Qiwei, Yang Xiuzhi, "Prediction of Audience Rating Based on Nolinear Auto-regressive(NAR) Model," *Video Engineering*, vol.39, no.4, pp. 79-81, Sep.2015.
- [25] Z. Duan, B. Gutierrez and L. Wang, "Forecasting Plug-In Electric Vehicle Sales and the Diurnal Recharging Load Curve," *IEEE Transactions on Smart Grid*, vol. 5, no. 1, pp. 527-535, Jan. 2014.
- [26] N. Korolko, Z. Sahinoglu and D. Nikovski, "Modeling and Forecasting Self-Similar Power Load Due to EV Fast Chargers," *IEEE Transactions on Smart Grid*, vol. 7, no. 3, pp. 1620-1629, May 2016.

- [27] Q. Dai, T. Cai, S. Duan and F. Zhao, "Stochastic Modeling and Forecasting of Load Demand for Electric Bus Battery-Swap Station," *IEEE Transactions on Power Delivery*, vol. 29, no. 4, pp. 1909-1917, Aug. 2014.
- [28] M. Alizadeh, A. Scaglione, J. Davies and K. S. Kurani, "A Scalable Stochastic Model for the Electricity Demand of Electric and Plug-In Hybrid Vehicles," *IEEE Transactions on Smart Grid*, vol. 5, no. 2, pp. 848-860, March 2014.
- [29] D. Wu, D. C. Aliprantis and K. Gkritza, "Electric Energy and Power Consumption by Light-Duty Plug-In Electric Vehicles," *IEEE Transactions on Power Systems*, vol. 26, no. 2, pp. 738-746, May 2011.
- [30] D. Gross, J. F. Shortle, J. M. Thompson, and C. M. Harris, "Fundamentals of queueing theory," *Technometrics*, vol. 41, no. 1, pp: 76-77, 2008.
- [31] A. Y. S. Lam, K. C. Leung and V. O. K. Li, "Capacity Estimation for Vehicle-to-Grid Frequency Regulation Services with Smart Charging Mechanism," *IEEE Transactions on Smart Grid*, vol. 7, no. 1, pp. 156-166, Jan. 2016.
- [32] P. Fan, B. Sainbayar and S. Ren, "Operation Analysis of Fast Charging Stations with Energy Demand Control of Electric Vehicles," *IEEE Transactions on Smart Grid*, vol. 6, no. 4, pp. 1819-1826, July 2015.
- [33] U. C. Chukwu and S. M. Mahajan, "V2G Parking Lot with PV Rooftop for Capacity Enhancement of a Distribution System," *IEEE Transactions on Sustainable Energy*, vol. 5, no. 1, pp. 119-127, Jan. 2014
- [34] Y. Sheffi, *Urban Transportation Network: Equilibrium Analysis with Mathematical Programming Methods*. Upper Saddle River, NJ, USA: Prentice Hall, 1985.
- [35] S. Bae and A. Kwasinski, "Spatial and Temporal Model of Electric Vehicle Charging Demand," *IEEE Transactions on Smart Grid*, vol. 3, no. 1, pp. 394-403, March 2012.

- [36] X. Dong, Y. Mu, H. Jia, J. Wu and X. Yu, "Planning of Fast EV Charging Stations on a Round Freeway," *IEEE Transactions on Sustainable Energy*, vol. 7, no. 4, pp. 1452-1461, Oct. 2016.
- [37] B. Ghosh, B. Basu and M. O'Mahony, "Multivariate Short-Term Traffic Flow Forecasting Using Time-Series Analysis," *IEEE Transactions on Intelligent Transportation Systems*, vol. 10, no. 2, pp. 246-254, June 2009.
- [38] M. Sommer, S. Tomforde and J. Haehner, "A Systematic Study on Forecasting of Traffic Flows with Artificial Neural Networks," in *ARCS 2015 - The 28th International Conference on Architecture of Computing Systems. Proceedings*, Porto, Portugal, 2015, pp. 1-8.
- [39] E. Y. Kim, "MRF model based real-time traffic flow prediction with support vector regression," *Electronics Letters*, vol. 53, no. 4, pp. 243-245, 2 16 2017.
- [40] M. T. Sánchez-Rico, R. García-Ródenas and J. L. Espinosa-Aranda, "A Monte Carlo Approach to Simulate the Stochastic Demand in a Continuous Dynamic Traffic Network Loading Problem," *IEEE Transactions on Intelligent Transportation Systems*, vol. 15, no. 3, pp. 1362-1373, June 2014
- [41] H. F. Yang, T. S. Dillon and Y. P. P. Chen, "Optimized Structure of the Traffic Flow Forecasting Model with a Deep Learning Approach," *IEEE Transactions on Neural Networks and Learning Systems*, vol. 28, no. 10, pp. 2371-2381, Oct. 2017.
- [42] A. Koesdwiady, R. Souza and F. Karray, "Improving Traffic Flow Prediction with Weather Information in Connected Cars: A Deep Learning Approach," *IEEE Transactions on Vehicular Technology*, vol. 65, no. 12, pp. 9508-9517, Dec. 2016.
- [43] W. Huang, G. Song, H. Hong and K. Xie, "Deep Architecture for Traffic Flow Prediction: Deep Belief Networks with Multitask Learning," *IEEE Transactions on Intelligent Transportation Systems*, vol. 15, no. 5, pp. 2191-2201, Oct. 2014.

- [44] Y. Lv, Y. Duan, W. Kang, Z. Li and F. Y. Wang, "Traffic Flow Prediction with Big Data: A Deep Learning Approach," *IEEE Transactions on Intelligent Transportation Systems*, vol. 16, no. 2, pp. 865-873, April 2015.
- [45] G. Wang, Z. Xu, F. Wen, and K. P. Wong, "Traffic-constrained multiobjective planning of electric-vehicle charging stations," *IEEE Trans. Power Del.*, vol. 28, no. 4, pp. 2363-2372, Oct. 2013.
- [46] Z. Liu, F. Wen, and G. Ledwich, "Optimal planning of electric-vehicle charging stations in distribution systems," *IEEE Trans. Power Del.*, vol. 28, no.1, pp. 102-110, Jan. 2013.
- [47] M. J. Mirzaei, A. Kazemi and O. Homaei, "A probabilistic approach to determine optimal capacity and location of electric vehicles parking lots in distribution networks," *IEEE Trans. Ind. Informat.*, vol. 12, no. 5, pp. 1963-1972, Oct. 2016.
- [48] K. Khalkhali, S. Abapour, S. M. Moghaddas-Tafreshi, and M. Abapour, "Application of data envelopment analysis theorem in plug-in hybrid EV Charging Station planning," *IET Gen., Transm., Distrib.*, vol. 9, no. 7, pp. 666-676, Apr. 2015.
- [49] H. Zhang, Z. Hu, Z. Xu, and Y. Song, "An integrated planning framework for different types of EV charging facilities in urban area," *IEEE Trans. Smart Grid*, vol. 7, no. 5, pp. 2273-2284, Sept. 2016.
- [50] X. Dong, Y. Mu, H. Jia, J. Wu, and X. Yu, "Planning of fast EV Charging Stations on a round freeway," *IEEE Trans. Sustain. Energy*, vol. 7, no. 4, pp. 1452-1461, Oct. 2016.
- [51] I. S. Bayram, A. Tajer, M. Abdallah, and K. Qaraqe, "Capacity planning frameworks for EV Charging Stations with multiclass customers," *IEEE Trans. Smart Grid*, vol. 6, no.4, pp. 1934-1943, Jul. 2015.
- [52] S. Shojaabadi, S. Abapour, M. Abapour, and A. Nahavandi, "Optimal planning of plug-in hybrid EV Charging Station in distribution network

- considering demand response programs and uncertainties," *IET Gener. Transmiss. Distrib.*, vol. 10, no. 13, pp. 3330-3340, Oct. 2016.
- [53] A. H. Hajimiragha, C. A. Canizares, M. W. Fowler, S. Moazeni, and A. Elkamel, "A robust optimization approach for planning the transition to plug-in hybrid EVs," *IEEE Trans. Power Syst.*, vol. 26, no. 4, pp. 2264-2274, Nov. 2011.
- [54] A. Hajimiragha, C. A. Canizares, M. W. Fowler, and A. Elkamel, "Optimal transition to plug-in hybrid EVs in Ontario, Canada, considering the electricity-grid limitations," *IEEE Trans. Ind. Electron.*, vol. 57, no. 2, pp. 690-701, Feb. 2010.
- [55] M. F. Shaaban and E. F. El-Saadany, "Accommodating high penetrations of EVs and renewable DG considering uncertainties in distribution systems," *IEEE Trans. Power Syst.*, vol. 29, no. 1, pp. 259-270, Jan. 2014.
- [56] I. Graabak, Q. Wu, L. Warland, and Z. Liu, "Optimal planning of the Nordic transmission system with 100% EV penetration of passenger cars by 2050," *Energy*, vol. 107, pp. 648-660, Jul. 2016.
- [57] W. Yao, C. Y. Chung, F. Wen, M. Qin, and Y. Xue, "Scenario-based comprehensive expansion planning for distribution systems considering integration of plug-in EVs," *IEEE Trans. Power Syst.*, vol. 31, no.1, pp. 317-328, Jan. 2016.
- [58] X. Lin, J. Sun, S. Ai, X. Xiong, Y. Wan, and D. Yang, "Distribution network planning integrating Charging Stations of EV with V2G," *Int. J. Elec. Power*, vol. 63, pp. 507-512, Dec. 2014.
- [59] W. Yao, J. Zhao, F. Wen, Z. Dong, Y. Xue, Y. Xu, and K. Meng, "A multi-objective collaborative planning strategy for integrated power distribution and EV charging systems," *IEEE Trans. Power Syst.*, vol. 29, no.4, pp. 1811-1821, Jul. 2014.

- [60] R. Deng, Z. Yang, M. Y. Chow, and J. Chen, "A survey on demand response in smart grids: Mathematical models and approaches," *IEEE Trans. Ind. Informat.*, vol. 11, no. 3, pp. 570–582, Jun. 2015.
- [61] Shao C, Wang X, Wang X, et al, "Layered and distributed charge load dispatch of considerable electric vehicles," *IEEE Trans. on Power Syst.*, 30(4):1858-1867, Jul. 2015.
- [62] T. V. Theodoropoulos, I. G. Damousis, and A. J. Amditis, "Demand-side management ICT for dynamic wireless EV charging," *IEEE Trans. Ind. Electron.*, vol. 63, no. 10, pp. 6623–6630, Oct. 2016.
- [63] M. Kisacikoglu, F. Erden, and N. Erdogan, "Distributed control of PEV charging based on energy demand forecast," *IEEE Trans. Ind. Informat.*, May 2017, doi: 10.1109/TII.2017.2705075.
- [64] P. You, Z. Yang, M. Chow, and Y. Sun, "Optimal cooperative charging strategy for a smart charging station of electric vehicles," *IEEE Trans. Power Syst.*, vol. 31, no. 4, pp. 2946–2956, Jul. 2016.
- [65] C. Kong, I. S. Bayram, and M. Devetsikiotis, "Revenue optimization frameworks for multi-class PEV charging stations," *IEEE Access*, vol. 3, pp. 2140–2150, 2015.
- [66] Y. Mou, H. Xing, Z. Lin, and M. Fu, "Decentralized optimal demand-side management for PHEV charging in a smart grid," *IEEE Trans. Smart Grid*, vol. 6, no. 2, pp. 726–736, Mar. 2015.
- [67] A. Kulvanitchaiyanunt, V. C. P. Chen, J. Rosenberger, P. Sarikprueck, and W. J. Lee, "A linear program for system-level control of regional PHEV charging stations," *IEEE Trans. Ind. Appl.*, vol. 52, no. 3, pp. 2046–2052, Jun. 2016.
- [68] X. Tan, G. Qu, B. Sun, N. Li, and D. H. K. Tsang, "Optimal scheduling of battery charging stations serving electric vehicle based on battery swapping," *IEEE Trans. Smart Grid*, Oct. 2017, doi: 10.1109/TSG.2017.2764484.

- [69] B. Sun, Z. Huang, X. Tan, and D. H. K. Tsang, "Optimal scheduling for electric vehicle charging with discrete charging levels in distribution grid," *IEEE Trans. Smart Grid*, Apr. 2016, doi: 10.1109/TSG.2016.2558585.
- [70] W. Kempton and J. Tomic, "Vehicle-to-grid power implementation: From stabilizing the grid to supporting large-scale renewable energy," *Journal of Power Sources*, vol. 144, no.1, pp. 280-294, Jun. 2005.
- [71] Q. Dai, T. Cai, S. Duan, and F. Zhao, "Stochastic modeling and forecasting of load demand for electric bus battery-swap station," *IEEE Trans. Power Del.*, vol. 29, no. 4, pp. 1909–1917, Aug. 2014.
- [72] Y. Zheng, Z. Y. Dong, Y. Xu, K. Meng, J. H. Zhao, and J. Qiu, "Electric vehicle battery charging/swap stations in distribution systems: comparison study and optimal planning," *IEEE Trans. Power. Syst.*, vol. 29, no. 4, pp. 1909-1917, Aug. 2014.
- [73] W. Tian, J. He, Y. Jiang, et al, "Multi-objective optimization of charging dispatching for electric vehicle battery swapping," *Power Syst. Tech.*, vol. 36, no. 11, pp. 25-29, 2012. (in Chinese)
- [74] Y. Yang, Z. Hu, and Y. Song, "Research on optimal operation of battery swapping and charging station for electric buses," *Proc. of the CSEE*, vol. 32, no. 31, pp. 35-42, 2012. (in Chinese)
- [75] S. Zhang, Z. Hu, Y. Song, et al, "Research on unit commitment considering interaction between battery swapping station and power grid," *Proc. of the CSEE*, vol. 32, no. 10, pp. 49-55, 2012. (in Chinese)
- [76] D. Zhang, Y. Jiang, W. Zhang, et al, "Economic operation of electric vehicle battery swapping station based on genetic algorithms," *Power Syst. Tech.*, vol. 37, no. 8, pp. 2102-2107, 2013. (in Chinese).
- [77] N. Yu, L. Tesfatsion, and C. C. Liu, "Financial bilateral contract negotiation in wholesale electricity markets using Nash Bargaining theory," *IEEE Trans. Power Syst.*, vol. 27, no.1, pp. 251-267, Feb. 2012.

- [78] D. Gately, "Sharing the gains from regional cooperation: A game theoretic application to planning investment in electric power," *Int. Econ. Rev.*, vol. 15, no. 1, pp. 195–208, 1974.
- [79] H. Liu, Y. Shen, Z. B. Zabinsky, C. C. Liu, A. Courts, and S. K. Joo, "Social welfare maximization in transmission enhancement considering network congestion," *IEEE Trans. Power Syst.*, vol. 23, no. 3, pp. 1105–1114, Aug. 2008.
- [80] F. Evans, J. M. Zolezzi, and H. Rudnick, "Cost assignment model for electrical transmission system expansion: An approach through the kernel theory," *IEEE Trans. Power Syst.*, vol. 18, no. 2, pp. 625–632, May 2003.
- [81] P. A. Ruiz, and J. Contreras, "An effective transmission network expansion cost allocation based on game theory," *IEEE Trans. Power Syst.*, vol. 22, no. 1, pp. 136–144, Feb. 2007.
- [82] Y. Tsukamoto and I. Iyoda, "Allocation of fixed transmission cost to wheeling transactions by cooperative game theory," *IEEE Trans. Power Syst.*, vol. 11, no. 2, pp. 620–629, May 1996.
- [83] A. G. Bakirtzis, "Aumann-Shapley transmission congestion pricing," *IEEE Power Eng. Rev.*, vol. 21, no. 3, pp. 67–69, 2001.
- [84] X. Tan and T. T. Lie, "Application of the Shapley value on transmission cost allocation in the competitive power market environment," *Proc. Inst. Elect. Eng., Gen., Transm., Distrib.*, vol. 149, no. 1, pp. 15–20, 2002.
- [85] Q. Lu, L. Chen, S. Mei, "Typical applications and prospects of game theory in power system," *Proceedings of the CSEE*, vol. 34, no. 29, pp. 5009-5017, Oct. 2014.
- [86] W. Su, H. Tahimi-Eichi, W. Zeng, and M. Chow, "A survey on the electrification of transportation in a smart grid environment," *IEEE Trans. Ind. Informat.*, vol. 8, no. 1, pp. 1-10, Feb. 2012.
- [87] Z. Darabi and M. Fedowsi, "An event-based simulation framework to examine the response of power grid to the charging demand of plug-in hybrid electric

- vehicles (PHEVs)," *IEEE Trans. Ind. Informat.*, vol. 10, no. 1, pp. 313-322, Feb. 2014.
- [88] L. P. Fernàndez, T. G. S. Romàin, R. Cossent, C. M. Domingo, and P. Friàas, "Assessment of the impact of plug-in electric vehicles on distribution networks," *IEEE Trans. Power Syst.*, vol. 26, no. 1, pp. 206-213, Feb. 2011.
- [89] K. Clement-Nyns, E. Haesen, and J. Driesen, "The impact of charging plug-in hybrid electric vehicles on a residential distribution grid," *IEEE Trans. Power Syst.*, vol. 26, no. 1, pp. 371-380, Feb. 2010.
- [90] Y. Ma, T. Houghton, A. Cruden, and D. Infield, "Modeling the benefits of vehicle-to-grid technology to a power system," *IEEE Trans. Power Syst.*, vol. 27, no. 2, pp. 1012-1020, May 2012.
- [91] Y. Saber and G. K. Venayagamoorthy, "Intelligent unit commitment with vehicle-to-grid: A cost-emission optimization," *J. Power Sources*, vol. 195, no. 3, pp. 898-911, Feb. 2010.
- [92] W. Yao, J. Zhao, F. Wen, Y. Xue and G. Ledwich, "A hierarchical decomposition approach for coordinated dispatch of plug-in electric vehicles," *IEEE Trans. Power Syst.*, vol. 28, no. 3, pp. 2768-2778, Aug. 2013.
- [93] P. Jong, A. Kiperstok, A.S. Sanchez, R. Dargaville and E.A. Torres, "Integrating large scale wind power into the electricity grid in the Northeast of Brazil," *Energy*, 2016, 100: 401-415.
- [94] C. Budischak et al., "Cost-minimized combinations of wind power, solar power and electrochemical storage, powering the grid up to 99.9% of the time," *J. Power Sources*, vol. 225, pp. 60-74, Mar. 2013.
- [95] A. Y. Saber and G. K. Venayagamoorthy, "Plug-in vehicles and renewable energy sources for cost and emission reductions," *IEEE Trans. Ind. Electron.*, vol. 58, no. 4, pp. 1229-1238, Apr. 2011.
- [96] G. Kyriakarakos, D. Piromalis, A. Dounis, and K. Arvanitis, "Intelligent demand side energy management system for autonomous polygeneration microgrids," *Appl. Energy*, vol. 103, pp. 39-51, Mar. 2013.

- [97] P. P. Varaiya, F. F. Wu, and J. W. Bialek, "Smart operation of smart grid: Risk-limiting dispatch," *Proc. IEEE*, vol. 99, no. 1, pp. 40-57, Jan. 2011.
- [98] J. Zhao, F. Wen, Z. Dong, Y. Xue and K. P. Wong, "Optimal dispatch of electric vehicles and wind power using enhanced particle swarm optimization," *IEEE Trans. Ind. Informat.*, vol. 8, no. 4, pp. 889-899, Jun. 2012.
- [99] T. Shekari, S. Golshannavaz and F. Aminifar, "Techno-economic collaboration of EV fleets in energy management of microgrids," *IEEE Trans. Power Syst.*, vol. 32, no. 5, pp. 3833-3841, Sept. 2017.
- [100] G. Carpinelli, F. Mottola, D. Proto and A. Russo, "A multi-objective approach for microgrid scheduling," *IEEE Trans. Smart Grid*, vol. 8, no. 5, pp. 2109-2118, Sept. 2017.
- [101] T. F. Robert, A. H. King, C. S. Harry, Rughooputh, and K. Deb, "Evolutionary multi-objective environmental/economic dispatch: stochastic vs deterministic approaches," KanGAL, Rep. 2004019, 2004, pp. 1-15.
- [102] M. A. Abido, "Environmental/economic power dispatch using multi-objective evolutionary algorithms," *IEEE Trans. Power Syst.*, vol. 18, no. 4, pp. 1529-1537, Nov. 2003.
- [103] M. R. Andervazh and S. Javadi, "Emission-economic dispatch of thermal power generation units in the presence of hybrid electric vehicles and correlated wind power plants," *IET Gener. Transm. Distrib.*, vol. 11, no. 9, pp. 2232-2243, 6 22 2017.
- [104] S. He, Q. H. Wu, and J. R. Saunders, "Group search optimizer: An optimization algorithm inspired by animal searching behavior," *IEEE Trans. Evol. Comput.*, vol. 13, no. 5, pp. 973-990, Oct. 2009.
- [105] B. Zhou, K.W. Chan, T. Yu and C.Y. Chung, "Equilibrium-inspired multiple group search optimization with synergistic learning for multi-objective electric power dispatch," *IEEE Trans. Power Syst.*, vol. 28, no. 4, pp. 3534-3545, Nov. 2013.

- [106] Q. Zhang and H. Li, "MOEA/D: A multi-objective evolutionary algorithm based on decomposition," *IEEE Trans. Evol. Comput.*, vol. 11, no. 6, pp. 712–731, Dec. 2007.
- [107] ZHU Dengyuan, CHANG Xiaofeng, "Matlab realization of grey prediction GM(1,1) model," *Journal of Henan University of Urban Construction*, vol.22, no.3, pp. 40-46, May. 2013. (in Chinese)
- [108] O. Abdel-Hamid, A. r. Mohamed, H. Jiang, L. Deng, G. Penn and D. Yu, "Convolutional Neural Networks for Speech Recognition," *IEEE/ACM Transactions on Audio, Speech, and Language Processing*, vol. 22, no. 10, pp. 1533-1545, Oct. 2014.
- [109] Y. Liang, J. Wang, S. Zhou, Y. Gong, N. Zheng, "Incorporating image priors with deep convolutional neural networks for image super-resolution," in *Neurocomputing*, vol. 194, no. 19, pp: 340-347, Jun. 2016.
- [110] A. Krizhevsky, I. Sutskever, and G. Hinton, "ImageNet classification with deep convolutional neural networks." *International Conference on Neural Information Processing Systems*, Curran Associates Inc. vol. 25, pp: 1097-1105, 2012.
- [111] S. G. Mallat, "A theory for multiresolution signal decomposition: the wavelet representation," *IEEE Transactions on Pattern Analysis and Machine Intelligence*, vol. 11, no. 7, pp. 674-693, Jul 1989.
- [112] H. Cramér, *Mathematical Methods of Statistics*, Princeton, NJ, USA: Princeton Univ., 1971.
- [113] G. Wang, Z. Xu, F. Wen and K. P. Wong, "Traffic-Constrained Multiobjective Planning of Electric-Vehicle Charging Stations," *IEEE Transactions on Power Delivery*, vol. 28, no. 4, pp. 2363-2372, Oct. 2013
- [114] M. J. Mirzaei, A. Kazemi and O. Homaei, "A Probabilistic Approach to Determine Optimal Capacity and Location of Electric Vehicles Parking Lots in Distribution Networks," *IEEE Transactions on Industrial Informatics*, vol. 12, no. 5, pp. 1963-1972, Oct. 2016.

- [115] S. Negarestani, M. Fotuhi-Firuzabad, M. Rastegar and A. Rajabi-Ghahnavieh, "Optimal Sizing of Storage System in a Fast Charging Station for Plug-in Hybrid Electric Vehicles," *IEEE Transactions on Transportation Electrification*, vol. 2, no. 4, pp. 443-453, Dec. 2016.
- [116] Dempster, A. P., et al. "Maximum Likelihood from Incomplete Data via the EM Algorithm." *Journal of the Royal Statistical Society. Series B (Methodological)*, vol. 39, no. 1, pp. 1-38, 1977.
- [117] C. Carson, S. Belongie, H. Greenspan and J. Malik, "Blobworld: image segmentation using expectation-maximization and its application to image querying," *IEEE Transactions on Pattern Analysis and Machine Intelligence*, vol. 24, no. 8, pp. 1026-1038, Aug 2002.
- [118] UK Department for Transport, *National Travel Survey*. [Online]. Available:https://www.gov.uk/government/uploads/system/uploads/attachment_data/file/79153/nts0501.xls.
- [119] F. Kelly, *Reversibility and stochastic networks*, Cambridge University Press New York, NY, USA: 2011.
- [120] Highways England, *Traffic Flow Data*, [Online]. Available: <http://tris.highwaysengland.co.uk/download/6e8f2a60-e4bc-4805-a5d2-d7f5c4a992db>
- [121] M. Hollander, D. Wolfe, and E. Chicken, *Nonparametric Statistical Methods*, Hoboken, NJ, USA: Wiley, 2014.
- [122] N. Neyestani, M. Y. Damavandi, M. Shafie-Khah, J. Contreras, J. P. S. Catalão, "Allocation of plug-in vehicles' parking lots in distribution systems considering network-constrained objectives," *IEEE Trans. Power Syst.*, vol. 30, no. 5, pp. 2643-2656, Sept. 2015.
- [123] G. E. Hinton, S. Osindero and Y. W. Teh, "A fast learning algorithm for deep belief nets," *Neural Computation*, vol. 18, no. 7, pp. 1527-1554, July 2006.
- [124] Geoffrey SO, Hinton E, Teh Y-W, "A fast learning algorithm for deep belief nets," *Neural Comput.*, vol. 18, no.7, pp. 1527-1554, Jul. 2006.

- [125] H. Wang, G. Wang, G. Li, J. Peng, Y. Liu, "Deep belief network based deterministic and probabilistic wind speed forecasting approach," *Applied Energy*, vol. 182, pp. 80-93, Nov. 2016.
- [126] M. J. Osborne and A. Rubinstein, *A course in game theory*. Cambridge, MA: MIT press, 1994.
- [127] B. Ken, *Game theory and the social contract*, MA, Cambridge: MIT Press, 1994.
- [128] A. E. Roth, and U. G. Rothblum, "Risk aversion and Nash's solution for bargaining games with risky outcomes," *Econometrica*, vol.25, no. 3, pp. 639-647, May 1982.
- [129] J. Nash and F. John, "The bargaining problem," *Econometrica*, vol.18, no. 2, pp. 155–162, 1950.
- [130] J. Nash, "Two-person cooperative games," *Econometrica*, vol. 21, no. 1, pp. 128–140, 1953.
- [131] S. Wang, Z. Y. Dong, F. Luo, K. Meng, and Y. Zhang, "Stochastic collaborative planning of EV charging stations and power distribution system", *IEEE Trans. Ind. Informat.*, vol. 14, no. 1, pp.321-331, Jan. 2018.
- [132] M. Lavorato, M. J. Rider, A. V. Garcia, and R. Romero, "A constructive heuristic algorithm for distribution system planning," *IEEE Trans. Power Syst.*, vol. 25, no.3, pp. 1734-1742, Aug. 2010.
- [133] W. Liu, Q. Wu, F. Wen, and J. Østergaard, "Day-ahead congestion management in distribution systems through household demand response and distribution congestion prices," *IEEE Trans. Smart Grid*, vol. 5, no. 6, pp. 2739-2747, Nov. 2014.
- [134] N. O'Connell et al., "Day-ahead tariffs for the alleviation of distribution grid congestion from electric vehicles," *Electr. Power Syst. Res.*, vol. 92, pp. 106-114, Nov. 2012.

- [135] J. Kennedy and R. C. Eberhart, "A discrete binary version of the particle swarm algorithm," in Proc. IEEE Int. Conf. Syst., Man, and Cybernetics, Orlando, FL, 1997, pp. 4104-4108.
- [136] X. Zhang, K. W. Chan, X. Yang, Y. Zhou, K. Ye, and G. Wang, "A comparison study on electric vehicle growth forecasting based on grey system theory and NAR neural network," in *IEEE Int. Conf. on Smart Grid Communication*, pp. 711-715, Sydney, Nov. 2016.
- [137] R. D. Zimmerman and C. Murillo-Sanchez, "MATPOWER 6.0b1 User' Manual," [Online]. Available: <http://www.pserc.cornell.edu/matpower/>
- [138] J. Hetzer, D. C. Yu and K. Bhattarai, "An economic dispatch model incorporating wind power," *IEEE Trans. on Energy Convers.*, vol. 23, no. 2, pp. 603-611, Apr. 2008.
- [139] J. Park, K. Lee, J. Shin, and K. Y. Lee, "A particle swarm optimization for economic dispatch with nonsmooth cost functions," *IEEE Trans. Power Syst.*, vol. 20, no. 1, pp. 34-42, Feb. 2005.
- [140] S.-L. Andersson, A. K. Elofsson, M. D. Galus, L. Göransson, S. Karlsson, F. Johnsson, and G. Andersson, "Plug-in hybrid electric vehicles as regulating power providers: Case studies of Sweden and Germany," *Energy Policy*, vol. 38, no. 6, pp. 2751-2762, Jun. 2010.
- [141] J. Tomić and W. Kempton, "Using fleets of electric-drive vehicles for grid support," *J. Power Sources*, vol. 168, no. 2, pp. 459-468, Jun. 2007.
- [142] F. N. Lee, M. Lin and A. M. Breipohl, "Evaluation of the variance of production cost using a stochastic outage capacity state model," *IEEE Trans. Power Syst.*, vol. 5, no. 4, pp. 1061-1067, Nov. 1990.
- [143] Q. Zhang and H. Li, "MOEA/D: A multi-objective evolutionary algorithm based on decomposition," *IEEE Trans. Evol. Comput.*, vol. 11, no. 6, pp. 712-731, Dec. 2007.

- [144] A. Jaszkiewicz, "On the performance of multiple-objective genetic local search on the 0/1 knapsack problem – A comparative experiment," *IEEE Trans. Evol. Comput.*, vol. 6, no. 4, pp. 402–412, Aug. 2002.
- [145] C. A. Coello Coello, G. B. Lamont, and D. A. Van Veldhuizen, *Evolutionary Algorithms for Solving Multi-Objective Problems*. Norwell, MA, USA: Kluwer, 2002.
- [146] K. Deb, A. Pratap, S. Agarwal, and T. Meyarivan, "A fast and elitist multi-objective genetic algorithm: NSGA-II," *IEEE Trans. Evol. Comput.*, vol. 6, no. 2, pp. 182–197, Apr. 2002.
- [147] B. Zhou, K.W. Chan, T. Yu and C.Y. Chung, "Equilibrium-inspired multiple group search optimization with synergistic learning for multi-objective electric power dispatch," *IEEE Trans. Power Syst.*, vol. 28, no. 4, pp. 3534-3545, Nov. 2013.
- [148] E. Zitzler, K. Deb, and L. Thiele, "Comparison of multiobjective evolutionary algorithms: Empirical results," *Evol. Comput.*, vol. 8, no. 2, pp. 173–195, 2000.
- [149] K. Deb, *Multi-Objective Optimization Using Evolutionary Algorithms*. Chichester, U.K.: Wiley, 2001.
- [150] Q. Li, M. Liu and H. Liu, "Piecewise normalized normal constraint method applied to minimization of voltage deviation and active power loss in an AC–DC hybrid power system," *IEEE Trans. Power Syst.*, vol. 30, no. 3, pp. 1243-1251, May 2015.
- [151] S. Agrawal, B. K. Panigrahi and M. K. Tiwari, "Multi-objective particle swarm algorithm with fuzzy clustering for electrical power dispatch," *IEEE Trans. Evol. Comput.*, vol. 12, no. 5, pp. 529-541, Feb. 2008.
- [152] R. Zimmerman, C. Murillo-Sánchez, and R. Thomas, "MATPOWER: Steady-state operations, planning and analysis tools for power systems research and education," *IEEE Trans. Power Syst.*, vol. 26, no. 1, pp. 12-19, Feb. 2011.
- [153] R. A. Horn and C. R. Johnson, *Matrix Analysis*. Cambridge, U.K.: Cambridge Univ. Press, 1985.

- [154] V. Vahidinasab and S. Jadid, "Normal boundary intersection method for suppliers' strategic bidding in electricity markets: An environmental/economic approach," *Energy Conversion and Management*, vol. 51, no. 6, pp. 1111–1119, Jun. 2010.
- [155] D. Mustard, "Numerical integration over the n-dimensional spherical shell," *Math. Comput.*, vol. 18, no. 88, pp. 578-589, Oct. 1964.
- [156] G. Hinton, and R. Salakhutdinov, "Reducing the Dimensionality of Data with Neural Networks," *Science*, vol. 313, pp. 504-507, Jul. 2006.
- [157] G. Hinton, "Training products of experts by minimizing contrastive divergence," *Neural Comput.*, vol. 14, no. 8, pp. 1771-1800, Aug. 2002.
- [158] H. B. Azad, S. Mekhilef and V. G. Ganapathy, "Long-Term Wind Speed Forecasting and General Pattern Recognition Using Neural Networks," *IEEE Transactions on Sustainable Energy*, vol. 5, no. 2, pp. 546-553, April 2014.
- [159] Q. Wang and B. M. Hodge, "Enhancing Power System Operational Flexibility with Flexible Ramping Products: A Review," *IEEE Transactions on Industrial Informatics*, vol. 13, no. 4, pp. 1652-1664, Aug. 2017.
- [160] H. Wang, G. Li, G. Wang, J. Peng, H. Jiang, and Y. Liu, "Deep learning based ensemble approach for probabilistic wind power forecasting," *Applied Energy*, vol. 188, pp. 56-70, Feb. 2017.
- [161] T. V. Vu, D. Gonsoulin, F. Diaz, C. S. Edrington and T. El-Mezyani, "Predictive Control for Energy Management in Ship Power Systems Under High-Power Ramp Rate Loads," *IEEE Transactions on Energy Conversion*, vol. 32, no. 2, pp. 788-797, June 2017.
- [162] J. Hu, M. R. Sarker, J. Wang, F. Wen and W. Liu, "Provision of flexible ramping product by battery energy storage in day-ahead energy and reserve markets," *IET Generation, Transmission & Distribution*, vol. 12, no. 10, pp. 2256-2264, 5 29 2018.
- [163] F. C. Schweppe, M. C. Caramanis, R. D. Tabors, R. E. Bohn, *Spot Pricing for Electricity*, MA, Boston: Kluwer, 1988.

- [164] R. J. Green, "Competition in generation: The economic foundations", *Proc. IEEE*, vol. 88, no. 2, pp. 128-139, Feb. 2000.
- [165] D. Feng, Z. Xu, J. Zhong and J. Ostergaard, "Spot Pricing When Lagrange Multipliers Are Not Unique," *IEEE Transactions on Power Systems*, vol. 27, no. 1, pp. 314-322, Feb. 2012.
- [166] R. A. Gallego, A. B. Alves, A. Monticelli, and R. Romero, "Parallel simulated annealing applied to long term transmission network expansion planning," *IEEE Trans. Power Syst.*, vol. 12, no. 1, pp. 181–188, Feb. 1997.
- [167] Highways England, Traffic Flow Data, [Online]. Available: <http://tris.highwaysengland.co.uk/detail/trafficflowdata>
- [168] Highways England, Monthly Summary Data, [Online]. Available: <http://tris.highwaysengland.co.uk/detail/monthlysummarydata>
- [169] K. Qian, C. Zhou, M. Allan and Y. Yuan, "Modeling of Load Demand Due to EV Battery Charging in Distribution Systems," *IEEE Transactions on Power Systems*, vol. 26, no. 2, pp. 802-810, May 2011.
- [170] D. Singh, R. K. Misra and D. Singh, "Effect of Load Models in Distributed Generation Planning," *IEEE Transactions on Power Systems*, vol. 22, no. 4, pp. 2204-2212, Nov. 2007.
- [171] J. Medina, N. Muller and I. Roytelman, "Demand Response and Distribution Grid Operations: Opportunities and Challenges," *IEEE Transactions on Smart Grid*, vol. 1, no. 2, pp. 193-198, Sept. 2010.
- [172] S. P. Lloyd, "Least squares quantization in PCM," *IEEE Transactions on Information Theory*, vol. 28, no. 2, pp. 129–137, 1982.
- [173] M. H. Amini, O. Karabasoglu, M. D. Ilić, K. G. Boroojeni and S. S. Iyengar, "ARIMA-based demand forecasting method considering probabilistic model of electric vehicles' parking lots," *2015 IEEE Power & Energy Society General Meeting*, Denver, CO, pp. 1-5, 2015.
- [174] Qiming Sun *et al.*, "Charging load forecasting of electric vehicle charging station based on support vector regression," *2016 IEEE PES Asia-Pacific*

- Power and Energy Engineering Conference (APPEEC)*, Xi'an, pp. 1777-1781, 2016.
- [175] Hecht-Nielsen, "Theory of the backpropagation neural network," International 1989 Joint Conference on Neural Networks, Washington, DC, USA, 1989, pp. 593-605 vol. 1.
- [176] Y. LeCun, "LeNet-5, convolutional neural networks," [Online], Available: <http://yann.lecun.com/exdb/lenet/>
- [177] J. Tanida, et al. "Parallel distributed processing model with local space-invariant interconnections and its optical architecture." *Applied Optics*, vol. 29, no. 32, pp. 4790-4797, Nov. 1990.
- [178] C. M. Bishop, *Neural Networks for Pattern Recognition*, London, U. K.: Oxford Univ. Press, 1996.
- [179] A. Hoke, A. Brissette, K. Smith, A. Pratt and D. Maksimovic, "Accounting for Lithium-Ion Battery Degradation in Electric Vehicle Charging Optimization," *IEEE Journal of Emerging and Selected Topics in Power Electronics*, vol. 2, no. 3, pp. 691-700, Sept. 2014.
- [180] R. Spotnitz, "Simulation of capacity fade in lithium-ion batteries", *J. Power Sources*, vol. 113, no. 1, pp. 72-80, Jan. 2003.
- [181] A.Y. Khinchine, *Mathematical Methods in the Theory of Queueing*, New York: Dover Publications, 1960.
- [182] A. Santos, N. McGuckin, H. Y. Nakamoto, D. Gay, and S. Liss, *Summary of Travel Trends: 2009 National Household Travel Survey*, U.S. Department of Transportation Federal Highway Administration, Washington, DC, USA, Rep. FHWA-PL-11022, Jun. 2011.
- [183] Hecht-Nielsen, "Theory of the backpropagation neural network," International 1989 Joint Conference on Neural Networks, Washington, DC, USA, 1989, pp. 593-605 vol. 1.

- [184] D. G. Kendall, “Stochastic processes occurring in the theory of queues and their analysis by the method of the imbedded Markov chain” , The Annals of Mathematical Statistics, vol. 24, no. 3, pp. 338 – 354, Sep. 1953.
- [185] M. Simpson and T. Markel. (2012). Plug-In Electric Vehicle Fast Charge Station Operational Analysis with Integrated Renewables. [Online]. Available: <http://www.nrel.gov/docs/fy12osti/53914.pdf>, accessed Oct. 14, 2018.
- [186] Idaho National Lab. EV Project Quarterly and Annual Report Data. [Online]. Available: <https://avt.inl.gov/project-type/data>, accessed Oct. 14, 2018.